UNIVERSITY OF SOUTHAMPTON

A NON-TACTILE SENSOR FOR ROBOT CONTROL

by Sean James Wellington

UNIVERSITY OF SOUTHAMPTON

ABSTRACT

FACULTY OF ENGINEERING AND APPLIED SCIENCE

ELECTRICAL ENGINEERING

Master of Philosophy

A NON-TACTILE SENSOR FOR ROBOT CONTROL

by Sean James Wellington

A non-tactile sensor has been developed for use in robot control and general vision applications. The sensor operates using a mechanically scanned laser, with reflected light from the surface to be imaged sensed using a simple detector. Initially the sensor was intended for one pass weld seam tracking, however, a number of additional applications have been investigated.

The light detector has a non-linear response, with the output signal corrupted by noise caused by the surface texture of the workpiece and the tolerances of the scanning mechanism. Signal processing is performed using a combination of analogue and digital signal processing. Noise reduction has been achieved using filtering and signal averaging, while software routines have been devised to reject erroneous scan data.

Thresholding techniques are used to detect the position of a discontinuity; for example, a weld seam or any significant surface defects. In addition, geometric inspection and dimensional measurements may be performed by detecting the edges of an object.

The sensor system has been interfaced to a gantry robot, with seam tracking accomplished at speeds appropriate for Metal Inert Gas (MIG) arc welding.

Surface classification is possible using the scanner output signal to characterise a surface. Statistical methods have been used to compare scan signatures from different surfaces.

The limitations of the simple laser scanner are identified, and where possible, suitable enhancements are proposed. It is speculated that improving the sensor performance will permit seam tracking at the higher speeds required for AGV guidance or sealant application.

Acknowledgement

I am indebted to my supervisor, Dr. Richard Crowder. Without his support and guidance this work would not have been completed.

This research has been supported solely by my employer, Southampton Institute of Higher Education. The Institute has provided all materials, equipment and technical support for the project as part of their staff development programme.

Several colleagues have been generous with their time. I must thank Graham King, John Bolt and Geoff Wharam for many useful discussions and conscientious proof-reading of the completed text.

Sean Wellington
December 1992

Contents

List of Tables and Illustrations

Tables

Figures

Chapter 1
Introduction

1.1 Background

The UK robot population has been steadily increasing over the last ten years. The greater part of this expansion is due to heavy investment by the major automotive manufacturers. In 1990 some 34.8% of the total UK robot population was employed in the automotive industry **[1]** and it is clear that current robot technology is best suited to the simple, repetitive tasks found on assembly lines. The limited use of robot technology can be ascribed to a number of factors:

1) The limited range of tasks that can be performed effectively.
2) The high cost of the equipment.
3) Difficulties associated with installing, programming and commissioning new high technology equipment.
4) Social considerations when replacing traditional jobs with automated systems.

If the use of industrial robots is to be increased, systems must be developed which are easy to use, cost effective, versatile and capable of undertaking more complex tasks. Current robot systems use expensive jigging to accurately locate components and tools at fixed positions within the robot work-space. It is widely recognised that a new generation of sensors are required to achieve the twin goals of increased task complexity and reduced dependency on a highly structured work-cell environment **[2]**. These sensors should be flexible, cost effective and easy to interface to a wide range of robot controllers. At present, many commercial sensor systems are designed specifically for a range of robots produced by a single manufacturer.

Although robots are being used in increasingly diverse applications including mushroom picking and sheep shearing **[3]**, the majority of installed robot systems are found in

the engineering industry. Table 1 shows a comparison of the key applications of industrial robots in the UK.

Application	Total at 12/90	During 1990
Injection Moulding (1989)	1212	n/a
Spot Welding	1010	157
Arc Welding	679	118
Machine Loading	634	7
Assembly	606	10

Table 1 Key robot applications in the UK
(source: British Robot Association **[1]**)

1.2 The Industrial Robot

Industrial robots are automatic manipulators which are freely programmable in at least three axes of motion and designed for industrial use. The robot may be programmed to perform handling or manufacturing tasks fully automatically, possibly in response to sensor information.

1.2.1 Robot Anatomy

Commercial robots are available in a wide range of sizes, shapes and physical configurations. When describing the anatomy of a robot a distinction is made between the main or primary axes which allow the robot to reach any point within the work-space and the secondary axes which allow the required orientation of the end-effector. The robot axes perform either sliding (translational) or rotational movements. These two types of motion are combined in various manners depending on the particular robot configuration.

The joint notation scheme **[4]** (pp20-32) is used to describe the three main axes of a robot, starting from the joint nearest the base and ending with the joint nearest the robot wrist. Most commercial robots possess one of four basic configurations (Table 2).

Robot Configuration	Joint Notation
Polar (Spherical coordinate)	RRT
Cylindrical	RTT
Cartesian (X-Y-Z)	TTT
Jointed Arm (Revolute coordinate)	RRR

Key: T = Translational axis
R = Revolute axis

Table 2 Basic robot configurations
(source: Groover *et al* **[4]**)

The main application areas of the basic configurations are identified by Hartley **[5]** (pp13-26). Cartesian robots are used for 'pick and place' operations, applying sealant and most assembly tasks. Cylindrical and polar robots are used for material handling and spot-welding, while jointed arm robots are used in applications which require high dexterity such as arc welding, paint spraying and fettling.

1.2.2 Robot Actuation

A number of techniques are used to produce the mechanical movements of the robot. The power source may be hydraulic, pneumatic or electric. Typical robot actuators are described by Coiffet and Chirouze **[6]** (pp83-105) and Miller **[7]**.

Hydraulic Actuators

Hydraulic drives are used for large robots with high load capacity. Mineral oil at pressures of approximately 100 bar is supplied via control valves to either rotary or linear actuators. Problems include pollution caused by oil leaks, elimination of air from the system and the need for piping, a pump, and accumulator.

Pneumatic Actuators

Pneumatic actuators employ air at a typical pressure of 10 bar. It is not possible to obtain accurate position control or high drive forces as the air will tend to compress. Rotary or

linear actuators are available and these devices are simple and clean, although a suitable air supply is required. Pneumatic drives are often used in rudimentary 'pick and place' applications and to control simple robot end-effectors.

Electric Actuators

Although advances in electric motor technology have led to an increased use of electric drives for industrial robots, these devices cannot yet match the power of hydraulic actuators. Traditionally robots have used DC servo systems, although brushless motors have become more popular with the development of electronic control. Electric motors are compact, reliable and easily controlled using a computer. Brushless motors offer exceptionally high reliability, long life and spark-free operation **[8]**.

1.2.3 Robot Control

The robot is controlled by a computer which uses sensor derived data to generate the actuator control signals. The control strategies employed are described by Todd **[9]** (pp44-45).

Point-to-Point (PTP) Control

The robot is positioned at specified points within the work-space. The robot can be programmed to move between two or more points but the path followed will be unspecified. The axes involved in the movement are independent, and hence the end-effector speed cannot be controlled.

Continuous Path (CP) Control

The robot can be programmed to follow a smooth trajectory which is defined as a series of closely spaced points. There is a permanent mathematical relationship between all the axes involved in the movement and the path that is followed.

The sensors used by a robot may be divided into two categories; internal sensors monitor the condition of the robot, while external sensors monitor the robot environment.

Internal Sensors

Position sensors are fitted to each axis of the robot and used by the controller to generate the actuator control signals. In addition, sensors may be used to measure velocity and acceleration. A range of internal sensors are described by Coiffet and Chirouze **[6]** (pp107-120).

External Sensors

The use of external sense is application dependent and a wide range of sensors are available using both tactile and non-tactile measurement techniques. A selection of external sensors are presented by Pugh **[10][11]**.

The difference between the so called first and second generation of industrial robots is broadly one of sensing. First generation robots have little or no external sense, while second generation (intelligent) robots use information provided by external sensors to modify their actions in accordance with variations in the environment. Second generation robots have a two level hierarchical control system (Table 3).

Lower Level Internal Sensors	Sensed information is used for position control
Higher Level External Sensors	Sensed information is used to adapt the task program in response to changes in the environment.

Table 3 Hierarchical control system

1.2.4 Programming the Robot

The two basic programming methods used with industrial robots are described by Mair **[12]** and shown in Table 4.

On-line programming ("teach-by-showing") techniques use a human operator to enter the required movements using the robot itself. This can be achieved by manually guiding the end-effector through the series of movements (lead-through) or by using a teach pendant. Lead-through programming is ideally

suited to applications such as paint spraying or arc welding where a smooth trajectory must be recorded and the skill of the human operator may be transferred directly to the robot. At present, the teach pendant is the most widely used programming method for industrial robots. Complex programs may be devised, although on-line programming techniques are time-consuming and inflexible.

Off-line (Indirect)	Implicit	Task oriented languages
	Explicit	Structured programming languages
		Primitive motion languages
On-line (Direct)	Teach by pendant	
	Teach by lead-through	

Table 4 Robot programming techniques
(source: Mair **[12]**)

Off-line programming does not require the use of the robot and this type of programming has some important advantages:

1) The robot can work productively while a new program is being devised.
2) There is potential for full integration into Computer Aided Engineering (CAE) systems.
3) Programs may be devised to cope with unusual or unexpected conditions.
4) The advantages of sensory feedback and adaptive control may be fully exploited.

Robot programming languages may be divided into two categories; explicit and implicit. With an explicit language the programmer must specify the position of the end-effector and each movement in detail. Primitive motion languages resemble BASIC, while structured programming languages such as VAL-II and AML are more like Pascal and support sensory feedback and interfacing **[4]** (pp214-289). A version of the VAL programming language, modified for use with arc welding robots, is described by Pavone **[13]**. A considerable number

of explicit programming languages are available for commercial use, but none has become universally accepted because of imperfections and incompatibilities between different robot types **[6]** (pp132-133).

Implicit (task-level) programming languages use program statements which refer to the robot task or goal. For example, the command "Grasp Bolt" will automatically initiate the required series of movements. The robot control system will plan the end-effector trajectory using a model of the robot environment held in the computer **[14]**.

1.3 The Arc Welding Process

Arc welding is used to make long continuous joints in which an airtight seal is normally required between the two pieces of metal being joined. An electrode in the form of a rod or wire is used to supply a high current, typically between 100A and 300A at voltages of 10V to 30V. The arc generated between the welding rod and the metal parts to be joined produces a very high temperature causing a pool of molten metal to fuse the two pieces together. The welding rod may be used to contribute to the molten pool, depending on the technique being used.

Metal Inert Gas (MIG) Welding

The most common arc welding process in which the electrode consists of a wire of the same or a similar material to the workpiece. The arc melts a small pool of the workpiece metal and also the tip of the electrode. Automatic wire feed is used to compensate for the fusion of the wire into the weld pool, thus maintaining a constant arc gap. MIG welding is normally used for welding steel.

Tungsten Inert Gas (TIG) Welding

A tungsten element is used to establish the arc. Tungsten has a very high melting point, so the electrode does not melt and contribute to the weld pool. If filler metal is to be added to the weld it must be done separately from the welding electrode. TIG welding is used for welding aluminum, copper and stainless steel.

In both these techniques the molten pool must be protected from atmospheric gases to prevent oxidisation of the joint. To achieve this the arc zone is flooded with an inert gas mixture, typically 85% argon 15% carbon dioxide. Considerable heat is generated by the welding process and the torch must be cooled using a supply of water or air.

Welding is a skilled job, with long training periods and poor working conditions. The welding process causes noise and fumes, with danger from splashes of molten metal. The eye hazard is considerable, and the operator must wear heavily tinted eye protection which means he is effectively blind until the arc is struck.

1.4 Robot Welding

The welding processes that have been successfully automated through the use of industrial robots are identified by Mangold **[15]** (Table 5) and described by Smith **[16]**.

Metal Inert Gas (MIG)
Tungsten Inert Gas (TIG)
Spot
Laser
Submerged Arc
E-Beam

Table 5 Types of robot welding process (source: Mangold **[15]**)

At the end of 1990 a total of 679 robots were employed for arc welding, although this represents 11% of the total robot population, it is evident that only a fraction of the potential market has chosen to invest in robot technology.

Arc welding represents an obvious application for industrial robot systems, however a number of problems can be identified **[5]** (pp79-94):

1) The robot must have sufficient accuracy and repeatability.
2) A robot is not as manoeuvrable as a human operator, causing problems with inaccessible welds.
3) The robot must be able to locate the start of the weld seam.
4) The robot must be able to track the seam so that the weld can be correctly positioned.
5) Robots are expensive.

Addressing these problems; the latest generation of industrial robots are highly dexterous, with improved drive mechanisms and a repetition accuracy better than ±0.2mm. By careful design of both the work-cell and the workpiece the number of welds that cannot be performed by robots can be reduced. Techniques here include mounting the workpiece on a rotary table and designing components specifically for automated manufacture.

Simple welds may be performed by indexing the workpiece and relying on the accuracy of the robot to follow the contour of the weld seam. For longer, more complex welds, the robot must be equipped with sensors to locate and follow the seam. Without effective sensors, arc welding robots are restricted to short welds. Indeed, past experience has shown that robots are most effective when large numbers of short welds are to be performed **[5]** (pp79-94).

The robot may traverse the welding gun faster, and with higher welding currents than a human operator. The resulting welds are more consistent and of a higher quality. The improved quality may mean fewer welds are required on a component to obtain the required strength, leading to yet higher productivity.

Appleton and Williams **[17]** describe some typical robot welding systems, while the latest generation of industrial welding robots are described by Rooks **[18]**.

1.5 Aims of the Research Programme

The initial aim of this research was to design and develop a low cost sensor system for use in seam tracking applications. Many industrial robot are used for arc welding, yet relatively few commercial seam tracking systems exist. Existing sensors are expensive and none has gained wide-spread acceptance. Seam tracking is also used for glue or sealant application and Automatic Guided Vehicle (AGV) navigation.

Machine vision principles have been employed in the sensor design and automated inspection represents an important secondary application. Automated visual inspection techniques may be used to form a simple pass/fail decision based on the general appearance of an item or to obtain specific quantitative measures of characteristics such as surface finish or component dimensions.

The main requirements of the sensor system can be identified:

1) The sensor should be rugged; visual inspection may take place in an environment with extreme temperature ranges and considerable airborne contamination, while the arc welding process generates considerable heat, visible and invisible radiation, smoke and red hot "spatter".
2) The sensor should be compact so that it may be operated in a confined space; for example, when tracking a fillet joint.
3) It is widely recognised that the most effective location for sensors is on the robot manipulator itself, at or near the end-effector **[19]**. The sensor should have low weight so that it may be mounted directly on a robot arm.
4) The sensor interface should have a low data bandwidth to facilitate connection to a wide range of robot control systems. Data rates between the sensor controller and robot control system may be reduced by using the sensor controller to preprocess the sensed data.

5) The sensor system should be versatile and easily tailored to a particular application. Many sensor systems are custom-built for a particular task and a considerable amount of time may be required for installation and commissioning.

1.6 Concluding Remarks

The use of industrial robots has not become as widespread as was originally envisaged by both industry and academe. One major restriction of existing robot systems is the limited range of tasks that can be performed effectively. This problem will be reduced by the efficient use of sensed data to adapt and control the actions of the robot.

Some benefits of sensory feedback are clear in the application of robots to arc welding. Without sensory feedback, the robot must simply move the welding torch along a predefined path, while the workpiece is held in a fixed position. Feedback of torch and seam position will allow accurate positioning of the weld without expensive fixturing, it will also provide compensation for deformation of the workpiece caused by the heat of the welding process.

The aim of this reseach programme was to develop a sensor system for use in arc welding and general vision applications. The few commercial seam tracking systems which exist are very expensive, and often designed for use with a single type of robot controller.

Chapter 2
Sensors for Arc Welding

At present most robot welding systems are used for Metal Inert Gas (MIG) welding but Tungsten Inert Gas (TIG) welding is becoming increasingly popular.

Welding is a complex multivariable control problem and a manual welder requires skill and judgement to control the welding process. The position of the weld pool will be continuously adjusted to ensure the weld is correctly positioned, while compensation for weld gap variation is achieved by altering the welding speed and the amount of filler metal added. If the welding process is to be successfully automated, the robot must be able to emulate a manual welder by performing the following operations:

1) Position the torch at the start of the seam.
2) Initiate the welding operation.
3) Move the torch smoothly along the required welding path, maintaining the appropriate torch orientation and arc gap.
4) Adjust the welding speed or the quantity of filler metal supplied to compensate for variations in the weld gap.

Often, welding parameters such as arc current, voltage and wire feed (if applicable) are controlled automatically by a dedicated controller, while the robot guides the torch along the seam. The first generation of robot welding systems simply moved the torch along a pre-taught path with the joints to be welded presented to the robot in a consistent position and orientation **[20]**. The robots have no sensory feedback and cannot compensate for variations in component dimensions or deformation of the workpiece caused by the heat of the welding process.

Sensors are required to locate the weld seam and then guide the torch along the seam. Extensive research carried out by industry and academic institutions around the world have

yielded many different ideas, but relatively few commercial sensor systems exist [21][22].

The sensors used for arc welding may be divided into three categories; tactile, arc parameter and non-tactile.

2.1 Tactile Sensors

Tactile sensors used to locate the start of the seam include electro-mechanical probes and wire touch sensors such as the *Tomkat "Seamfind"* system from NEI Thompson [23]. The tip of the welding torch is used to "feel" for the weld seam, with the pre-programmed search pattern dependant on the type of joint to be welded.
The simplest seam tracking devices use rollers that run along the weld seam, although these are unsuitable if tack welds have been used or the seam deviates substantially from a straight line. An alternative approach uses a probe oscillated from side to side just ahead of the torch [4] (pp400-401). This technique is only suitable if the weld geometry allows the probe to make contact with the sides of the seam.

Tactile sensors are inexpensive but inflexible and prone to wear and damage. They do not permit control of the welding process.

2.2 Arc Parameter Sensors

Sometimes known as "through the arc" sensing, the arc current or voltage is monitored as the welding torch is moved from side to side across the seam [24]. Through the arc sensing requires no additional hardware, but it is only suitable if the weld geometry permits the weaving action of the torch. Arc sensing systems are described by Cook *et al* [25] and Munezane *et al* [26].

2.3 Non-Tactile Sensors

Non-tactile sensors are divided into two categories. In a *one-pass* system, the seam is tracked during the welding process, while in a *two-pass* system, the position of the seam is determined with the arc off and the joint is then welded in a

separate operation. Two-pass sensors, although less complex, are slower and cannot compensate for deformation of the workpiece during the welding process.

Most non-tactile sensors have some form of machine vision. Alternative devices using capacitive, ultrasonic or eddy-current techniques have been the subject of some research, but few practical systems exist.

2.3.1 Laser Ranging Systems

Smati *et al* describe the operation of range finders using optical triangulation, time-of-flight, and shadow-cast measurement techniques **[27]**.

Laser ranging sensors can be used to locate the start of a weld seam. One commercial example is the ASEA Seamfinder which is a distance sensor based on the principle of optical triangulation **[28]**. A modulated infrared laser is directed at the workpiece and reflected light is focused onto a sensor array. The sensor output is filtered and the position of the beam on the array indicates the distance between the sensor and workpiece. In use, the sensor is moved across the surface and the weld seam is indicated by a change in the measured height. The position of the seam is determined by combining searches in three directions. Seamfinder has an accuracy of ±0.4mm and will detect fillet, butt and lap joints. The sensor output can be used to select the correct welding parameters **[29]**. Longer welds can be accomplished by searching for points along the seam and then interpolating between these reference positions.

Seamfinder operates with a large stand-off height, hence minimising problems with spatter. Additional environmental protection is provided by a forced air flow and replaceable glass windows.

2.3.2 Laser Scanning Systems

Vision systems employing scanning lasers are cheap and simple. They are widely used in seam tracking applications. Commercial sensors include the Oldelft Seampilot and the ASEA Lasertrak.

Seampilot is used to measure the surface profile of a workpiece in a plane perpendicular to the direction of robot motion. The sensor uses a helium-neon laser which is focused and mechanically scanned across the workpiece at a rate of 10 scans/s. The helium-neon laser is used because it has a wavelength of 632nm which corresponds to a window in the broad spectrum of radiation produced by the arc. A viewing mirror directs light reflected from the workpiece onto a linear CCD array camera. The image data are then interpreted by a computer to yield the profile of the seam. The sensor is mounted 20mm in front of the welding torch (*"look-ahead"*) and the combination of sensor and torch is called a "tandem". The Seampilot measures stand-off height and lateral position relative to a reference point in the plane of sensor measurement. The sensor data are then transformed into robot based coordinates to correct the torch position. The Seampilot sensor is described by Verbeek *et al* **[30]** and Oomen and Verbeek **[31]** who identify a number of methods for seam tracking with a look-ahead sensor:

1) Direct feedback - the seam position data is fed directly to the robot controller. This technique is only satisfactory when the tandem vector is reasonably parallel to the seam.
2) Proportional Speed - the speed of the robot motion in a direction perpendicular to the programmed trajectory is made proportional to the offsets measured by the sensor. Again, this technique is only satisfactory when the tandem vector is reasonably parallel to the seam.
3) Tractrix - the seam offset data is used to shift the robot trajectory and rotate the tandem vector so as to minimise the offsets. This technique requires a method of rotating the tandem vector.

4) Delayed shift - the sensor is located in front of the welding torch and this results in a time delay between the sensor passing over a particular point on the workpiece and the welding torch passing over the same point. To compensate for this delay, data from the sensor is stored, and then used to correct the robot trajectory after an appropriate time delay.

The Seampilot system can control the welding process automatically by identifying the joint type and checking that it is suitable for welding. The system then selects a weave pattern or straight weld, corrects the orientation and position of the torch and measures the root gap to adjust fill levels. In addition, the sensor can detect and compensate for tack welds [32].

The use of Seampilot for the production of military vehicles is described by Bangs [33]. Sensor temperature is regulated by a closed-loop water cooling system and the camera lens is protected by a gas shroud.

ASEA Lasertrak [34] is an intelligent one-pass seam tracking system based on the ASEA Seamfinder. It is argued by Edling [35] that sensors using separate computer systems are often difficult to program and suffer from interfacing problems. Lasertrak is totally integrated into the robot control system with the sensor mounted 20mm ahead of the torch and orientated by a "turning unit". A semiconductor laser is scanned across the workpiece by means of mirrors, with light reflected from the workpiece and detected by a sensor array. The output from the light sensitive detector is used to determine the position of the weld seam and adapt the welding parameters according to the programmed joint type. Programming is performed using menus, where search or track arguments are added to the normal robot positioning instructions.

Lasertrak will operate with lap, fillet and butt joints with a typical accuracy of ±0.4mm, a tracking speed of 0-20 mm/s and a searching speed of 0-100 mm/s.

Research at MTS Systems Corporation in Minneapolis, USA has yielded a vision based sensor using a helium-neon laser scanned across the workpiece at 200Hz by means of an acousto-optic cell **[36]**. Reflected light is sensed by a photo-detector and the device has an accuracy of ±0.025mm over a 25mm scan range. A separate range sensor, using the principle of optical triangulation, is used to measure the distance between sensor system and workpiece.

2.3.3 Two-Dimensional Vision with Image Processing

Sensors using conventional CCD cameras include those proposed by Yen *et al* **[37]** and Wezenbeek **[38]** which use optical interference filters to view the weld pool directly. In both systems the camera is completely separate from the welding torch.

A seam guiding system using uniform illumination of the workpiece is proposed by Drews *et al* **[39]**. The sensor is mounted ahead of the welding torch, with reflected light detected by a linear photo-sensitive array. The authors also describe a sensor using two laser diodes to illuminate the workpiece. Reflected light is detected by a linear array of photodiodes such that each photodiode is associated with a particular point on the workpiece. The edges of the seam are identified by differentiating the image data, the sensor can be used for seam tracking and control of the welding process as described by Drews and Kuhne **[40]**.

Brzakovic and Khani **[41]** describe a vision system that determines the boundary of a weld pool from images acquired by a coaxial viewing system (the camera is aligned with the welding electrode). Image processing, using Hough and Fourier transforms, is performed using a VAX 11/785 computer at a rate of 1 frame/s.

2.3.4 Two-Dimensional Vision with Structured Lighting

Torch stand-off height is determined by projecting a suitable light pattern onto the workpiece and observing the image produced **[42]** (pp94-95). The camera can either be combined

with the welding torch in a single package or mounted separately.

Vision systems using a camera combined with the welding torch

The Metatorch optical seam tracking system has found extensive use in industrial applications. The device was originally developed at Oxford University and comprises sensor and MIG welding torch packaged in a cylinder 57mm in diameter. The sensor uses the principle of active triangulation, with infrared laser diodes (wavelength 830nm) used to project a structured light pattern on the workpiece in front of the weld pool. A solid state CCD camera is used to view the light pattern and the image is processed to provide real-time control of the torch position. The Metatorch system is described by Clocksin *et al* **[43]** and the device has been used in many practical applications **[44][45]**.

A water cooling system is used to regulate the sensor temperature. The CCD camera is protected from molten spatter by a replaceable window and a forced air flow is used to prevent smoke obscuring the field of view. Arc glare is eliminated by an optical interference filter with a pass-band of 10nm centred at 830nm.

Seam tracking for lap, fillet and butt joints is achieved by analysing the stripe produced on the workpiece. An initial sensor pass (*"Vision Teach"*) is used to generate a model of the workpiece from samples taken approximately every 2mm along the seam. During a welding operation the camera image is compared with the seam model using a template matching process and the difference is used to correct the lateral position and stand-off height. A rule based system for interpreting the weld seam images produced by Metatorch is described by Huang Nan *et al* **[46]**.

Control of the welding process is achieved by measuring the weld gap and adjusting the wire feed rate and welding speed as appropriate. The prototype Metatorch was developed in 1980 and is capable of welding thin sheet steel with an accuracy of

±0.5mm using ASEA and KUKA robots. Variants on the original sensor include a compact sensor which is mounted on a separate welding torch and a high accuracy version intended for TIG welding **[47][48]**.

A number of the difficulties associated with one-pass control of arc-welding have been successfully overcome. It is noted by Clocksin *et al* **[43]** that adequate seam tracking can be achieved with a software loop time of 250ms. Degradation of the glass window which protects the camera can be prevented by careful design of the spatter guards and by providing a flow of clean air over the sensor **[48]**.

Richardson *et al* **[49]** suggest seam tracking systems for MIG and TIG welding using a CID camera integrated with the torch. A narrow band optical filter is used to allow observation of a laser line projected onto the arc pool. The system can be used to track the seam and control the welding process for butt and fillet joints.

Vision systems using a separate camera

Smith and Lucas **[50]** extend the work originally presented by Clark *et al* **[51]** and use a band of light from a semiconductor laser projected onto the workpiece approximately 10mm ahead of the arc. A CCD camera with coherent fibre-optic bundle is used to view the workpiece, with image processing performed by an Intel 8086 microprocessor. The vision processing software is implemented using PL/M in conjunction with the RMX-86 real-time operating system and will produce an 8-bit error value, in 2's complement form, along with an 8-bit value indicating the seam width. The sensor computer is connected to the robot controller via a conventional RS232 serial link and the maximum update rate is 10 s^{-1} which corresponds to a position update every 0.1mm at a typical TIG welding speed of 1 mm/s.

The sensor is suitable for tracking butt joints and has been interfaced to a PUMA robot with a VAL-II controller. The use of the coherent fibre-optic bundle allows the camera to be

separate from the weld head and hence reduces the weight which must be carried by the robot thus minimising problems due to heat and electro-magnetic interference. Cooling of the sensor is provided by a forced air flow.

The combination of CCD camera with fibre-optic bundle is also employed by Koskinen *et al* **[52]**. A line is projected onto the workpiece using a helium-neon laser and the camera image is processed by a microcomputer with Intel 80286 micro-processor. A PUMA robot is controlled with an accuracy of ±0.5mm in the horizontal plane and ±1mm in the vertical plane. The image processing software is implemented using PL/M and Pascal, with the RMX-86 operating system, giving a typical processing speed of 8 frames/s.

Brown *et al* **[53]** make use of a 256 pixel line scan CCD camera focused 15mm ahead of the weld pool. Image processing is performed by two 8-bit microprocessors and seam tracking speeds of between 5 and 25 mm/s have been achieved with a resolution better than 0.6mm and an update frequency of 40Hz.

A two-pass seam tracking system is described by Wang **[54]**. Coherent illumination is provided by a white light source which projects a line on the workpiece perpendicular to the seam. A solid-state camera is used as the image sensor, with image processing performed by an Intel 8088 microprocessor programmed in assembly language. The operator must enter the joint type, welding sequence, exposure time, root gap and plate thickness before welding can commence. The sensor has an accuracy of ±0.4mm and will tolerate a maximum deviation of 7mm from the pre-programmed seam path.

2.4 Concluding Remarks

It is clear that manual welders rely on visual feedback to position the torch, move the torch along the seam and adjust the filler metal deposition rate. Consequently, arc parameter and tactile sensors have limited capability when compared with vision based systems.

The majority of vision based seam tracking systems make use of structured lighting in conjunction with an area array camera. A spectral filter may be used to isolate the structured light pattern from the radiation produced by the arc. Laser scanning systems also find widespread use. The laser is focused and scanned across the workpiece, with reflected light directed onto a linear photosensitive array.

Seam tracking systems using a camera integrated with the welding torch are often preferred because the welding torch cannot temporarily obscure the camera field of view. The disadvantages of this arrangement are that customers are restricted to a particular type of welding torch and the sensor is situated in a particularly vulnerable position.

Practical arc welding sensors must be designed to operate reliably in the hostile environment produced by the welding process. The sensor must be cooled and protected from smoke and airborne debris, while a compact sensor package is required to reduce the number of inaccessible weld seams. Commercial vision-based seam tracking systems are expensive and it is clear that more cost-effective and reliable devices are required.

Chapter 3
Design of the Laser Scanner

The aim of this research was to produce a low cost sensor system for seam tracking or general vision applications. One-pass seam tracking presents a major technical challenge, with the main difficulties identified by Thomas **[55]**.

1) The sensor must cope with a range of surface types, ranging from shiny new steel to matt black oxide.
2) The joint may be no larger than scratches on the surface of the workpiece.
3) The arc is brighter than the sun, containing a broad spectrum of visible and invisible radiation.
4) Considerable heat is produced near the arc zone, with additional problems caused by smoke and red hot "spatter".

It was argued in Chapter 2 that some form of machine vision is essential for effective weld seam tracking. Conventional vision systems using CCD or CID cameras are expensive, and must often be tailored to one particular application; for example, bin picking, assembly or inspection **[56]**.

The simplest type of camera is the "flying spot" scanner **[57][58]**. Light from a high intensity source is focused and scanned across the surface to be imaged, while reflected light is sensed by a collection system incorporating a photo-detector. In practise, the light source is nearly always a laser because a high intensity focused beam is required. To produce a two dimensional image the linescan camera must be mechanically scanned in the second plane however this motion is inherent in applications such as seam tracking and vehicle guidance.

The advantages and disadvantages of the laser scanner over other imaging systems may be summarised:

Advantages

1. Small scanning elements permit high scan rates and hence good resolution.
2 The use of coherent light to illuminate the workpiece will mean that any background illumination, for example the arc light, can be rejected using suitable filters.
3. A single scanning element (projector) may be used with several light detectors so that an object or surface may be analysed from several different angles.

Disadvantages

1. Lasers present a considerable eye hazard.
2. The single wavelength of most lasers means that it can be difficult to detect certain colour features of the workpiece.
3. Problems may arise when inspecting objects such as glass due to interference between light reflected from the upper and lower surfaces. Slabodsky **[59]** reviews the techniques used for inspecting glass and notes that the performance of a laser flying spot scanner can be improved by using a number of separate projectors and light detectors at different angles or by using reflective tape under the glass sheet with two separate light detectors.

The flying spot scanner consists of three main components; the light source, scanning element and light detector.

3.1 Light Source

As stated previously, the light source used in flying spot cameras is nearly always a laser because a high intensity light spot is required. A 0.6mW helium-neon gas laser with a wavelength of 633nm (red) has been selected for this project. This is a compact, durable, low cost device, classified as a Class 1 laser by the *British Standard Specification for Radiation Safety of Laser Products*, BS7192 **[60]**. Class 1 lasers are inherently safe, that is the maximum permissible exposure level cannot be exceeded under any condition and the device may be used in unsupervised areas. It is noted by

Verbeek *et al* **[30]** that a wavelength of 633nm corresponds to a window in the spectrum produced by the arc. A spectral filter may be used to isolate the laser light from the background radiation.

3.2 Scanning Element

A laser will produce a narrow beam of light and hence a relatively small scanning element is required. There are several techniques employed to scan the laser beam; these include rotating pyramid or polygon mirrors, oscillating mirrors and acousto-optic deflectors. The simplest method, preferred in almost all surface inspection systems, is the rotating polygon mirror driven at high speed by a synchronous electric motor.

The scanning mechanism adopted is a polygon mirror mounted directly on the shaft of a dc stepper motor. Accurate control of the scan rate is achieved by varying the stepping rate of the motor, while the large inertia of the mirror will tend to reduce the discrete stepping action of the motor.

3.3 Light Detector

Conventional linescan cameras commonly use photo-multipliers, photodiodes or linear photosensitive arrays **[58]**. The scanning system will be used with surfaces ranging from an almost perfect mirror to matt black and these will reflect vastly different amounts of light. To prevent saturation or overload of the light detector in changing operating conditions it must be possible to vary either the sensitivity of the detector or the laser power output. The laser selected has a constant output and therefore to simplify the design and minimise the cost of the scanner it was decided to use a light detector with variable sensitivity. This will preclude the use of light detectors that have a fixed sensitivity, for example the linear CCD.

The light detector consists of a Perspex rod, mounted in an aluminium tube, with a photodiode attached at each end. (Figure 1). The detector has an aperture of 100mm x 6mm and

the photodiodes are IPL33 devices from Integrated Photomatrix Ltd.

A schematic of the laser scanner is shown in Figure 2. The laser beam is scanned across the workpiece by the rotating polygon mirror, with reflected light sensed by the light detector. Unlike conventional linescan cameras there is no beam forming or focusing.

The laser light sensed by the detector will be dependant on surface finish and texture. A specular surface (for example high quality aluminium or steel) has a mirror like reflection characteristic. Light is reflected in a narrow beam as shown in Figure 3(a). An uneven (diffuse) surface such as paper will scatter light in all directions, some towards the light detector as shown in Figure 3(b). Most practical surfaces produce a combination of specular and diffuse reflection.

The position of a discontinuity is determined when light is either reflected directly from the discontinuity and collected by the detector or scattered causing a reduction in the measured light level. Position is resolved from the point on the light detector which receives this change in light level.

3.4 Laser Scanner Geometry

The laser and polygon mirror must be arranged in a configuration that will give the required scan length and scan rate.

3.4.1 Scan Length

The light detector has an aperture length of 100mm and hence the laser beam must be scanned across about 120mm on the workpiece.

3.4.2 Scan Rate

The sensor is intended for use in diverse applications including:

1) Seam tracking when mounted on a robot arm.

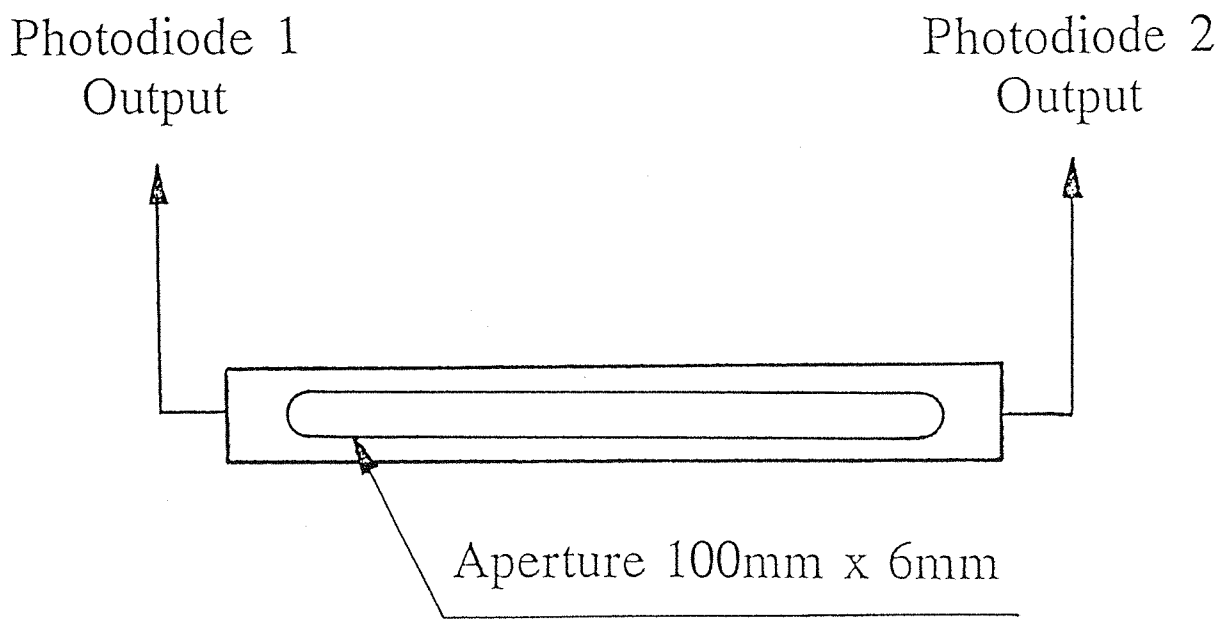

Fig.1 The light detector

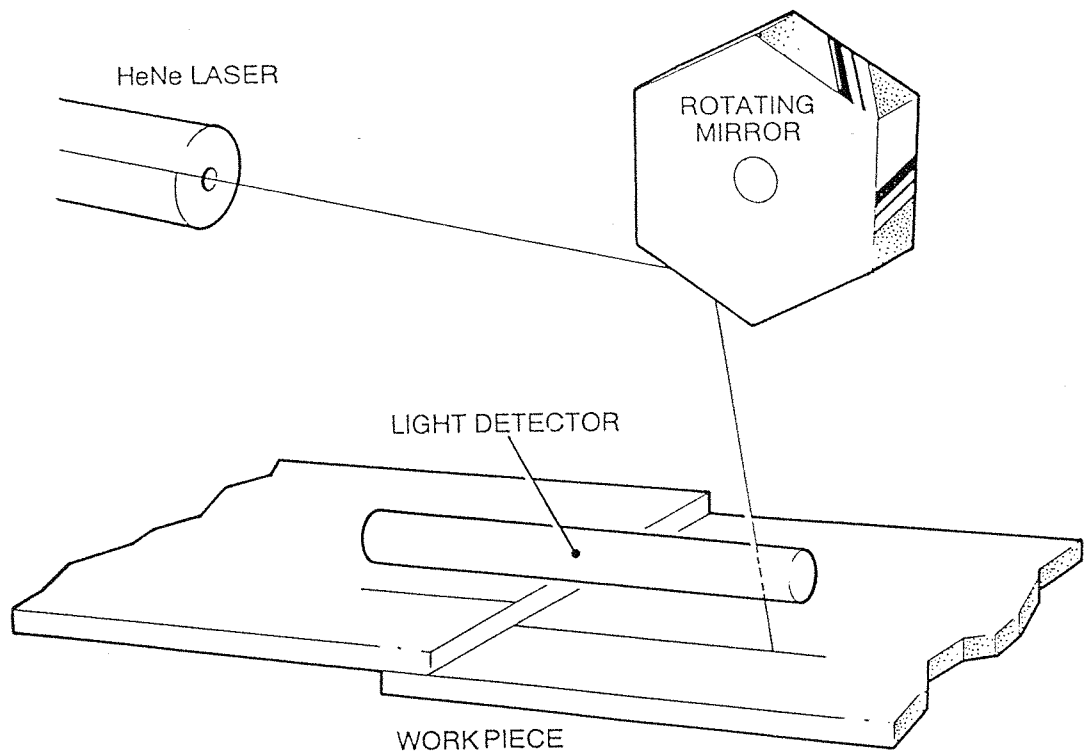

Fig.2 Schematic diagram of the laser scanner

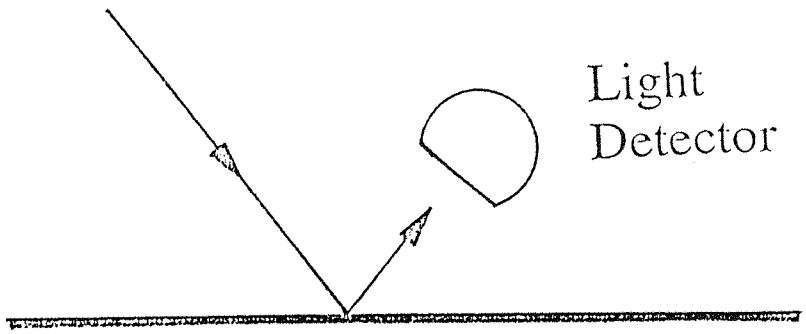

Fig.3(a) Specular surface

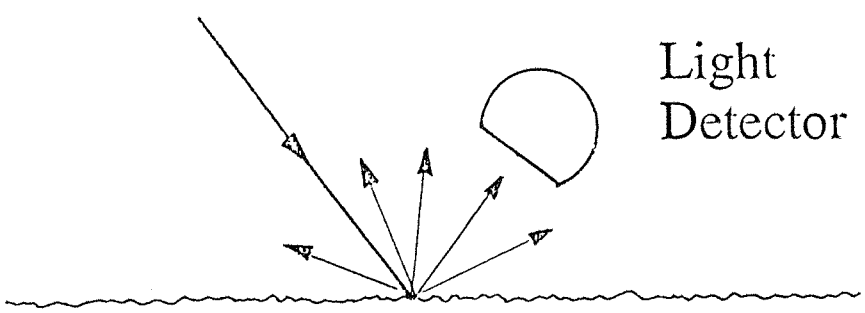

Fig.3(b) Diffuse surface

Fig.3 Reflection from specular and diffuse surfaces

2) AGV guidance - a modified form of seam tracking.
3) Vision.

In general, all these tasks fall into one of two broad categories; real time control or vision, and the scan rate can be estimated for each:

Real time control

For optimum performance the sensor system should provide new lateral position data at the maximum rate supported by the robot controller. A typical industrial robot controller will update the control loops every 5 - 10ms which suggests a minimum scan rate of 100 - 200 s^{-1}.

Welding is carried out at comparatively slow speeds and it may not be necessary to correct the robot trajectory at this maximum rate. In practise, the required update rate will be dictated by factors such as the dynamics of the robot, the complexity of the weld seam and the accuracy required. Also, it may be necessary to operate the sensor at high speed when searching for the start of the seam.

The operating speed required for one-pass seam tracking may be estimated by comparing the performance of some typical seam tracking systems. It can be seen from Table 6 that vision based systems operate with a processing speed in the order of 10 frames/s, while the sensor employing a scanned laser has a scan rate of 10 s^{-1}.

Vision

Figure 4 shows how the laser beam is scanned across the workpiece. For a laser spot diameter of 2mm the time taken to move the scanner must be less than the time for one complete scan as this will ensure total coverage of the workpiece by the laser beam. A graph showing scan rate plotted against tracking velocity is shown in Figure 5.

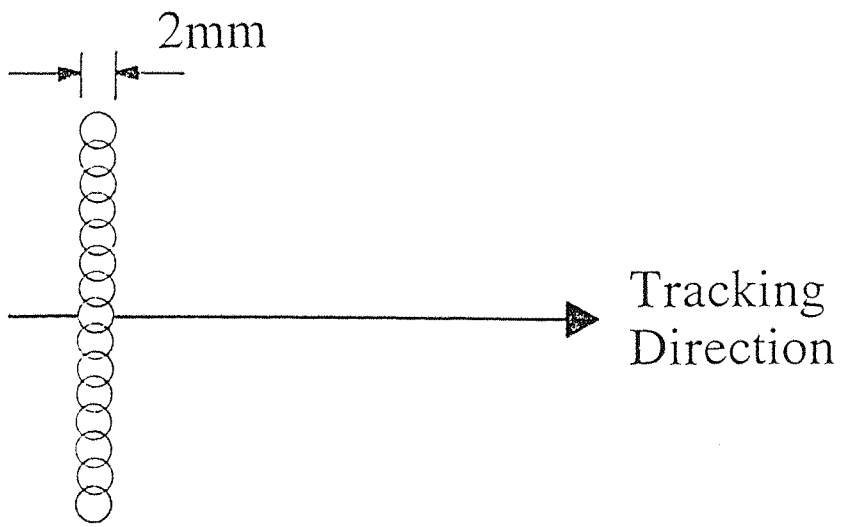

Fig.4 Scanning the laser

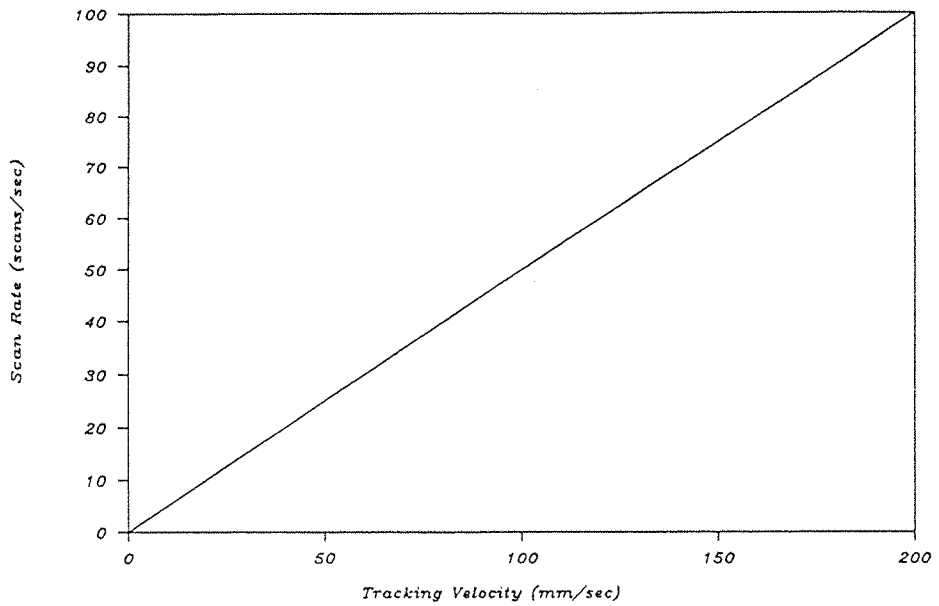

Fig.5 Scan rate plotted against tracking velocity

Seam Tracking System	Operating Principle	Operating Speed
Verbeek *et al* [30]	Mechanically scanned laser with a linear array CCD camera	10 scans/s
Clocksin *et al* [43]	Structured lighting with an area array CCD camera	4 frames/s
Brzakovic and Khani [41]	Area array CCD camera	1 frame/s
Smith and Lucas [50]	Structured lighting with an area array CCD camera and coherent fibre-optic bundle	10 frames/s
Koskinen *et al* [52]		8 frames/s

Table 6 Operating speeds of seam tracking systems

The basic configuration of the laser scanner is shown in Figure 6. The scan rate is determined by the speed of mirror rotation and the number of faces on the mirror. Increasing the number of faces will increase the scan rate but reduce the scan length for a given mirror-workpiece displacement. A mirror must be selected which has a maximum number of faces yet still gives a scan length of 120mm. In addition, the mirror should be small and light in order to reduce the load on the drive motor and hence maximise the scan rate.

A complex relationship exists between the number of sides on the mirror, scan length and stand-off height and an iterative procedure was used to design the scanner.

3.4.3 Reflection from an n-sided Polygon

If the incident ray is parallel to the central axis of the polygon we have from Figure 6

$$\theta_1 = \frac{360^\circ}{n} \qquad 3.1$$

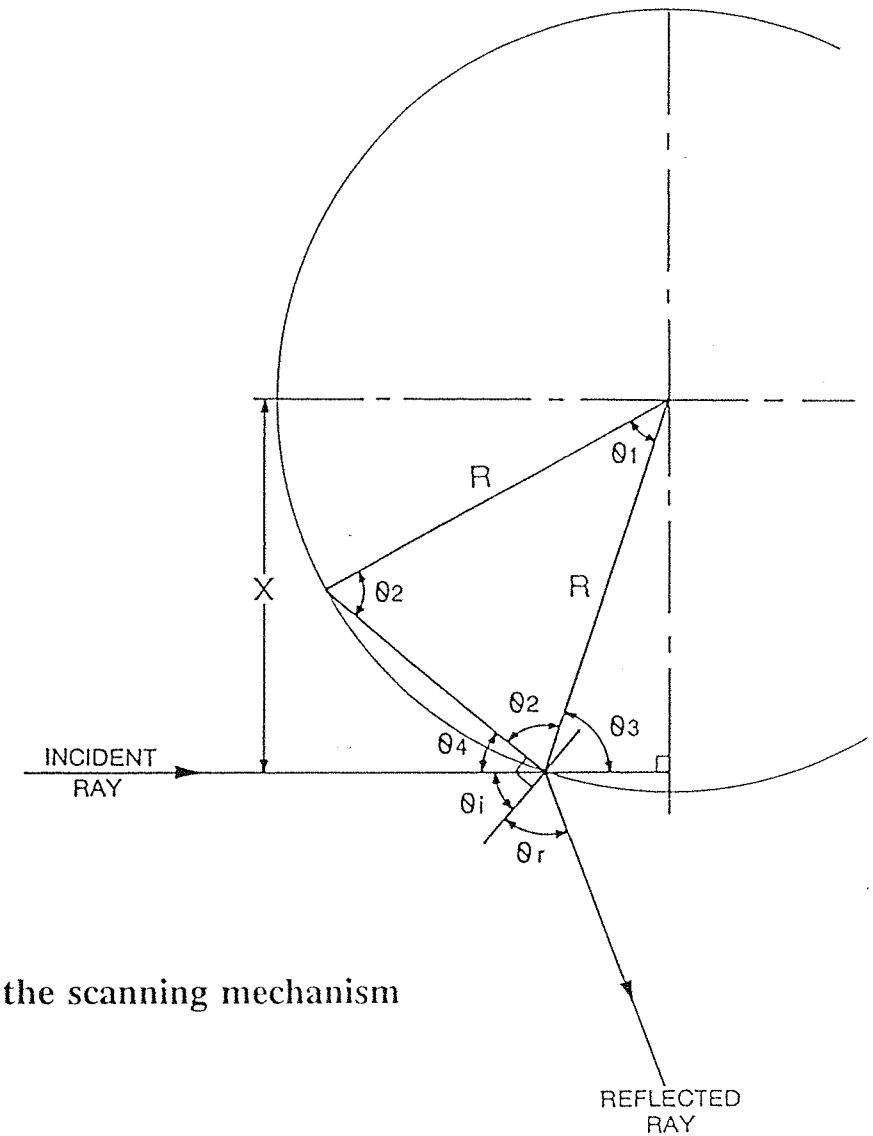

Fig.6 Geometry of the scanning mechanism

$$\theta_2 = \frac{180^\circ - \frac{360^\circ}{n}}{2} \qquad 3.2$$

$$\theta_3 = Sin^{-1}\frac{X}{R} \qquad 3.3$$

Where: The polygon has n sides.
X = Distance of the incident ray from the central axis of the polygon.
R = Radius of the polygon.

$$\theta_4 = 180^\circ - \theta_2 - \theta_3 \qquad 3.4$$

$$\theta_i = 90^\circ - \theta_4 \qquad 3.5$$

Hence

$$\theta_i = Sin^{-1}\frac{X}{R} - \frac{360^\circ}{2n} \qquad 3.6$$

The total angle between incident and reflected ray is θ_{min}

$$\theta_{min} = 2\theta_i \qquad 3.7$$

So

$$\theta_{min} = 2\left(Sin^{-1}\frac{X}{R} - \frac{360^\circ}{2n}\right) \qquad 3.8$$

If the polygon is rotated so that the incident ray strikes the other end of the mirror face θ_i will increase by θ_1 and the total angle between incident and reflected ray will increase to θ_{max}

$$\theta_{max} = 2\left(Sin^{-1}\frac{X}{R} + \frac{360^\circ}{2n}\right) \qquad 3.9$$

It can be seen that the light beam is reflected through a total angle of $2\left(\frac{360^\circ}{n}\right)$

A computer simulation was used to investigate the effect of varying the ratio $\frac{X}{R}$ and the number of faces on the mirror. The results obtained are shown in Table 7 and indicate that a mirror with 8 sides will scan the laser beam through a total angle of 90°.

n	θ_{min}	θ_{max}	$\theta_{max}-\theta_{min}$
5	25.18	169.18	144.00
6	37.18	157.18	120.00
7	45.75	148.61	102.86
8	52.18	142.18	90.00
9	57.18	137.18	80.0
10	61.18	133.18	72.0

Table 7 Reflections from an n-sided polygon for $\frac{X}{R} = 0.75$

3.4.4 Calculation of the Stand-off distance

It is clear that in order to obtain a scan length of 120mm the scanner must be operated at a fixed distance from the workpiece. The distance between the point of reflection on the polygon and the workpiece may be calculated as follows.

Referring to Figure 7 we have:

R = Radius of polygon.

X = Distance of the incident ray from the central axis of the polygon.

H = Distance from the point of reflection on the polygon to the workpiece.

L = Scan length.

For a mirror with 8 sides and $\frac{X}{R} = 0.75$

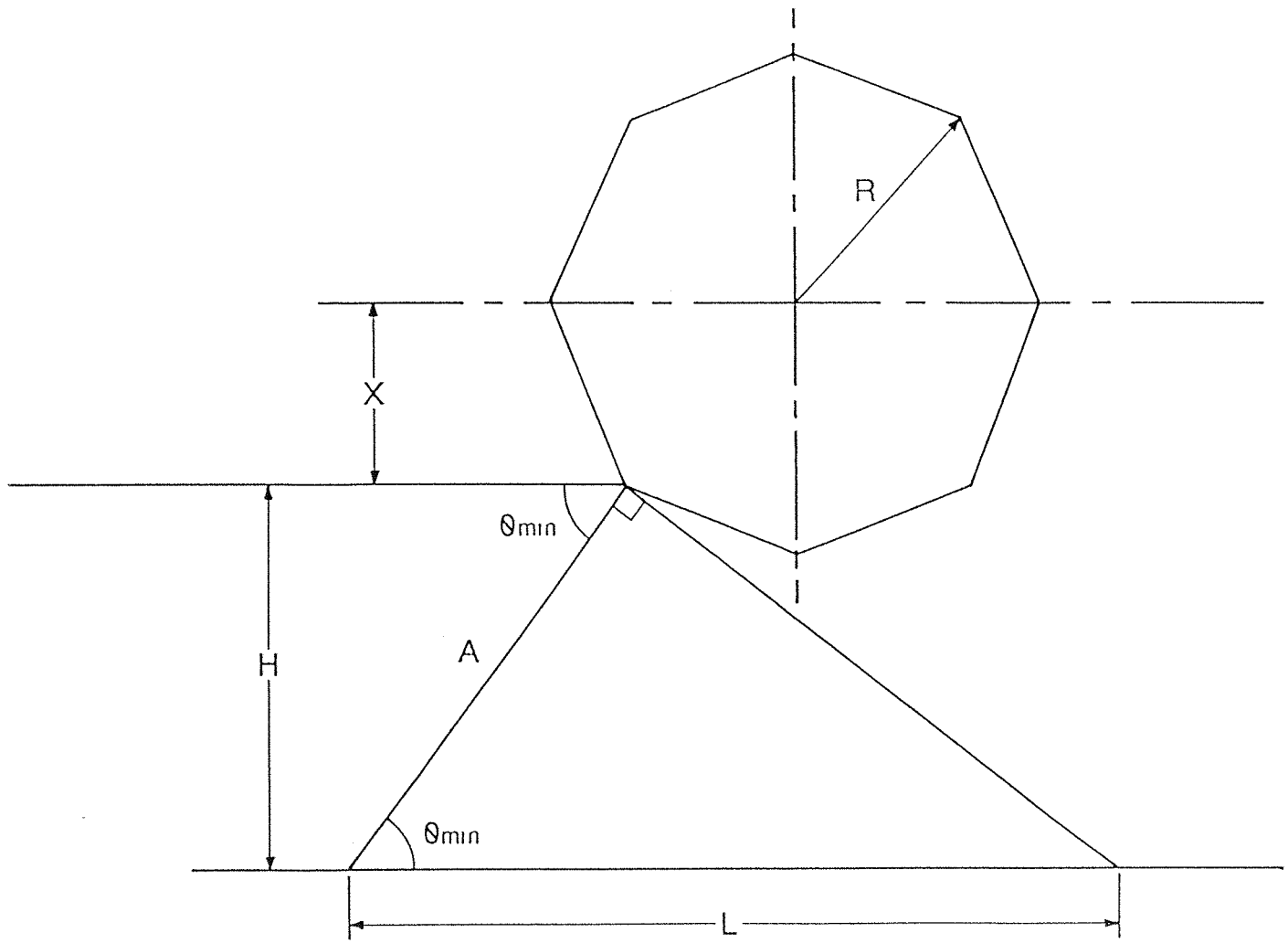

Fig.7 Determination of scan length and stand-off height

$$Cos\ \theta_{min} = \frac{A}{L} \qquad 3.10$$

$$Sin\ \theta_{min} = \frac{H}{A} \qquad 3.11$$

$$H = ASin\ \theta_{min} = LCos\ \theta_{min} Sin\ \theta_{min} \qquad 3.12$$

$$H = \frac{LSin\ 2\theta_{min}}{2} \qquad 3.13$$

θ_{min} = 52.18° and L = 120mm giving H = 58.1mm

Thus a mirror with 8 sides will give a scan length of 120mm with a distance of 58.1mm between the point of reflection on the polygon and the workpiece. If the mirror is manufactured with a radius of 20.0mm (37.0mm across flats) the distance required between the incident ray of the laser and the central axis of the polygon is 15.0mm.

3.5 The Prototype Laser Scanner

An appropriate configuration of laser and mirror has been determined and these components are fixed in a suitable chassis. The mirror is fabricated from extruded aluminium and mounted directly on the shaft of a stepping motor. The prototype laser scanner is shown in Figure 8 and Figure 9.

The mirror places a considerable burden on the motor and this limits the maximum stepping rate which can be achieved. In practise, the motor will stall if the stepping rate exceeds 360 rpm and to ensure reliable operation the rate is limited to 300 rpm.

With a 1.8° step angle and an 8-sided mirror the maximum scan rate of the laser across the workpiece is given by

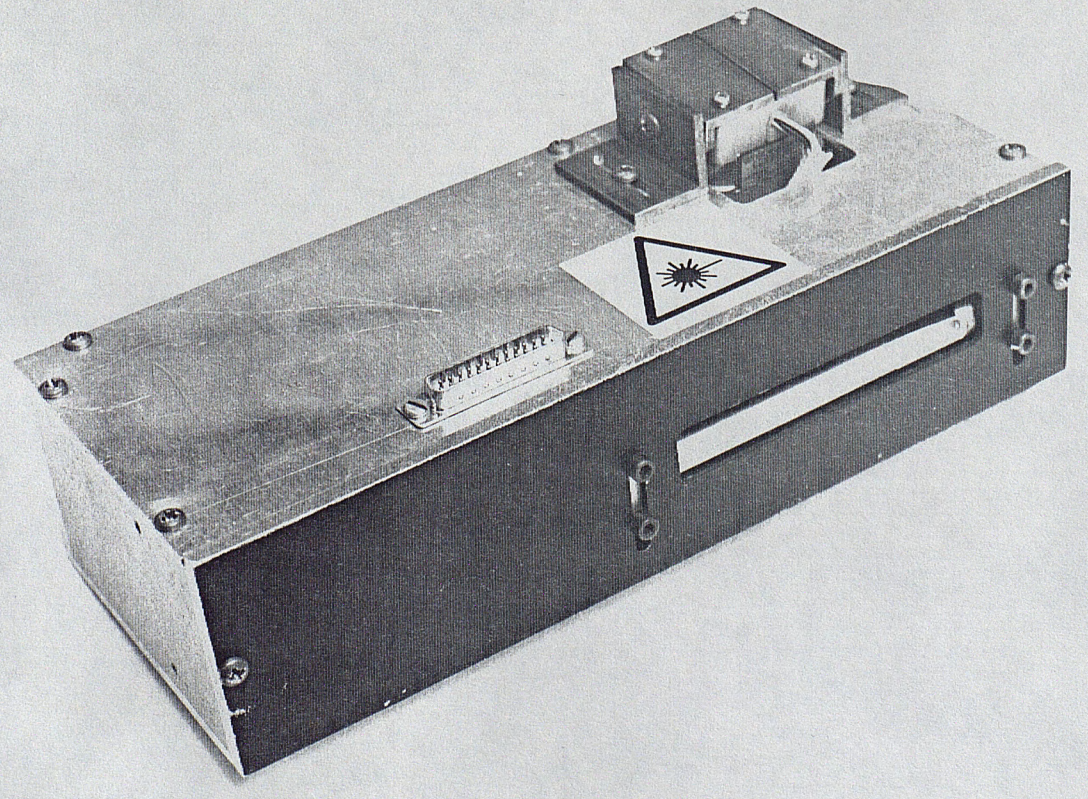

Fig.8 The prototype laser scanner - External

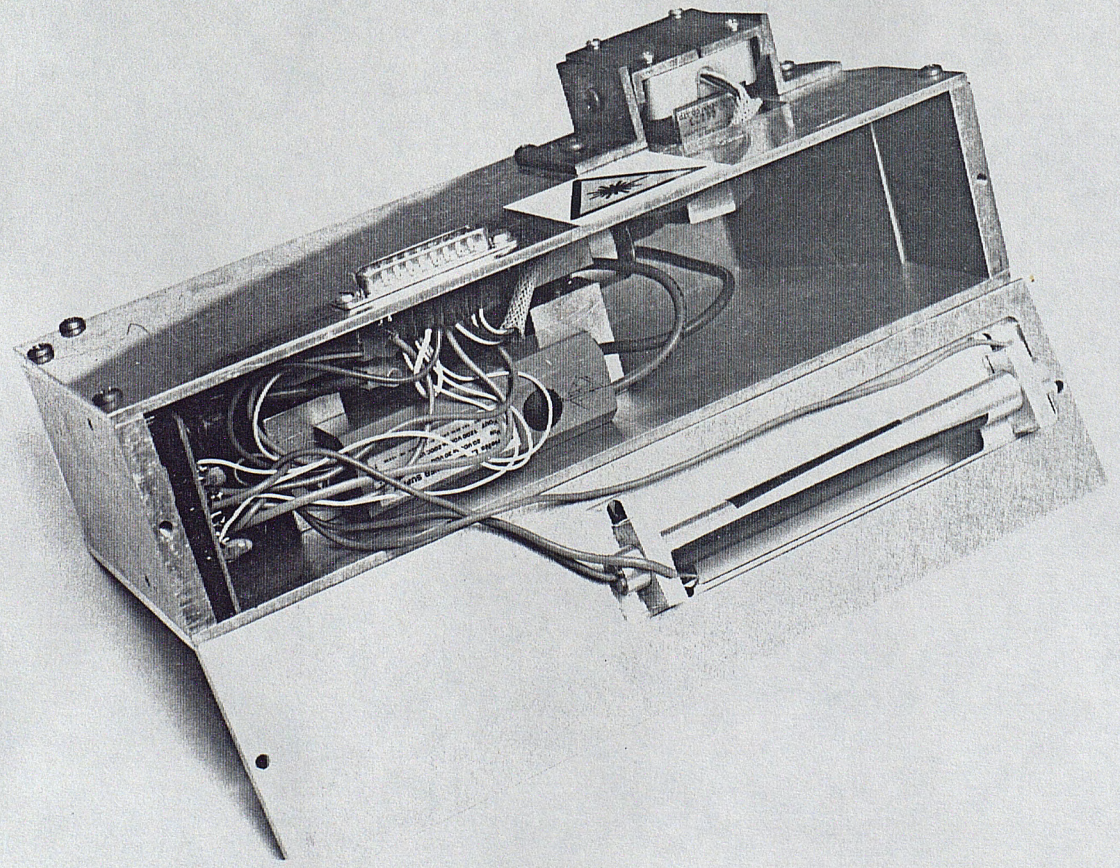

Fig.9 The prototype laser scanner - Internal

$$Scan\ rate = \frac{1000\ x\ 1.8}{360}\ x\ 8 = 40\ scans/s \qquad 3.14$$

From Section 3.4.2 a scan rate of 40 s^{-1} appears adequate for weld seam tracking, although this may prove unsuitable for vision applications when high resolution is needed.

The total weight of the prototype laser scanner is 2.4kg (including the cable which connects the scanner to the sensor controller). This additional weight must be carried by the robot, along with the required tool.

3.6 Concluding Remarks

A low-cost "flying-spot" laser scanner has been devised. The cost of the main components was approximately £200 at 1992 prices. The beam from a 0.6mW helium-neon laser is scanned across the surface to be imaged, with reflected light sensed by a simple detector. A surface defect will change the reflection characteristics of the laser from the workpiece and the position of a discontinuity is resolved from the point on the light detector which detects the change in received light level.

Chapter 4
Signal Processing

4.1 Photo-diode Amplifiers

The light detector has been described in Chapter 3 and consists of two photo-diodes attached to the ends of a translucent Perspex rod. To obtain a usable output the photo-diodes are connected to buffer amplifiers mounted in the scanner head. The scanner is connected via screened cables to a signal conditioning module situated close to the robot controller. This arrangement has the following advantages:

1) Minimises the number of components that must be situated close to the welding torch.
2) Minimises the weight and size of the scanner hardware which must be carried by the robot arm.
3) Amplifies the photo-diode signals to ensure adequate signal to noise ratio.

At the signal conditioning module the photo-diode signals are subtracted using a differential amplifier with high common mode rejection **[61]**. This will cancel changes in the output signals caused by variations in ambient light level and reduce the common mode noise in the individual photo-diode signals.

A schematic of the amplifier arrangement is shown in Figure 10. The circuit was tested by recording the output voltage with the laser light source applied directly to the detector (Figure 11). The results obtained are shown in Figure 12.

Comments

1) The differential amplifier is saturated when the laser is applied close to the photo-diodes at the ends of the light detector. This problem will not occur during normal operation because the laser intensity will be reduced by reflection from the work piece.
2) The output signals from the photo-diodes are not exactly symmetrical. This is due to differences in the

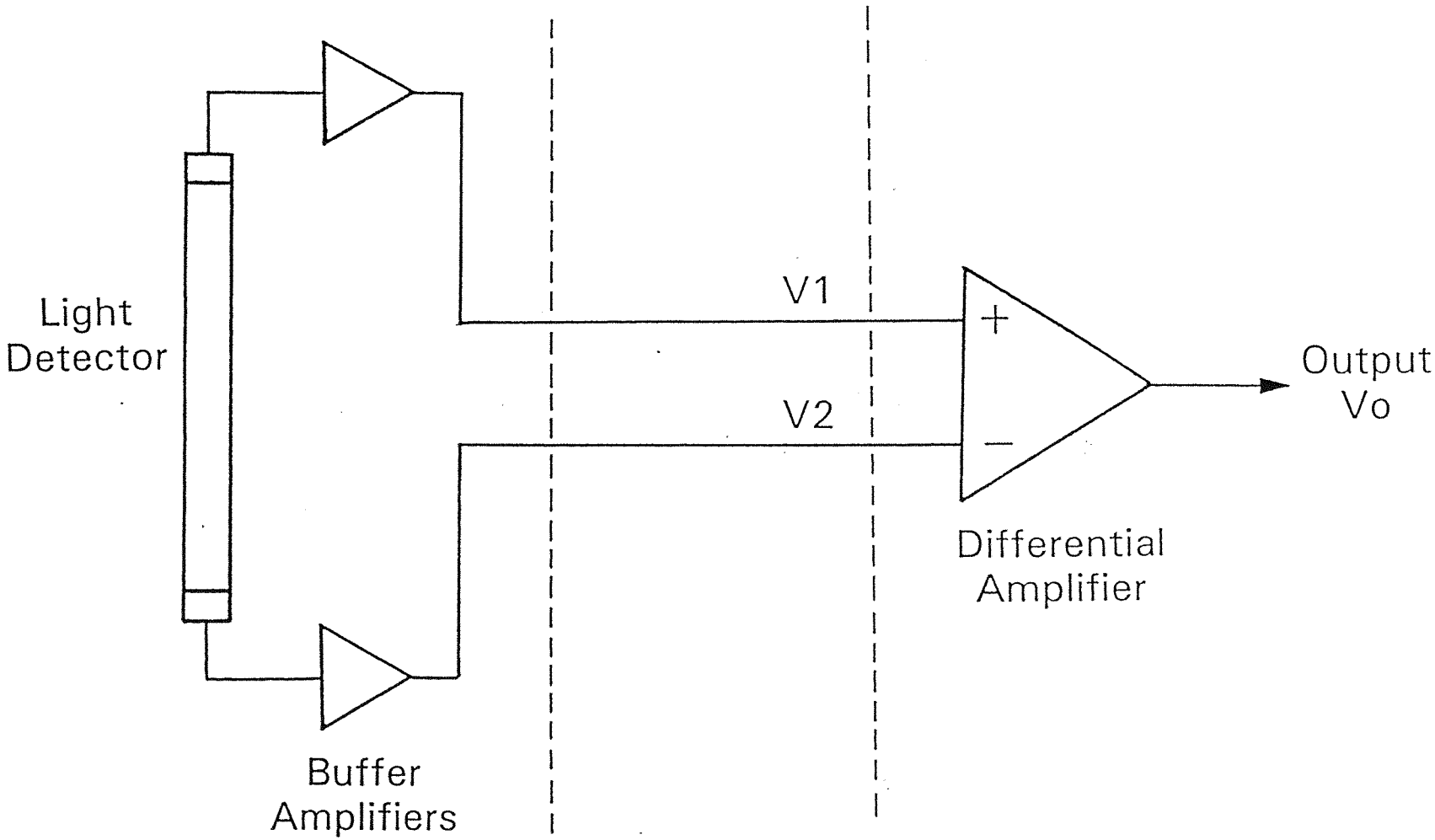

Fig.10 Initial signal processing

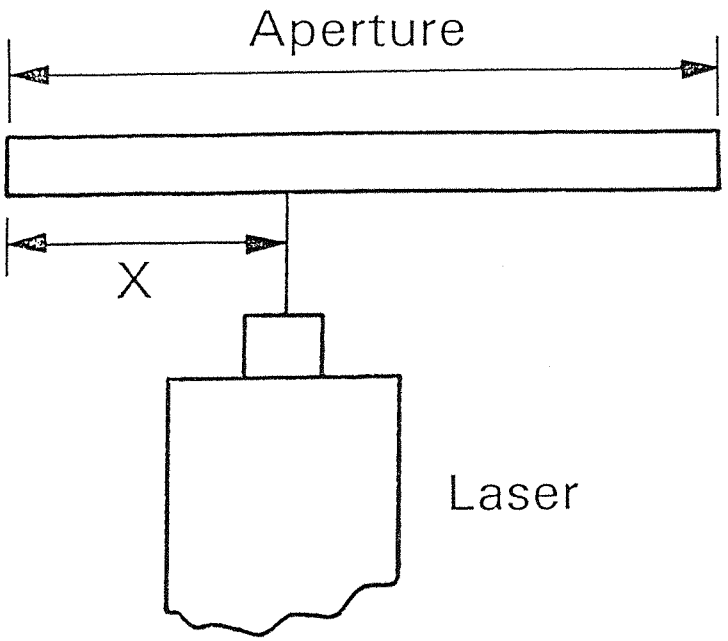

Fig.11 Testing the light detector response

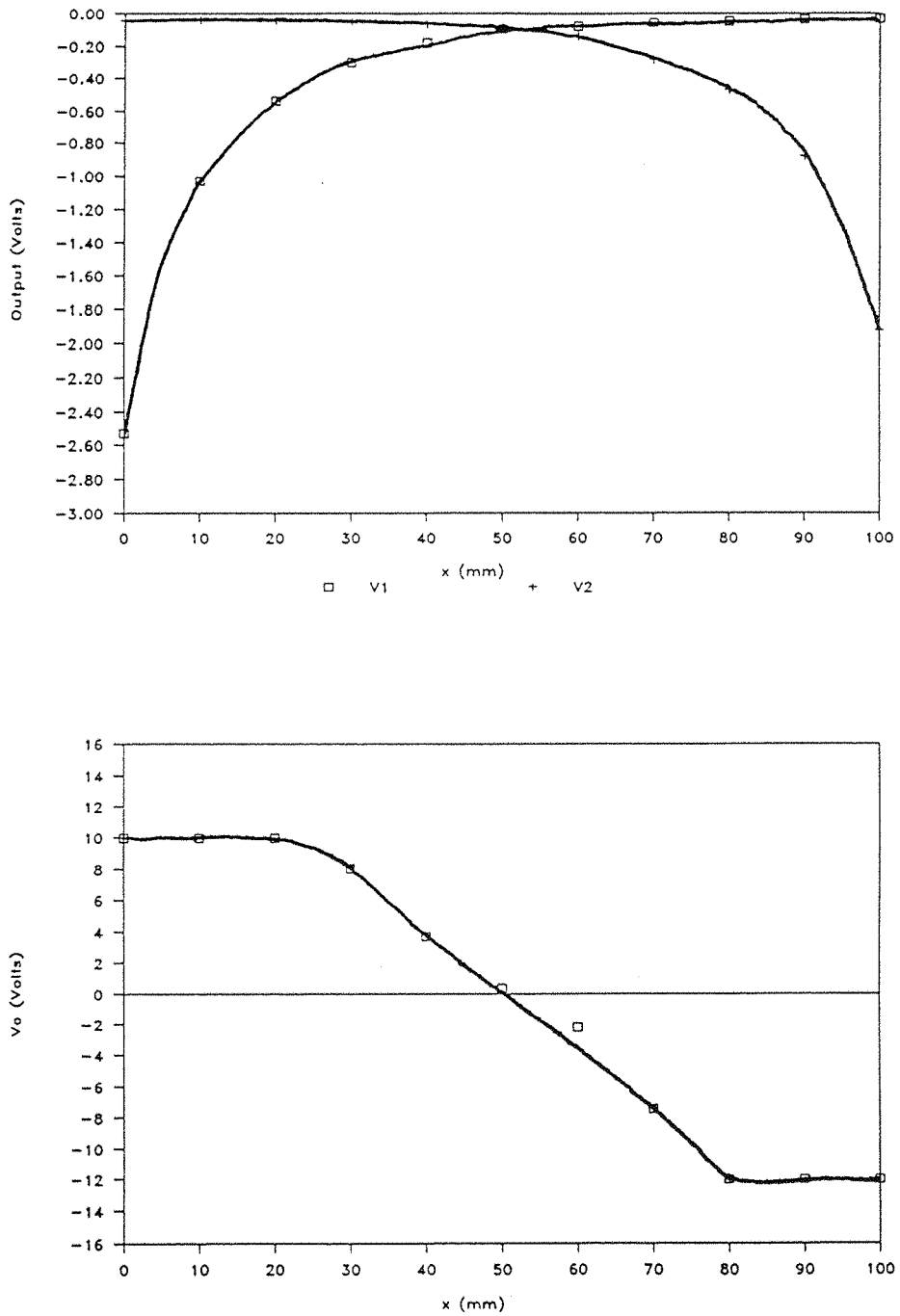

Fig.12 Light detector output plotted against position of the laser beam

characteristics of the photo-diodes, component tolerances and non-uniformities in the light detector construction.

3) The light detector has a "blind spot" (approximately at the centre of the aperture) when the photo-diode signals are equal corresponding to a difference output of zero.

4.2 Bandpass Filter

The scanner output is an ac signal with a fundamental frequency of n Hz (for a scan rate of n s^{-1}) and considerable high frequency noise. The noise is caused by small imperfections on the surface being imaged and interference from the high voltage laser power supply which is situated close to the light detector. A low pass filter will reduce these unwanted components, however, care must be taken to ensure that signals from discontinuities above the detection threshold are not degraded. An additional high pass filter section will eliminate any DC offsets in the preceding amplifier stages.

The bandpass filter has a Butterworth response and is implemented from a second order high pass section cascaded with a second order low pass section [62]. Initially the filter was set with a high frequency break point of 2kHz and a low frequency break point of 10Hz. During tests on a range of surfaces it was observed that high frequency noise is reduced, whereas major surface discontinuities give a well-defined output. Figure 13 shows the effect of the bandpass filter. The detector output signal is produced by a diffuse surface with coarse texture and the high frequency component of the signal is considerably reduced. Band-limiting the light detector output signal will preclude detection of small surface defects. The low pass filter cut-off frequency must be chosen carefully to ensure that significant surface features will be detected. In practice, the contrast between significant and insignificant surface features will be application dependent and the criteria employed for discrimination may be highly subjective.

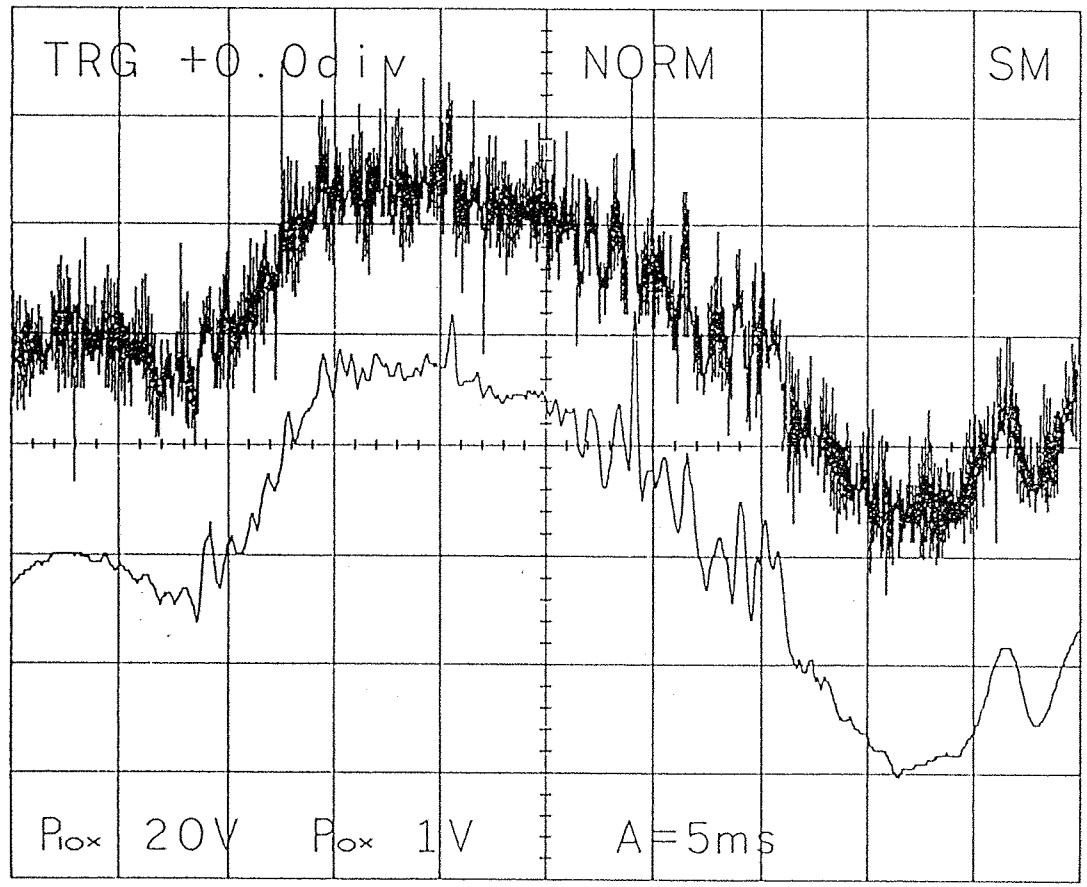

Fig.13 Filtering the light detector output

4.3 Start of Scan Sensor

The position of a discontinuity is measured relative to the leading edge of the light detector aperture. This reference position cannot be resolved directly from the light detector output; if a discontinuity is located near the leading edge of the detector aperture there may not be a clearly defined signal at the start of the scan. To overcome this problem and provide a reliable synchronising signal an additional photo-detector is mounted inside the scanner chassis. The laser is scanned across this detector at the beginning of every scan (Figure 14). The start of scan sensor is connected to a comparator which gives an output signal at TTL logic levels.

There is a short delay between the start of scan pulse and the actual start of scan caused by the overlap of the laser scan at the ends of the light detector aperture. The laser is scanned across the start of scan sensor which gives a TTL pulse, the laser must then be scanned across approximately 10mm on the work piece before reflected light is sensed by the detector. This time delay effectively shifts the light detector output by a fixed amount relative to the start of scan pulse.

4.4 Signal Processing

The signal processing system must perform a number of functions:

1) Seam Tracking

Determine the position of a surface discontinuity relative to the start of scan pulse. The scanner will be used with a wide range of surface types and textures and different seam configurations.

2) Surface Inspection

Provide some qualitative measure of surface finish and identify the position or extent of some surface blemish such as a scratch.

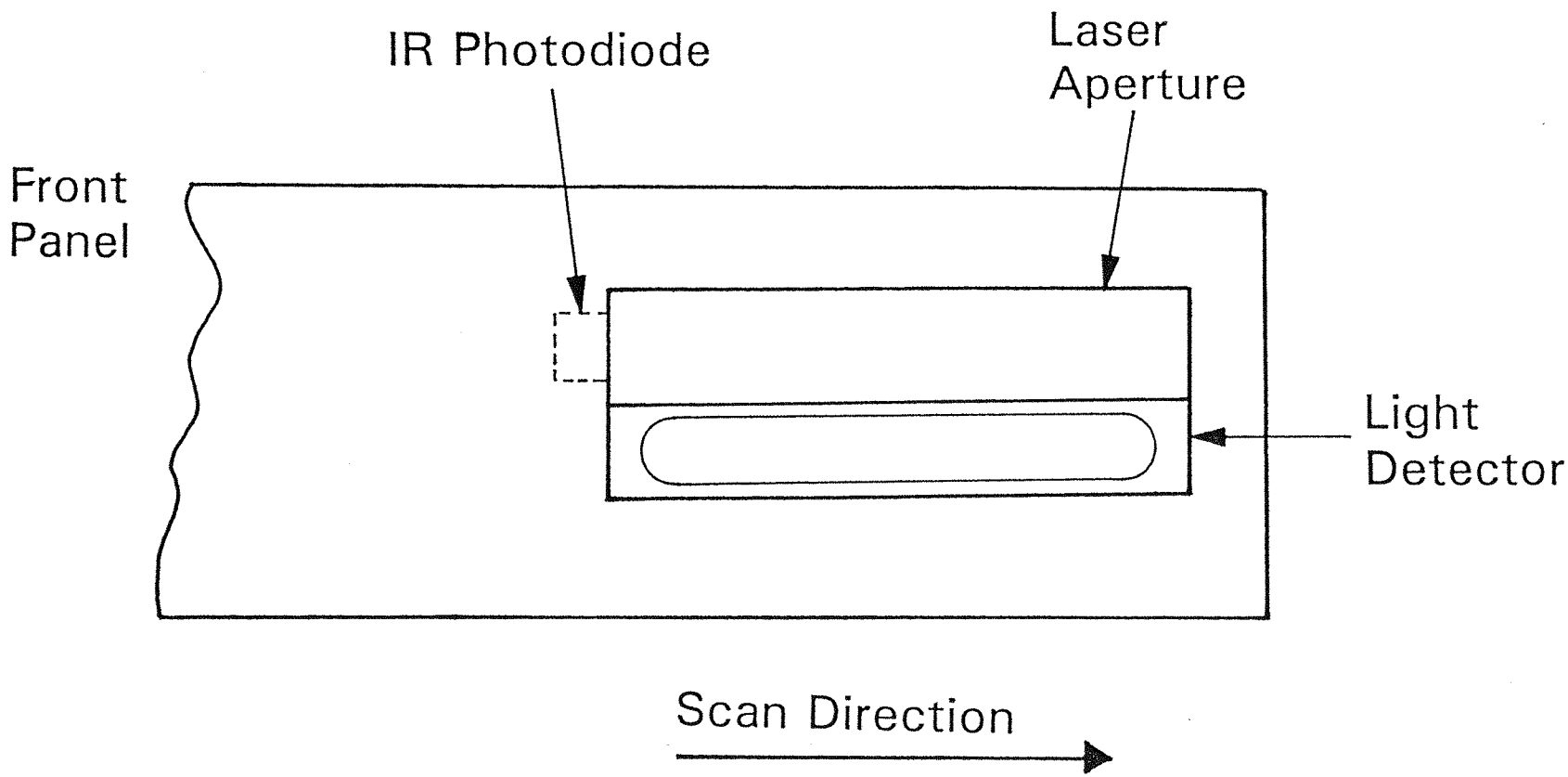

Fig.14 The start of scan sensor

A digital signal processing (DSP) system has been adopted to give maximum flexibility and simplify the interface to the robot controller.

4.5 Digital Signal Processing

The advantages of DSP systems are well known and include low cost, no drift and the provision of an adaptive response. A number of specialised DSP processors are available at comparatively low cost, however it was decided to use a standard IBM compatible PC/AT as the sensor controller. The PC/AT uses the Intel 80286 microprocessor which has no on-chip floating point Arithmetic and Logic Unit (ALU) and offers meagre performance when compared with a dedicated DSP processor. It was intended to use the PC as a development platform for the software routines and then, if necessary, port the algorithms to a faster processing system.

The PC/AT affords a number of advantages when used as a development system:

1) The computer hardware is readily available, along with a wide range of application software, compilers and assemblers.
2) The PC/AT bus (also known as Industry Standard Architecture) is an industry standard for data acquisition and control. A large number of expansion boards are available that connect directly to the bus. These devices include analogue and digital interface circuits, hardware timers etc.
3) The Intel 80287 maths co-processor may be added to speed the execution of floating point arithmetic operations.
4) Derivatives of the IBM PC are already widely used in industry.

The use of an IBM AT as a sensor controller is described by Beattie **[63]** who asserts that the device is suitable for processing data provided by the image acquisition system of the MetaTorch weld seam tracking system. Beattie recognises that the DOS operating system used with the PC range is not a

"real time" operating system but asserts that problems can be minimised by careful use of the DOS function calls.

To facilitate digital processing, the analogue output from the light detector must be sampled and a data acquisition module was used with the PC expansion bus. This included a 12 bit analogue to digital converter with a maximum conversion time of 35μs and a programmable timer to control the sampling rate. In addition, 16 digital input lines and 16 digital output lines are provided and these are used to interface the sensor system to the robot controller and monitor the start of scan sensor.

Unless otherwise stated, all software has been implemented using the 'C' programming language. The Borland Turbo C compiler was chosen because it supports DOS function calls and allows in-line assembly language statements if additional speed is required [64].

The computer polls for the start of scan pulse and then initiates an analogue to digital conversion. The converted value is stored directly in memory which permits the maximum possible sampling frequency. When a complete image has been collated the required information is extracted from the data. This process is analogous to a conventional vision system using a CCD camera, the complete image is transferred to memory before any processing is performed.

4.5.1 Sampling Rate

A High Level Language (HLL) program was written to sample the analogue to digital converter output and store the converted values directly in memory. In tests the PC/AT achieved a maximum sampling rate of approximately 10kHz and thus the sampling rate has been limited to 8kHz to ensure error-free operation.

To prevent aliasing the minimum sampling frequency must be at least twice the highest frequency component present in the spectrum of the analogue signal [65]. In this case the

analogue signal is band-limited by a filter having an upper break frequency of 2kHz which will ensure aliasing does not occur.

4.5.2 Automatic Gain Control

The scanner must operate with a wide range of surface types which will reflect vastly different amounts of light and some form of automatic gain control (AGC) is required to ensure the light detector output does not exceed the ±10V range of the analogue to digital converter but is maintained close to these limits to ensure maximum resolution. A software programmable amplifier is used which provides gains of 1, 2, 4, 8 or 16 **[a]**. The gain control data is provided by the sensor controller and an outline of the development system is shown in Figure 15.

4.6 Concluding Remarks

To give maximum flexibility, a combination of analogue and digital signal processing techniques have been employed. The signals from the light detector are subtracted to reject common-mode noise and then filtered. The light detector output signal is scaled by a programmable gain amplifier before quantisation by a 12-bit analogue to digital converter. An additional photodiode is used to give a reference pulse at the start of every scan.

The industry standard PC/AT computer has been chosen as the sensor controller and signal processing algorithms are implemented using the 'C' programming language.

---

[a] Analog Devices AD526 Software Programmable Gain Amplifier

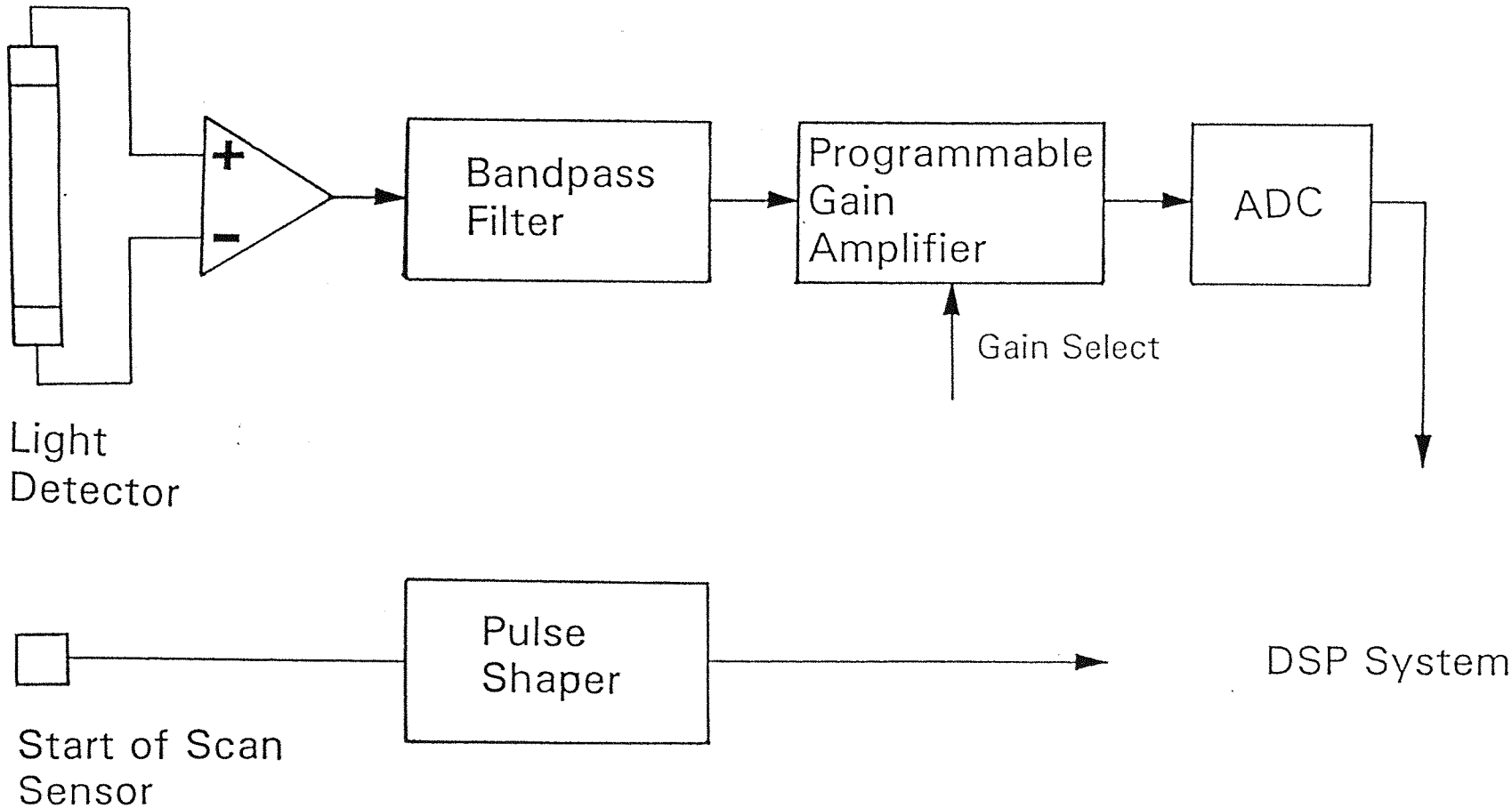

Fig.15 The signal processing system

Chapter 5
Detecting the Seam

5.1 The Sensor Scan-rate

A comparative study of existing seam tracking systems has found that image processing speeds in the order of 10 frames/s are employed. The scan rate of the prototype laser scanner is limited by two factors:

1) The maximum scan rate of the laser across the workpiece (40 scans/s from Equation 3.14).
2) The maximum sampling rate of the DSP system (8kHz using the prototype sensor controller).

To achieve the maximum sampling rate one complete scan is sampled and the converted values are stored in memory before any further signal processing is carried out. The overall operating speed of the seam tracking system is thus limited by the time taken to sample one complete scan and then extract the position of the seam from the data.

It is noted by Edling and Porsander **[28]**, Koskinen *et al* **[52]** and Wang **[54]** that a tracking accuracy of ±0.4mm is required for arc welding. The light detector has an aperture of 100mm and hence 250 samples will be required as the laser is scanned across the detector aperture.

With a sampling frequency of 8kHz the maximum scan rate will be given by

$$Maximum\ Scan\ Rate = \frac{8000}{250} = 32\ scans/s \qquad 5.1$$

Equation 5.1 will only apply when the laser is scanned across exactly 100mm on the workpiece. In practise there is an overlap of approximately 20mm at either end of the detector aperture. This overlap is required to ensure that the laser will be scanned across the full width of the detector aperture when the sensor is operated with a stand-off height which is less than the nominal operating value.

When the laser is scanned across 140mm a total of 350 samples will be required to give a resolution of ±0.4mm and hence the maximum scan rate is reduced to

$$Maximum\ Scan\ Rate = \frac{8000}{350} = 22\ scans/s \qquad 5.2$$

A scan rate of 20 s^{-1} has been selected for seam tracking. This will require 50ms to sample one complete scan, with a further 50ms available to process the scan data and hence correct the lateral position of the sensor every 100ms.

The prototype mirror face planes have axial offsets, resulting in considerable variation in signal amplitude from separate scans. This effect can be seen clearly in Figure 16 and the dimensions of the prototype mirror are given in Appendix 2. Compensation can be achieved by scaling the sampled scan data so that the magnitude of the peak sample is constant for every scan. Unfortunately, scaling the scan data requires a large number of floating-point computations, thus increasing the overall software loop time.

The light detector output signal is shown in Figure 17. It can be seen that the 20mm overlap of the laser scan at the leading edge of the detector aperture delays the collection of light reflected from the workpiece by 5ms (40 samples) after the start of scan pulse is received. Light from the workpiece is collected for a total of 32.5ms (corresponding to 260 samples) and hence the resolution of the sensor is given by

$$Resolution = \frac{100mm}{260} = 0.385mm \qquad 5.3$$

5.2 Detection of the Seam

The position of the seam must be determined from the one-dimensional scanner image signal. In conventional two-dimensional vision systems a discontinuity (point or line) can be detected using a spatial mask **[66]** (pp331-338) and although these techniques are easily modified for use with a

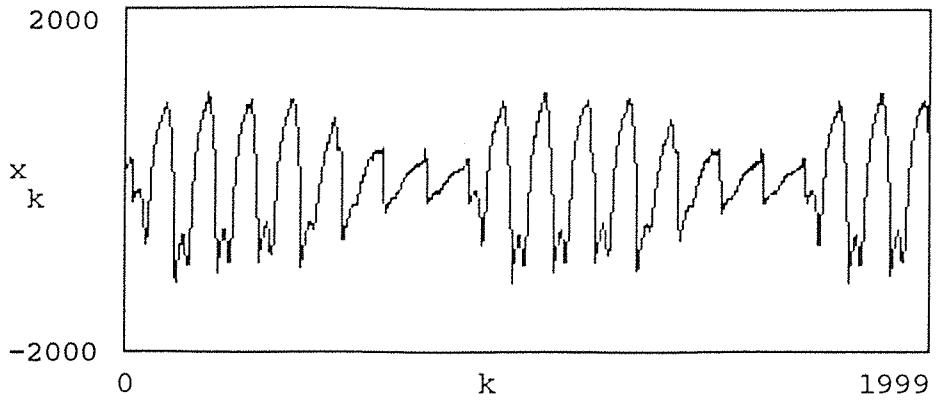

x_k is the signal amplitude

k is the sample number

Fig.16 Output signal for continuous scanning

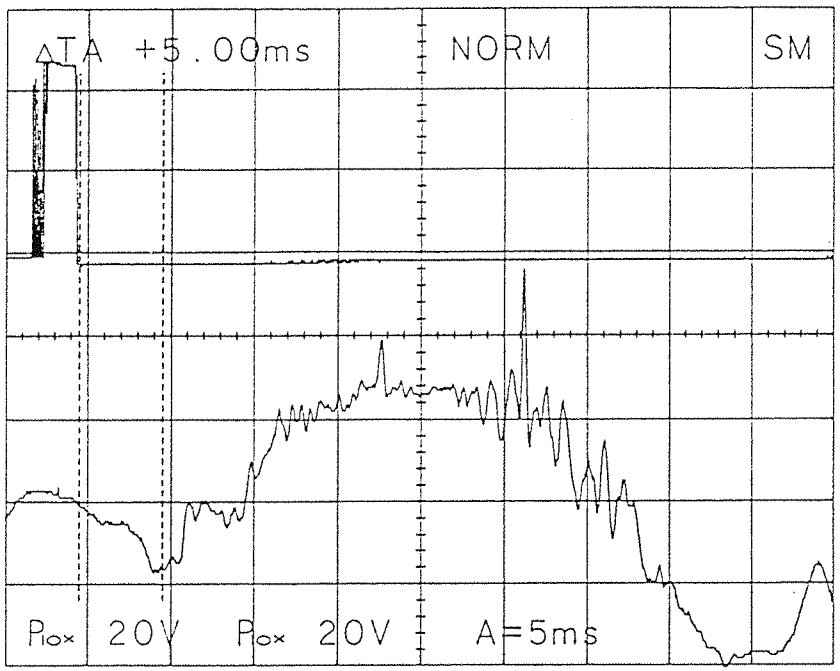

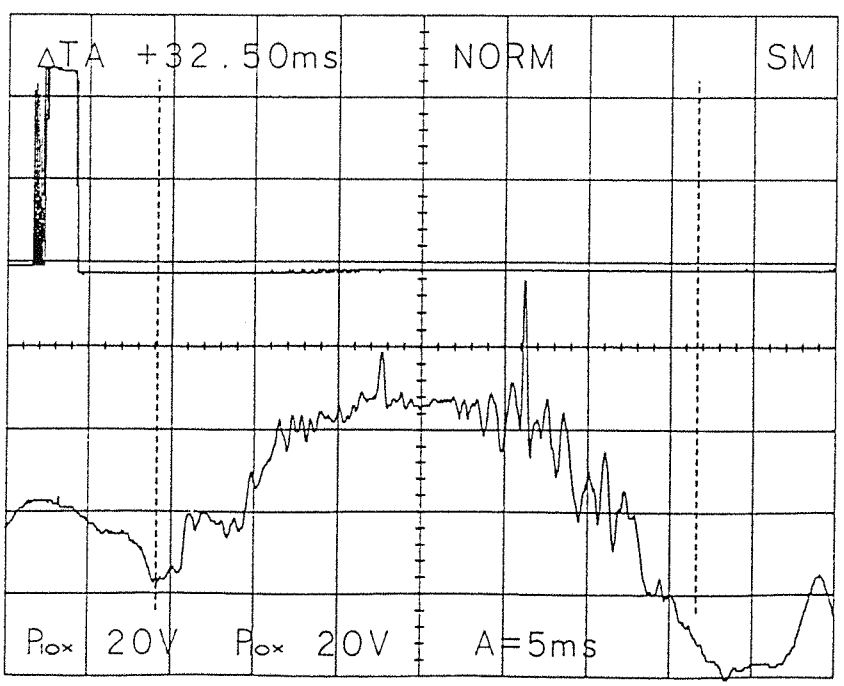

Fig.17 The relationship between start of scan pulse and light detector output

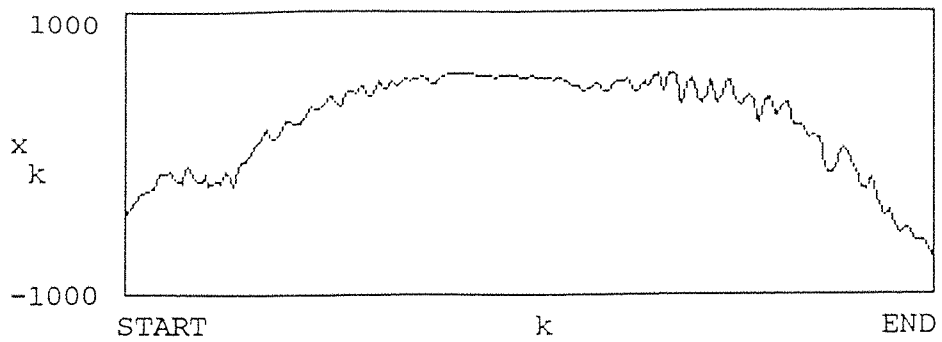

(a) Scan Data

x_k is the signal amplitude

k is the sample number

START = 40*

END = 300*

* There is a 5ms delay (40 samples) before the laser is scanned across the leading edge of the light detector aperture. The scan time is 27.5ms (260 samples).

Fig.18 Comparison of first order difference operators

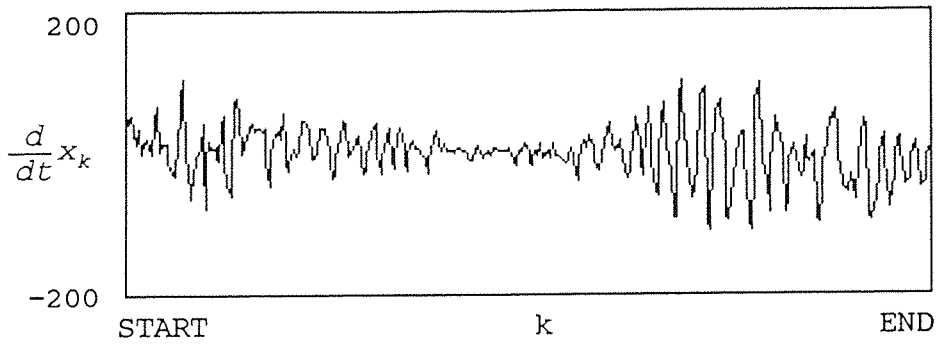

(b) First Order Forwards

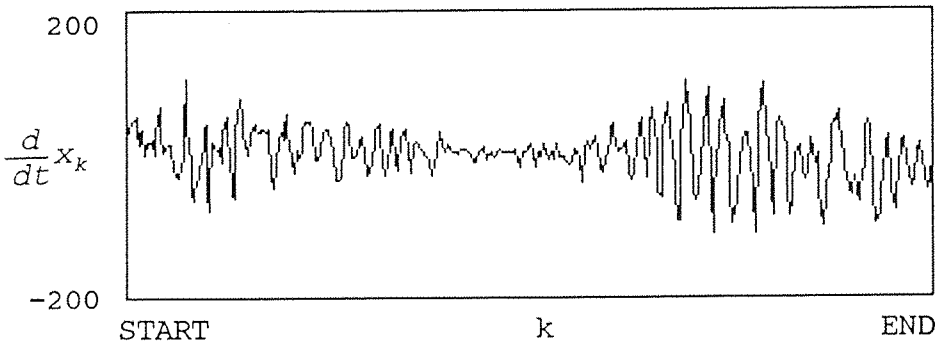

(c) First Order Backwards

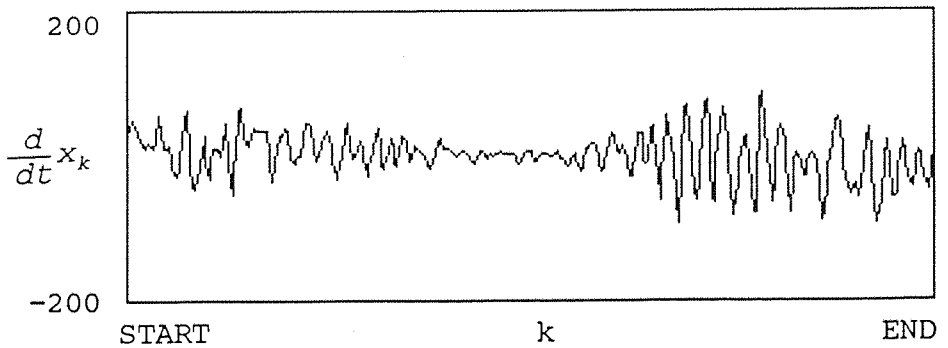

(d) Central Difference

one-dimensional image they are unsuitable because the light detector has a non-linear response, while most solid state cameras have uniform pixel sensitivity.

A number of enhancement techniques will highlight edges in an image, most notably differentiation and high pass filtering [66] (pp176-182). Unfortunately, both these techniques will inherently accentuate the high frequency noise component of the signal.

5.2.1 Differentiation

Sampled data can be differentiated using a simple first order difference operator [67] (pp227-234).

First Order Forwards $$\frac{d}{dt}x_k \approx x_{k+1} - x_k \qquad 5.4$$

First Order Backwards $$\frac{d}{dt}x_k \approx x_k - x_{k-1} \qquad 5.5$$

Central Difference $$\frac{d}{dt}x_k \approx \frac{x_{k+1} - x_{k-1}}{2} \qquad 5.6$$

Figure 18 gives the scanner output obtained from a diffuse surface and shows the results of differentiating this data using the above methods. It can be shown [67] (pp68-70) that the central difference technique is less accurate than the forwards or backwards difference operators but will attenuate high frequency differentials. This property will tend to reduce any noise present in the scanner output signal, an effect which is apparent in Figure 18.

The scan data can be differentiated using the central difference operator to attenuate high frequency noise and surface defects may be detected by applying a global threshold to the derivative values. The threshold level cannot be determined using the usual histogram techniques [68] due to the non-linear response of the light detector. It was found that an appropriate threshold level can be set empirically as shown in Figure 19(a) however this is unsatisfactory because the global threshold will only detect the position of the seam when the discontinuity is well defined and the surface is

uniform. Figure 19(b) shows the results obtained for a surface with poor finish where the position of the discontinuity cannot be detected against the background noise caused by uneven surface texture.

5.2.2 High Pass Filtering

Eliminating the low frequency components from the scanner signal will accentuate discontinuities in the image, along with any high frequency noise. A high pass filter may be implemented using time domain processing and many design techniques exist. In this case, we can use the Bilinear Transform to design a digital filter directly from an analogue prototype **[69]**.

The transfer function of a single-pole high pass filter with a break frequency of 600 rad/s is

$$H(s) = \frac{Ks}{s + 600} \qquad 5.7$$

The Bilinear Transform is

$$s = \frac{2}{T}\,\frac{1-z^{-1}}{1+z^{-1}} \qquad 5.8$$

Where T is the sampling period.

Substituting for s in the analogue transfer function with a sampling frequency of 8kHz gives

$$H(z) = \frac{Y(z)}{X(z)} = \frac{K'(1-z^{-1})}{1-0.928z^{-1}} \qquad 5.9$$

Hence the required difference equation is

$$y_k = x_k - x_{k-1} + 0.928y_{k-1} \qquad 5.10$$

The effect of this high pass filter on the scan data from Figure 19 is shown in Figure 20. Again, it can be seen that any small surface defects at the extremes of the detector

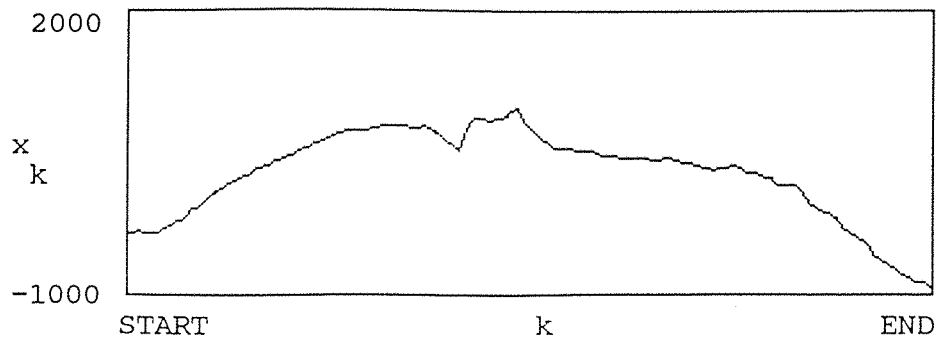

x_k is the signal amplitude

k is the sample number

START = 40

END = 300

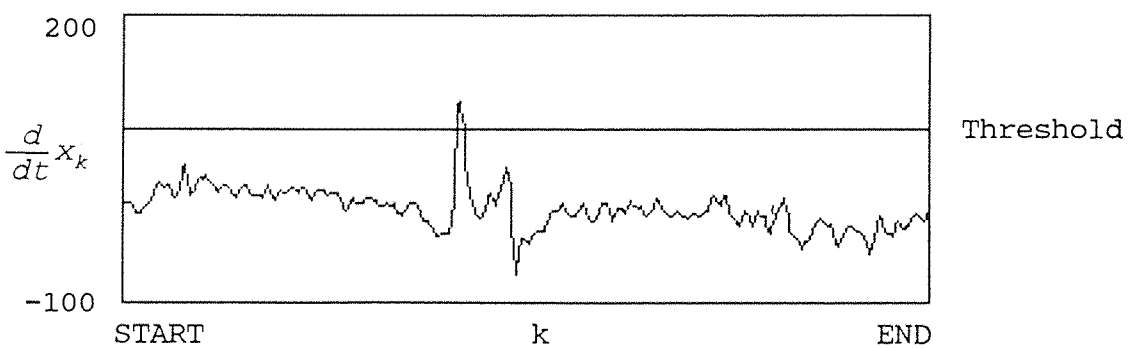

Fig.19(a) Seam detection using differentiation

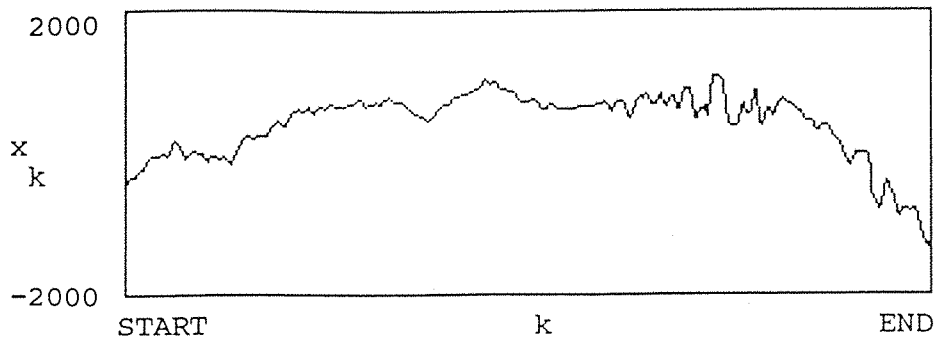

x_k is the signal amplitude

k is the sample number

START = 40

END = 300

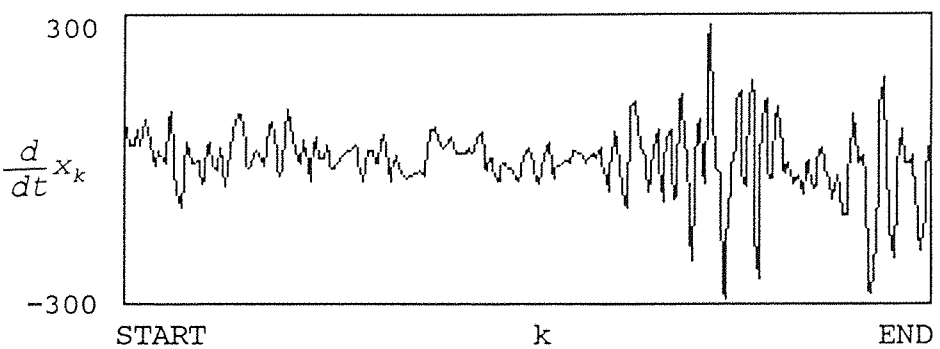

Fig.19(b) Seam detection using differentiation

First order high-pass filter

$$y_k = x_k - x_{k-1} - 0.928y_{k-1}$$

x_k is the signal amplitude

k is the sample number

START = 40

END = 300

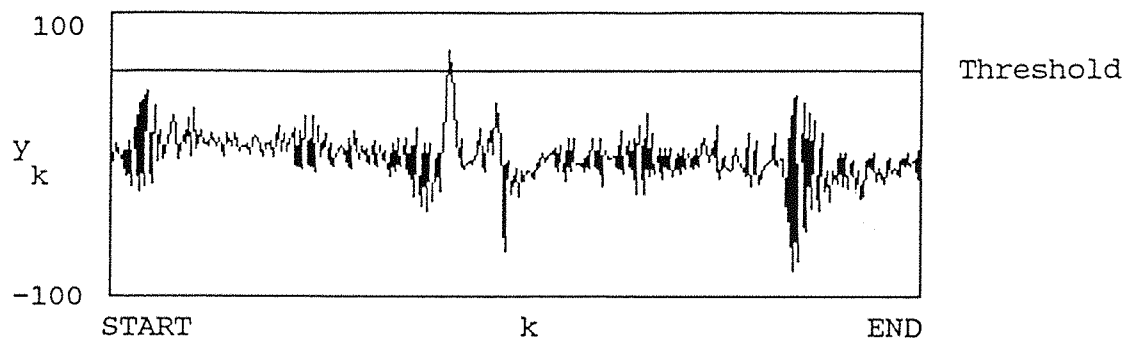

(a) The seam close to the scan centre - good surface finish

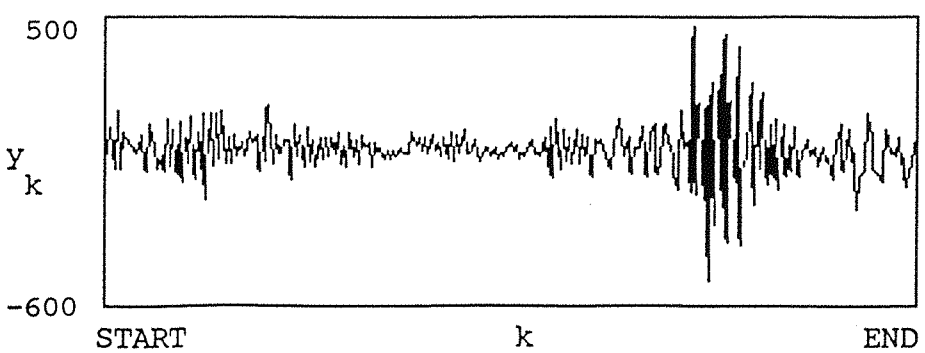

(b) The seam close to the scan centre - poor surface finish

Fig.20 Seam detection using high pass filtering

aperture cause large fluctuations in the output signal and a simple global threshold cannot be used to detect the position of a discontinuity.

It is apparent that the light detector has a non-linear response and hence it is not possible to detect the position of a discontinuity using a simple global threshold. The problem is compounded by the variation in the amplitude of the scanner output signal caused by inaccuracies in the polygon mirror used to mechanically scan the laser across the workpiece.

5.3 Seam Tracking Algorithm

For the purposes of testing and evaluation a seam has been simulated using a length of white tape. Figure 21 shows the output signal when the scanner is moved in increments of 20mm across this "seam". It can be seen that a significant peak is produced at either end of the detector aperture, although the peak is less pronounced at the centre of the scan. The uniform reflection from the discontinuity becomes more clearly defined as the scanner is moved across the seam. This undesirable effect is caused by the geometry of the scanning mechanism. The laser originates from a single point and hence is scanned through an arc. As a result, the scan speed and the angle of reflection of the laser from the workpiece vary with scan position. A derivation of the laser scan speed is given in Appendix 3. Discontinuities situated at the extremes of the detector aperture, where the scan speed is highest, will give high frequency components in the scanner output signal.

The position of a discontinuity may be determined by applying a global threshold to the differentiated scan data, however this will only operate reliably when the discontinuity is located away from the central region of the light detector. Instead, a two-stage algorithm has been employed. Initially the scan data is differentiated and a global threshold is applied to the positive peaks in the differentiated data. This will only detect the position of the seam near the ends of the detector aperture. If the global threshold fails to locate

x_k is the signal amplitude

k is the sample number

START = 40

END = 300

(a) Seam position = 20mm

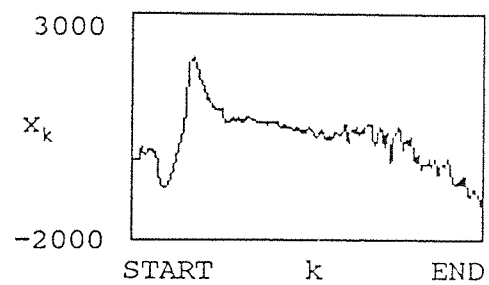

(b) Seam position = 40mm

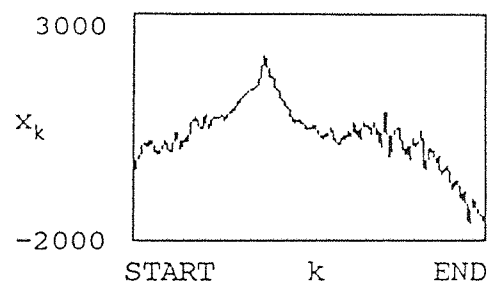

(c) Seam position = 60mm

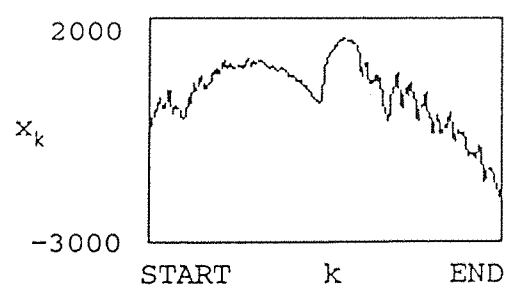

(d) Seam position = 80mm

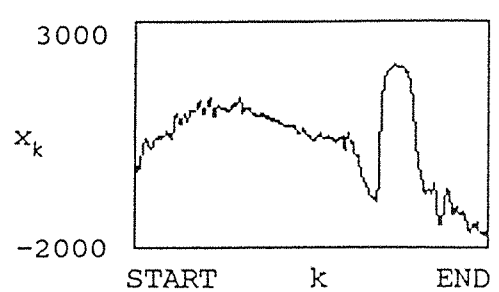

Fig.21 Scanner output resulting from changing seam position

the seam position the differentiated data is checked for regions where consecutive samples have low derivative values. The widths of these regions are compared with a pre-programmed threshold and a match indicates the seam position. The pseudo-code descriptions of the two seam detection algorithms are shown in Figure 22.

The seam detection algorithm will operate reliably with the following seam configurations:

1) Lap joints

A lap joint will cause a shadow, giving a temporary loss of reflected light. As a result, the light detector output will be negligible for a period dependent on the height difference which exists. In practice, the algorithm will operate reliably with a minimum sheet thickness of approximately 4mm.

2) Square butt joint

Clearly, no light will be reflected from the gap between the parts to be welded. A minimum root gap of 4mm is required for reliable detection.

3) Single V butt joints

A well-defined optical signal is produced by the bevelled edges of the two parts to be joined. This signal will be independent of the root gap.

The two-stage algorithm may also be used for tape following; for example in AGV guidance applications.

An outline flowchart of the seam tracking software is shown in Figure 23 and detailed descriptions are provided in Appendix 1. Initially, the programmable amplifier gain is set so that the analogue input does not exceed the ±10V range of the analogue to digital converter. One complete scan is then sampled and the converted values are stored in memory. To compensate for variations in the amplitude of the scanner output signal the converted values are scaled such that the magnitude of the peak sample is 2048. This permit the use of

```
Total=Max_Total=Width=Position=0

FOR i=START TO END
DO
     IF Diff[i] >= 0
     THEN
          Total=Total+Diff[i]
          Width=Width+1
     ELSE
          IF Total > Max_Total
          THEN
               Position=i-Width/2
               Max_Total=Total
          ENDIF
          Width=Total=0
     ENDIF
ENDFOR

IF Max_Total > THRESHOLD_1
THEN
     Seam_Position=Position
ELSE
     Width=Max_Width=0
     FOR i=START TO END
     DO
          IF (Diff[i] >= 0) AND (Diff[i] < THRESHOLD_2)
          THEN
               Width=Width+1
          ELSE
               IF Width > Max_Width
               THEN
                    Position=i-Width/2
                    Max_Width=Width
               ENDIF
          ENDIF
     ENDFOR
     IF Max_Width >= THRESHOLD_3
     THEN
          Seam_Position=Position
     ENDIF
ENDIF
```

Fig.22 Two-stage seam tracking algorithm

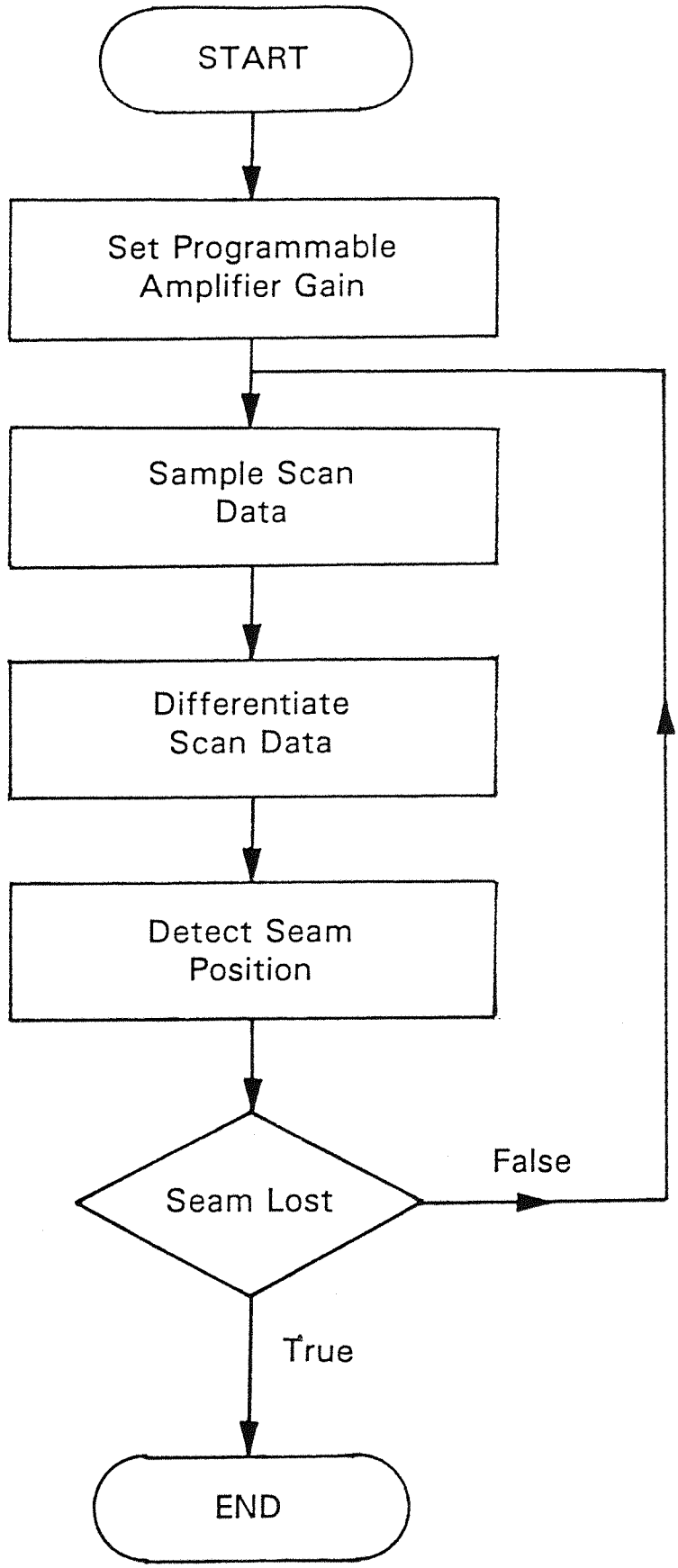

Fig.23 Seam tracking software - Flowchart

fixed thresholds to detect the seam position. The scan data is differentiated using the central difference technique and the seam detection algorithms are applied to the differentiated data. Three threshold values must be set before the scanner is used in a particular application:

Threshold 1 — The minimum magnitude of the positive peak in the differentiated data due to the required seam.

Threshold 2 — The maximum derivative value caused by the uniform reflection due to the required seam.

Threshold 3 — Related to the root gap of a butt joint, the height difference of a lap joint, or the tape width. Used in conjunction with Threshold 2.

5.4 Concluding Remarks

A two-stage seam detection algorithm has been devised that will operate with a range of seam configurations. The seam detection algorithm uses three threshold levels which must be established empirically before tracking commences.

Reliable seam detection is impeded by the non-linear response of the light detector and the simple scanning mechanism employed. The laser scan speed is variable, with higher scan speeds at the end of the detector aperture and therefore, the signal produced by a particular seam is position dependent.

Chapter 6
Seam Tracking

In seam tracking applications the laser scanner will be mounted on the robot arm, just ahead of the Tool Centre Point (TCP). Typically, the TCP will be the tip of the welding torch or a nozzle for adhesive application. It is argued by Verbeek *et al* **[30]** that this "look-ahead" arrangement will allow compensation for the delayed reaction of the robot controller. Such compensation is not possible using tracking systems mounted coaxially with the TCP.

The arrangement of tool and sensor is shown in Figure 24. The sensor is operated with a fixed stand-off height and hence the Z axis offset must be constant. To track a seam the sensor is moved at a constant velocity along the X axis and the sensed data are used to correct the lateral position of the TCP (Y axis). The look-ahead distance will be governed by geometric factors such as the dimensions of the weld torch, however intermediate data storage can be used to overcome the time lag between the passage of the sensor and the torch over any given point on the seam. This technique, known as "Delayed Shift", is described by Verbeek *et al* **[30]**.

6.1 Crocus Gantry Robot

The seam tracking software has been tested using a 3-axis gantry robot manufactured by Crocus Ltd. and installed at the University of Southampton.

The specification of the robot is summarised in Table 8. Each axis is controlled independently and a schematic diagram of the control system is shown in Figure 25. The axis prime mover is a permanent magnet DC motor driven by a servo drive unit having ±10V velocity command input. This velocity control signal is provided by a Smart Motion Control Card (SMCC) manufactured by Baldor ASR. The SMCC is a two-axis controller which is digitally programmed using ASCII characters from an RS232 serial interface. In the Crocus system two cards are daisy-chained to control the three robot axes (Figure 26).

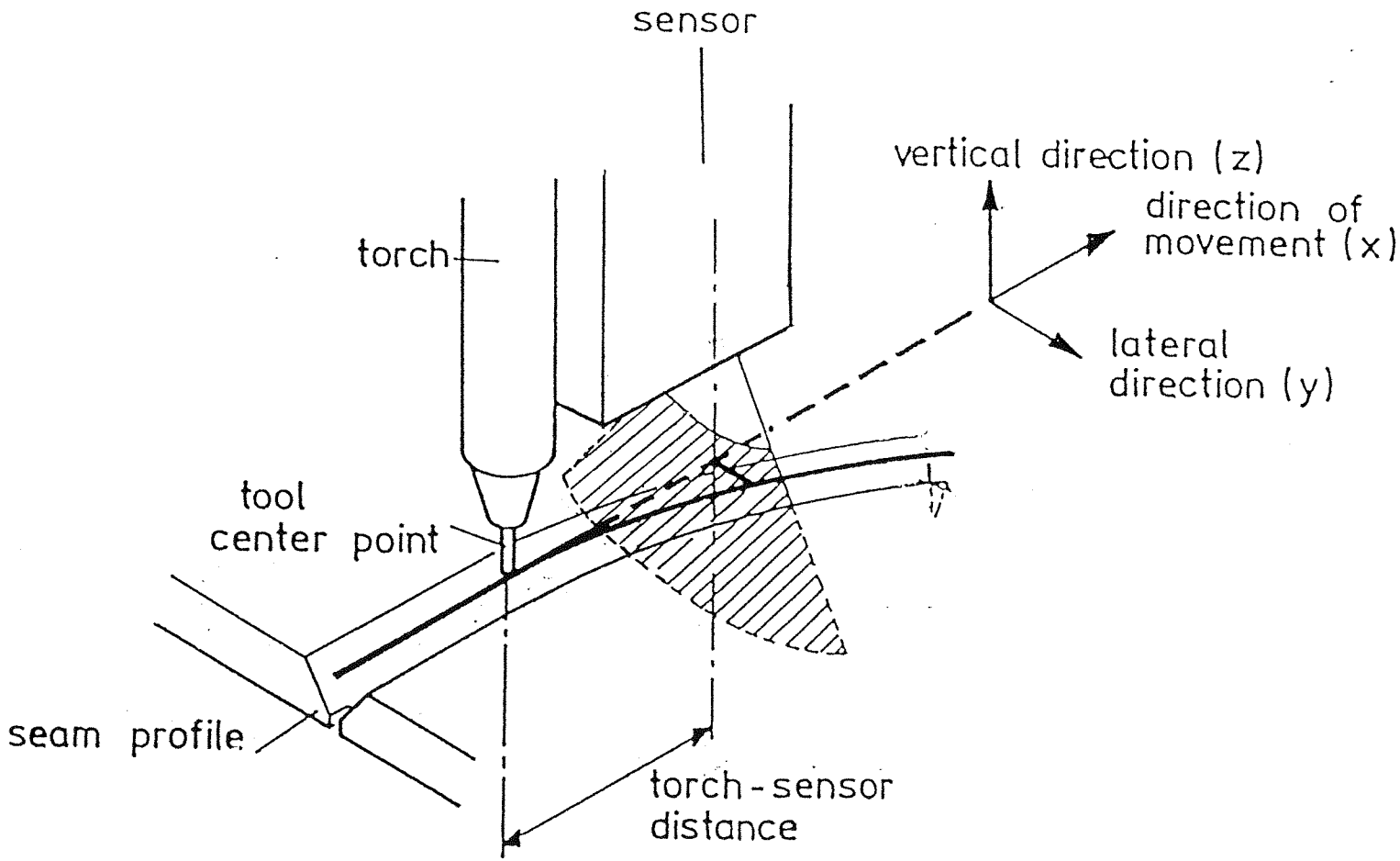

Fig.24 Using a look-ahead sensor

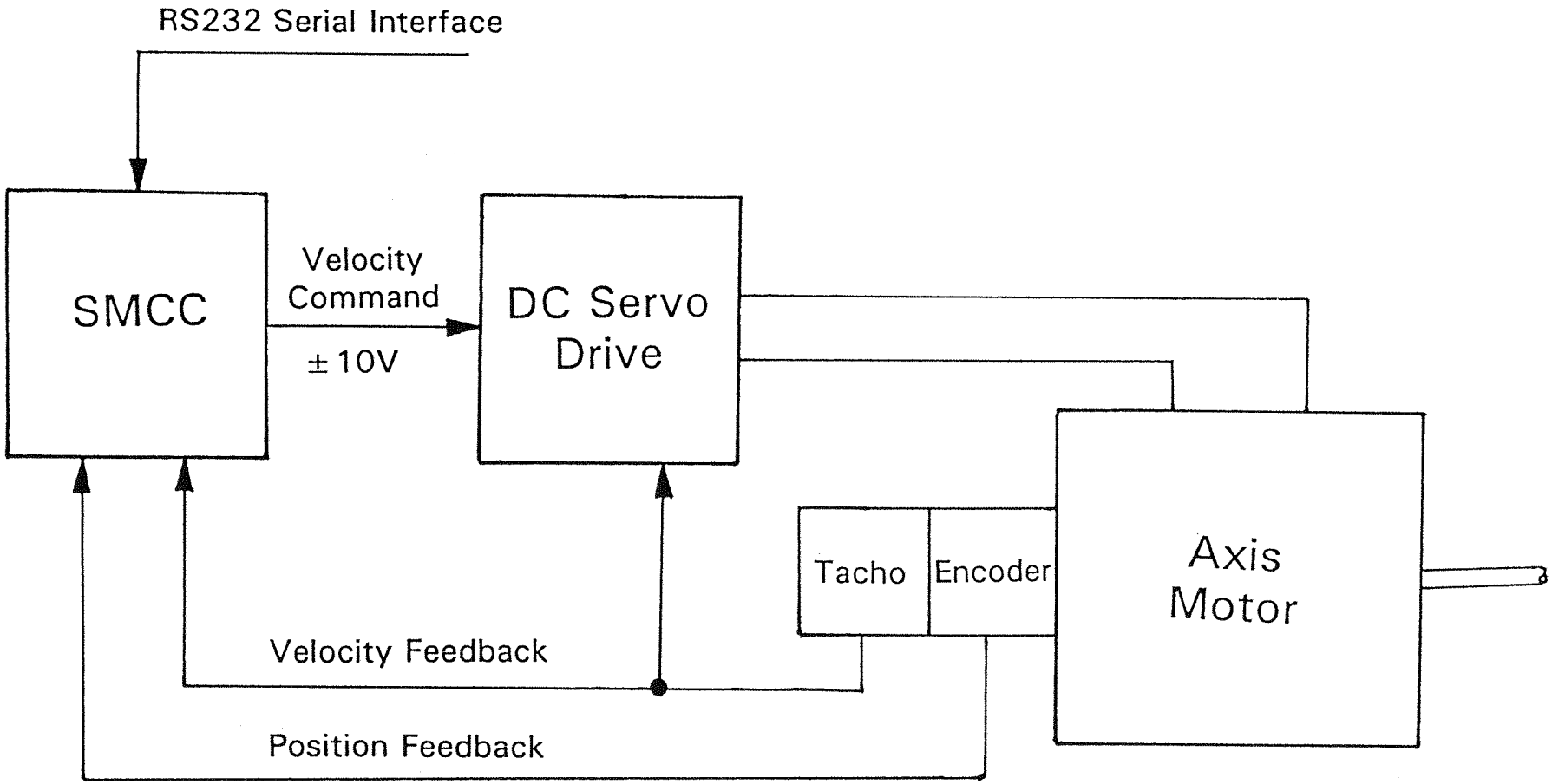

Fig.25 Robot axis position control

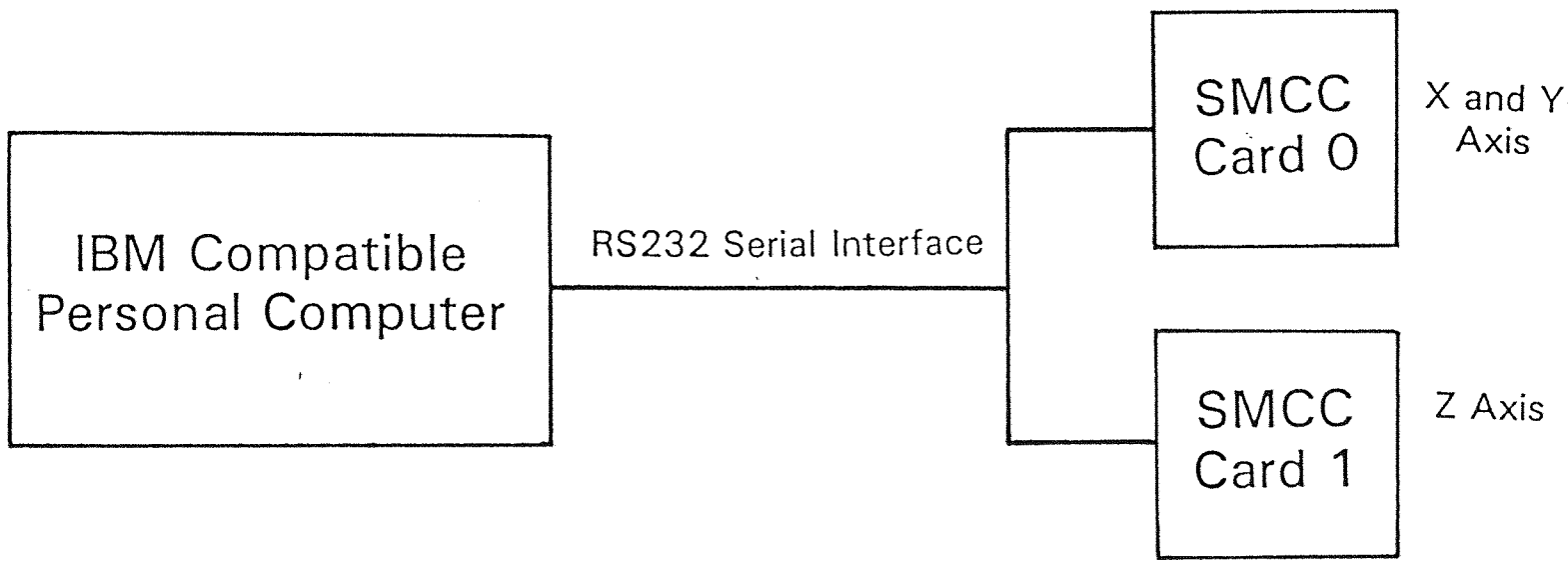

Fig.26 The robot control system

Travel	X Axis	1.0m
	Y Axis	0.78m
	Z Axis	1.0m
Maximum Travel Speed	X Axis	0.9m/s
	Y Axis	0.9m/s
	Z Axis	0.9m/s
Position Encoder Sensitivity	X Axis	69100 counts/m
	Y Axis	69100 counts/m
	Z Axis	69100 counts/m
Lift Capacity	40Kg	

Table 8 Crocus robot specification

The Crocus robot offers the following advantages when used as a test platform for the seam tracking software:

1) Gantry robots are frequently used for applications which require some form of seam tracking. Examples include arc welding, flame and water jet cutting.
2) The robot may be controlled directly in all three axes by means of ASCII character strings sent to the control cards from an IBM compatible personal computer.
3) The sensor must operate with a fixed stand-off height and this can be achieved simply by fixing the Z axis position.
4) The Crocus robot was available and experience with the control system had been gained during the course of another project.
5) The use of a cartesian robot simplifies the transformation from sensor based coordinates to world based coordinates.

An IBM compatible PC is used as the robot controller. High Level Language (HLL) programs are written to send control characters to the SMCC axis control cards. External devices are interfaced to the computer using a digital input/output card connected to the PC expansion bus.

6.2 Interfacing the Sensor System to the Robot

The sensor controller in interfaced to the robot controller using a total of 11 digital input/output lines (Figure 27). The function of the individual signal lines are given in Table 9.

Signal	Direction	Function
Error	Sensor → Robot	8-bit value in Sign-Magnitude format which indicates the difference between the actual seam position and the desired seam position (sensor based coordinate)
Data Valid	Sensor → Robot	A handshake line which indicates that the Error signal is valid 1 = Data Valid
Seam Present	Sensor → Robot	A handshake line which indicates that a seam has been located by the sensor 1 = Seam Present
System Tracking	Sensor ← Robot	A handshake line which indicates the current status of the robot 1 = Robot Tracking Seam

Table 9 Sensor interface signals

The Error value is in 8-bit Sign-Magnitude format and hence the error magnitude will be in the range ±127. This corresponds to the total sensor aperture length and thus the overall resolution of the sensor system is given by

$$Resolution = \frac{100mm}{254} = 0.394mm \qquad 6.1$$

This compares with the basic sensor resolution of 0.385mm from Equation 5.3.

6.3 Tracking a Seam

The experimental apparatus has been described above. The laser scanner is mounted on the end effector of a gantry (cartesian) robot, with the sensor controller connected to the robot controller via a parallel interface. A weld seam has been

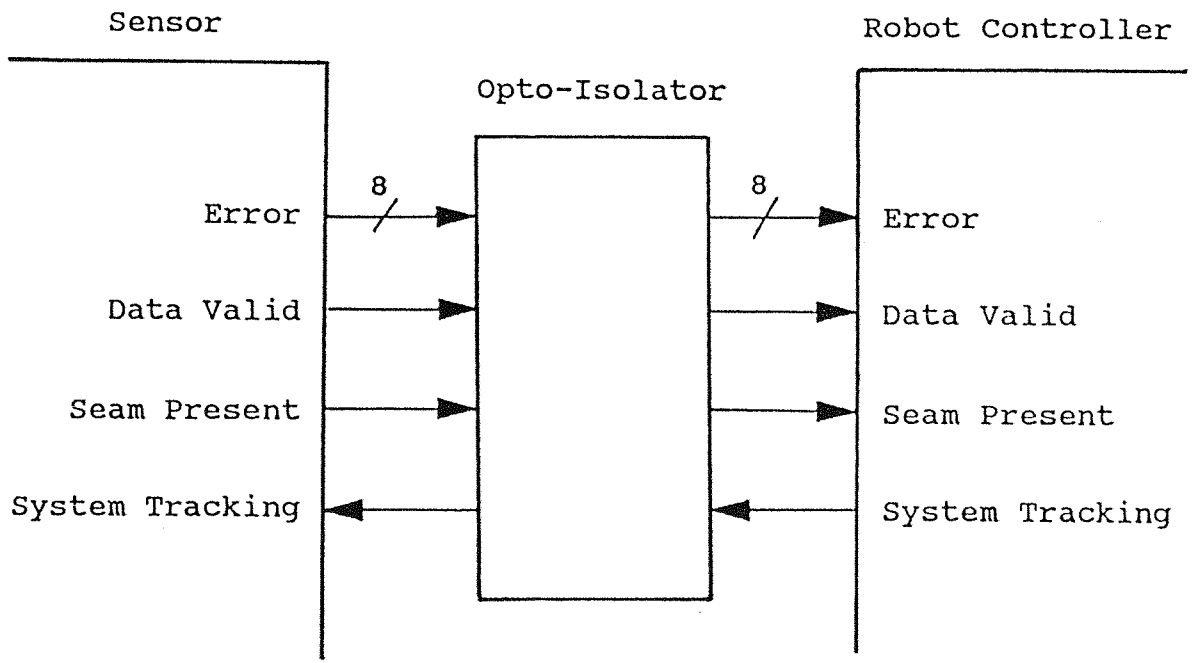

Fig.27 The robot-sensor interface

simulated using an 8mm wide strip of white tape against an irregular background. Figure 28 shows the experimental apparatus, while Figure 29 shows the laser scanner tracking the reference seam.

The thresholds used for seam detection were established empirically and these are given in Table 10.

Threshold	Value
1	2400
2	100
3	10

Table 10 Seam detection threshold levels

It is noted by Porsander and Sthen **[70]** that robots typically move the welding torch smoothly at velocities between 8 and 25mm/s. During the course of testing, various seam configurations have been tracked successfully at this velocity, including examples which deviate from a straight-line substantially more than any practical weld seam.

6.3.1 Sensor Resolution

The resolution of the sensor system was measured as 0.4mm using slip gauges to establish appropriate displacements of a reference seam. This value compares with the design figure of 0.394mm (Equation 6.1).

6.3.2 Software Loop Time

The original specification required a software loop time of 100ms for seam tracking. An optimum loop time of 200ms has been achieved, although this figure is variable because the control software is designed to reject scan data if the seam position cannot be determined with sufficient confidence. Tracking is only discontinued when five successive scans indicate that no seam is present. The control algorithms have been designed to improve system reliability. In particular, the following problems may be encountered when the sensor is operated in an industrial environment:

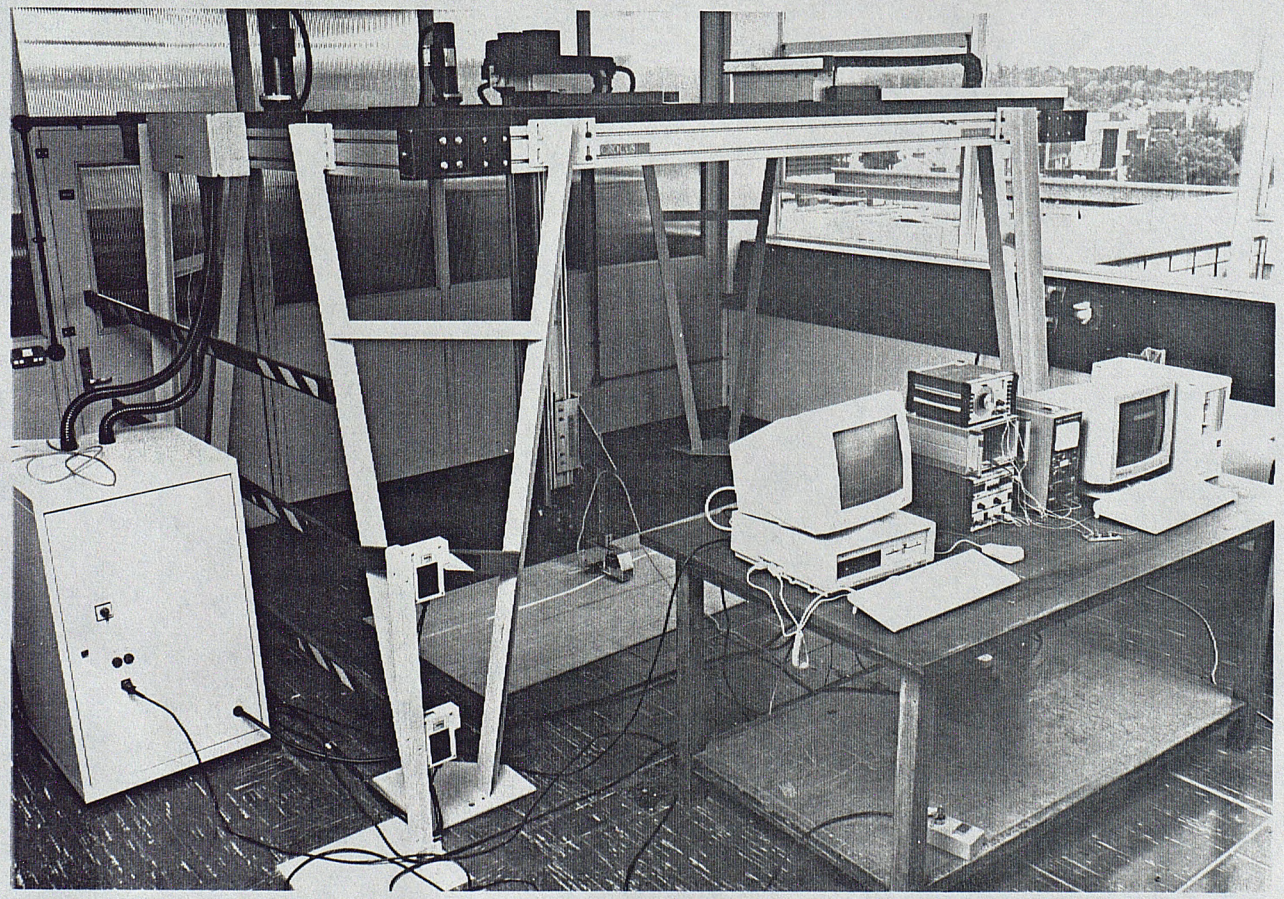

Fig.28 The experimental apparatus

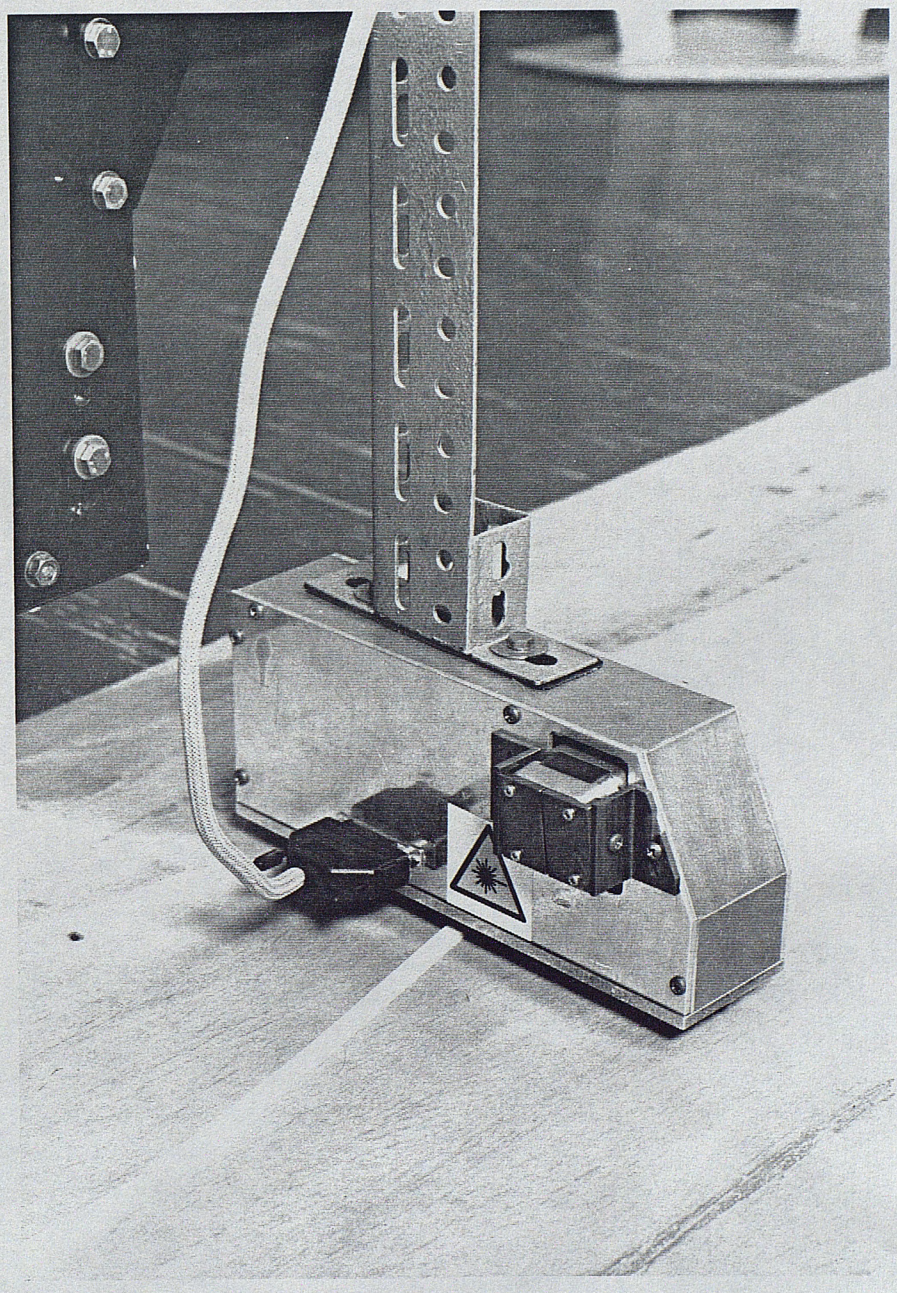

Fig.29 Tracking a seam

1) Variations in the scanner output signal caused by mechanical tolerances in the scanning mechanism.
2) Temporary occlusion of the light detector by smoke or fumes.
3) Noise induced by EM interference or optically, via the light detector.
4) Damage or contamination sustained by one or more faces on the polygon mirror.

The overall software loop time is dependent on operational factors such as surface texture, seam definition, stand-off height and system integrity. Tests on a range of surfaces and seam configurations yielded an average loop time of 210ms, substantially slower than the design figure for one-pass weld seam tracking. In Section 5.1 a scan rate of 20 s^{-1} was selected in order to achieve a software loop time of 100ms. This requires 50ms to sample the scan data, leaving 50ms to process the data and extract the seam position. Clearly, the 50ms time is insufficient for the latter task and this highlights two separate limitations:

1) The tasks of sampling the scan data and processing the data are performed sequentially. This is necessary to achieve the maximum possible sampling rate. Some form of autonomous I/O technique will relieve the main processor of this time-consuming task.
2) Sampling the sensor output signal can only commence at the beginning of each scan (every 50ms). The seam tracking software is not synchronised to the mechanically scanned laser and hence the program may be delayed while polling for the start of scan pulse.

6.4 Seam Tracking Results

A proportional control law has been adopted. Initially the sensor is positioned close to the start of the seam. The robot is then driven at constant speed along the seam (Y axis) with the lateral speed (X axis) controlled using the measured error. Direction is determined using the sign of the error, while the axis feed rate is proportional to the magnitude of

the error. The Z axis position (sensor stand-off height) is fixed at all times.

The following robot control parameters are selected by sending ASCII character strings to the SMCC axis control cards:

X axis feed rate
Y axis feed rate
Acceleration and deceleration time

The acceleration/deceleration time is the time taken to complete any programmed speed change. Axis feed rates are set using decimal values in the range 0 to 255, where 0 corresponds to a speed of zero, and 255 selects the maximum (reference) speed which is set using a separate string of control characters sent to the SMCC.

For the purposes of this work no attempt has been made to "fine-tune" the control parameters. Controller settings will be dependent on the particular robot used and this work has sought to prove that the sensor can be used for seam tracking, and not to establish a precise set of control parameters for a particular hardware configuration.

Testing has been achieved using a "reference" seam fashioned from white tape. The position of the seam has been established relative to the X and Y axes of the robot. Calibration was achieved by positioning the robot end-effector directly above the seam and recording the X and Y coordinates at intervals along the seam length. The calibration data are shown in Figure 30. For the purposes of testing and evaluation, the X and Y coordinates of the robot are periodically recorded when tracking a seam, along with the sensed error and the velocity command signal. Tracking accuracy for a particular control strategy may then be established by comparing the trajectory followed by the robot with the actual seam profile.

The results presented in the following section indicate the effects of

1) varying the control law
2) varying the robot acceleration/deceleration time
3) varying the tracking speed
4) filtering the error data

6.4.1 Varying the Control Law

The optimum control law has been established empirically. Initial tests were performed with a seam tracking speed of 25mm/s and an acceleration/deceleration time of 0.25s. The following examples are indicative of the results obtained:

Control Algorithm 1

```
IF Error < 3
THEN
     Velocity_Command=0

ELSE IF Error > 40
THEN
     Velocity_Command=Error*4

ELSE
     Velocity_Command=Error

ENDIF

IF Velocity_Command > 240
THEN
     Velocity_Command=250

ENDIF
```

A graph showing control algorithm 1 is shown in Figure 31(a). The results obtained are presented in Figure 32(a) and show a maximum tracking error of 18mm. As expected, there is a constant following error when tracking inclined sections of the seam. It can be seen that the velocity command is increased significantly when the error exceeds 40 resulting in an oscillatory response. This problem is particularly apparent when large following errors are present. The error magnitude provided by the sensor system will be in the range ±127 for a lateral position error of ±50mm. An error magnitude of 40 thus corresponds to a position error of 10mm. When the error is less than 3 the velocity command is set to 0. This dead-band is designed to prevent the robot oscillating about the seam when the tracking error is small. The velocity command value

must be limited so that the maximum axis feed rate of the robot is not exceeded.

Control Algorithm 2

```
IF Error < 3
THEN
     Velocity_Command=0

ELSE IF Error > 20
THEN
     Velocity_Command=Error*4

ELSE
     Velocity_Command=Error

ENDIF

IF Velocity_Command > 240
THEN
     Velocity_Command=250

ENDIF
```

Control algorithm 2 is shown in Figure 31(b). The velocity command is increased significantly when the error exceeds 20, giving the results shown in Figure 32(b). An oscillatory response is produced when tracking sloping sections of the seam where the following errors exceed 20 and the maximum tracking error is 48.4mm.

Control Algorithm 3

```
IF Error < 3
THEN
     Velocity_Command=0

ELSE IF Error > 40
THEN
     Velocity_Command=Error*2

ELSE
     Velocity_Command=Error

ENDIF

IF Velocity_Command > 240
THEN
     Velocity_Command=250

ENDIF
```

Control algorithm 3 is shown in Figure 31(c). The transition between the unity gain and high gain region of the controller characteristic is more gradual than previous examples. The controller has unity gain when the error is less than 40 and a gain of 2 when the error exceeds 40. Tracking results are presented in Figure 32(c) and show a smooth trajectory with a maximum error of 26mm.

This control algorithm appears to give the best overall results and has been employed in all subsequent tests. It is apparent that increasing the controller gain can reduce the tracking error, although oscillation may occur due to the discontinuous nature of the control strategies employed.

6.4.2 Varying the Robot Acceleration/Deceleration Time

The effects of varying the robot acceleration/deceleration time is shown in Figure 32(d) and Figure 32(e). Again, a tracking speed of 25mm/s has been employed. Increasing the acceleration/deceleration time to 0.5s increased the maximum tracking error to 28.4mm. Reducing the acceleration/ deceleration time to 0.117s had no discernable effect on tracking accuracy, with the maximum error unchanged at 26mm. The robot has a large mass and appears unable to respond rapidly to programmed speed changes.

6.4.3 Varying the Tracking Speed

Initial tests have been performed at a tracking speed of 25mm/s. Figure 32(f) shows the results for a tracking speed of 10mm/s. The maximum error is 18.4mm. Figure 32(g) shows a maximum error of 34mm for a tracking speed of 50mm/s.

6.4.4 Filtering the Error Data

Measurement noise can be reduced by filtering the error data. A three-point smoother has been employed; the error value is calculated by averaging the last three seam positions computed by the scanner. Seam tracking results are shown in Figure 32(h) and these show a clear reduction in measurement noise, with a maximum lateral position error of 24.4mm.

Smoothing the error data, although giving a reduction in measurement noise, degrades the frequency response of the sensor system. Averaging more than three points will further decrease the sensor performance, particularly when tracking sharp turns at high speed.

6.5 Concluding Remarks

It has been shown that the sensor can be used to track a seam, although it was decided not to pursue an ideal set of robot control parameters. The seam tracking accuracy will be governed by a number of factors in addition to the performance of the sensor itself:

1) The dynamics of the robot.
2) The software loop time of the IBM PC used as the robot controller.
3) The speed of the RS232 serial link used to connect the robot controller to the axis control cards.
4) The following errors cannot be eliminated using a simple proportional control law.

Considering these factors; while gantry robots have a rigid structure, the sensor has a weight of 2.4kg and is mounted on the end effector with the Z axis fully extended. When the robot is moved quickly the sensor tends to swing, rather like a pendulum, and this results in relative movement between the fixed end of the Z axis and the end effector. The robot controller is an IBM PC with an Intel 8086 microprocessor. Control software is written using the Pascal programming language and the loop time is substantially greater than that of the sensor. An RS232 serial link with a Baud Rate of 4800 is used to communicate with the axis control cards and the software loop time is further limited by the time taken to send data to the control cards.

Rudimentary control theory suggests that steady state following errors will not be eliminated using a proportional control law. The solution to this problem is well known. Increasing the controller gain will reduce the tracking error,

although this may give rise to an oscillatory response [71]. Poor results have been obtained using a constant controller gain. Large gain values cause an oscillatory response, while reducing the gain gives a sluggish response and large tracking errors. The control law which has been employed has unity gain for small position errors and a gain of two for larger position errors. This two-stage characteristic gives a rapid response when the error is large and then reduces the controller gain when the error is small, thus preventing overshoot.

It has been seen that an oscillatory response may be caused by an abrupt transition between the high gain and low gain regions of the controller characteristic. Careful choice of controller gains and break-points will eliminate this problem.

The sensor operates using the "look-ahead" principle and will be situated in front of the TCP in any practical application. The lateral error data produced by the sensor data indicates the difference between the current sensor position and the seam at a fixed distance ahead of the TCP. This problem can be overcome by delaying the error value. For example, with a tracking speed of 25mm/s and a software loop time of 200ms the error value should be delayed by 5 samples when the sensor is located 25mm ahead of the TCP.

In practice, tracking accuracy will be measured relative to the TCP rather than the sensor itself and this presents an additional difficulty when evaluating the overall performance of the seam tracking system. Often the sensor position lags the required seam position, especially when tracking sharp curves. In this situation, the error between the TCP and seam position will not equal the sensed position error. The actual error will be dependent on the seam configuration and the relationship between the sensor and tool.

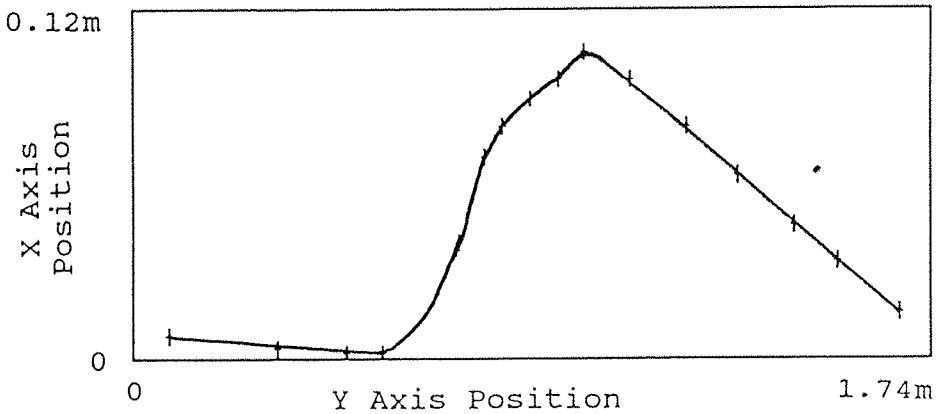

The X and Y axes do not have the same scales:

The total Y axis movement is 1.74m (120000 encoder counts)
The total X axis movement is 0.12m (8000 encoder counts)

Where 69100 encoder counts = 1m

All displacements are measured relative to the robot "home" position.

Fig.30 The reference seam relative to X and Y axis coordinates

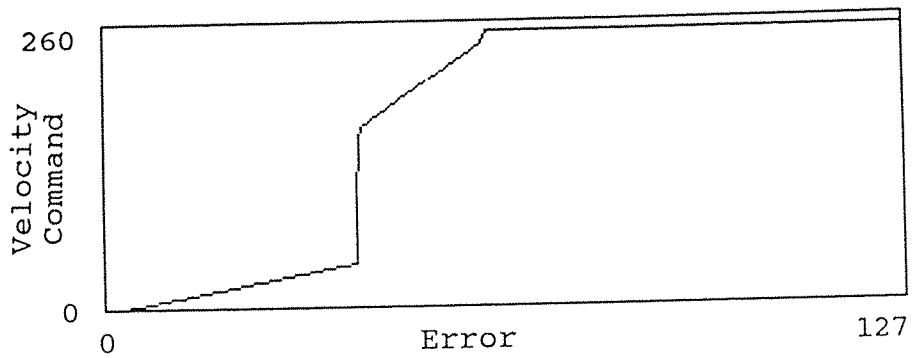

Fig.31(a) Control Algorithm 1

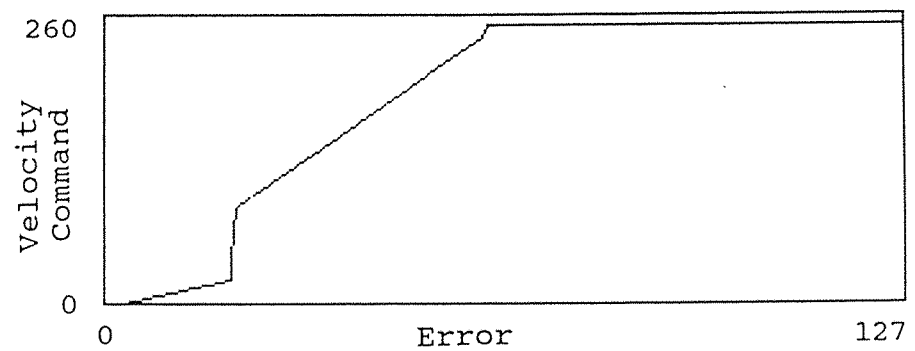

Fig.31(b) Control Algorithm 2

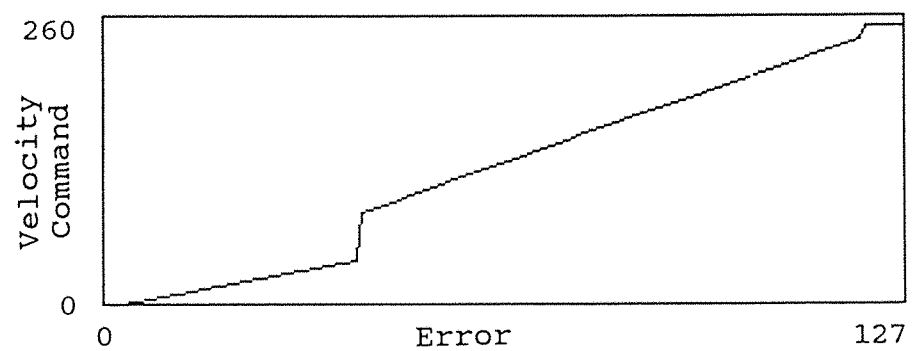

Fig.31(c) Control Algorithm 3

Fig.31 Proportional control algorithms

Tracking Speed = 25mm/s
Acceleration/Deceleration time = 0.25s

Measured error plotted against Y axis position

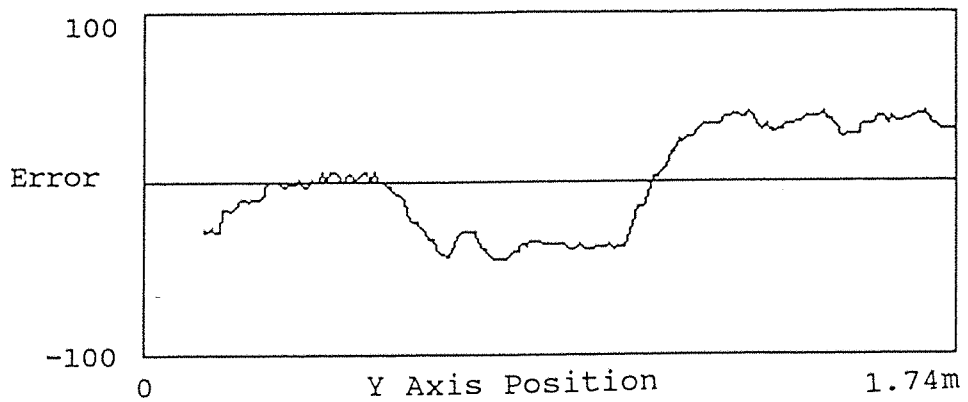

X axis velocity command plotted against Y axis position

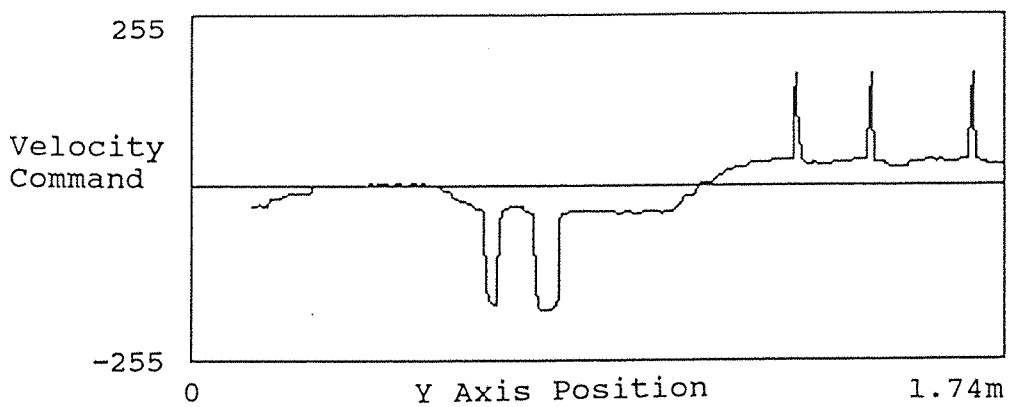

X axis position plotted against Y axis position

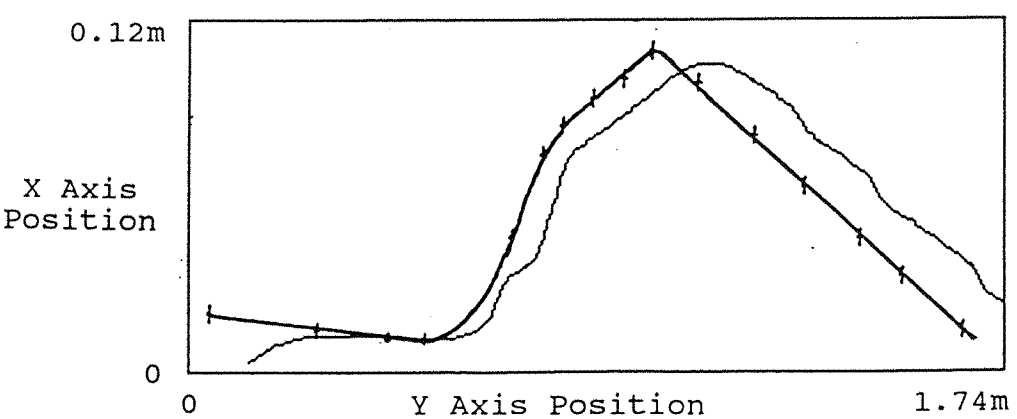

Fig.32(a) Seam tracking results

Tracking Speed = 25mm/s
Acceleration/Deceleration time = 0.25s

Measured error plotted against Y axis position

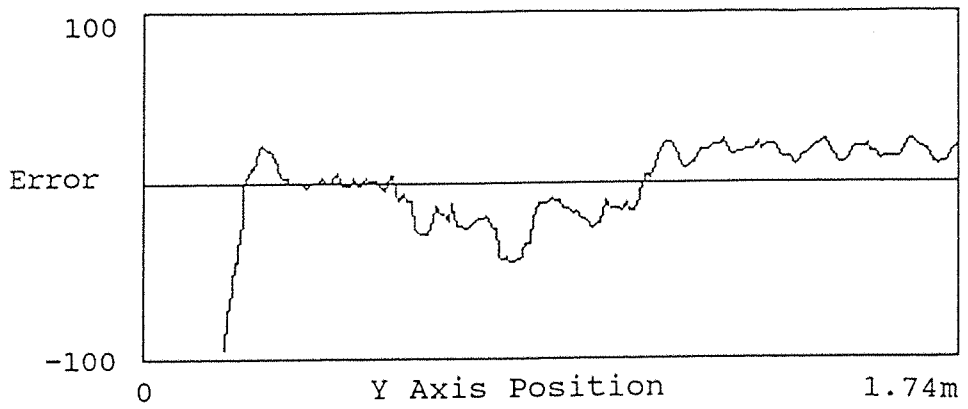

X axis velocity command plotted against Y axis position

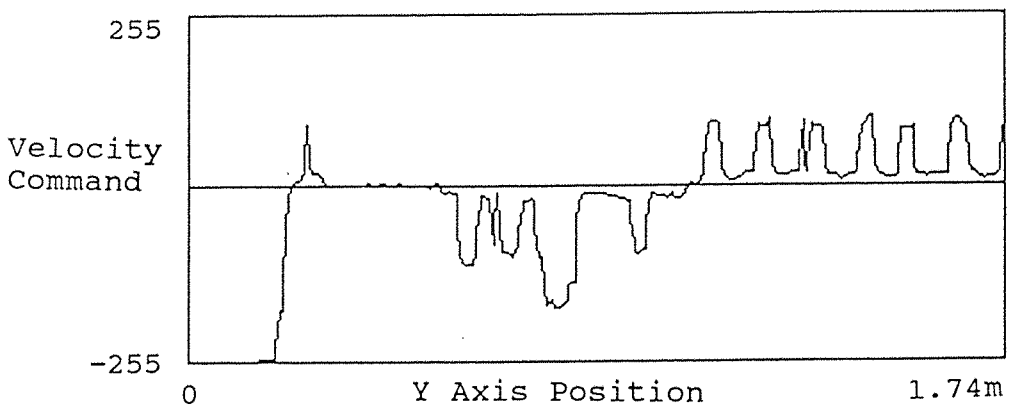

X axis position plotted against Y axis position

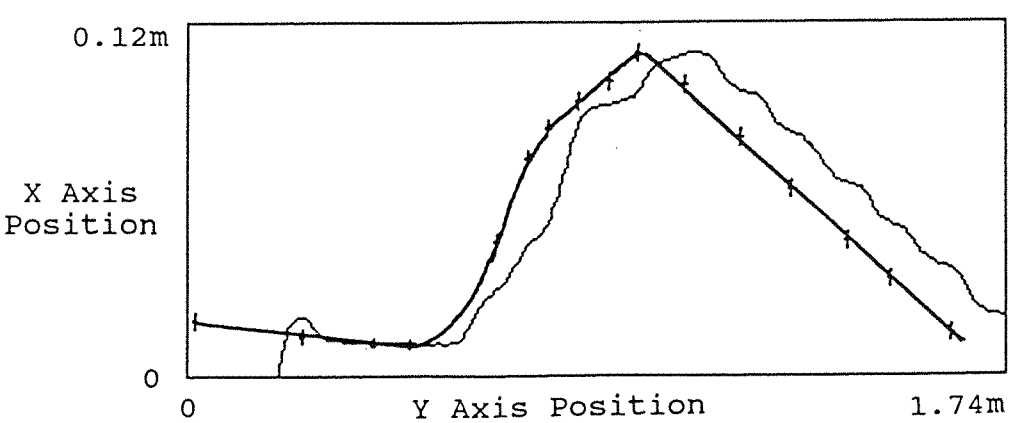

Fig.32(b) Seam tracking results

Tracking Speed = 25mm/s
Acceleration/Deceleration time = 0.25s

Measured error plotted against Y axis position

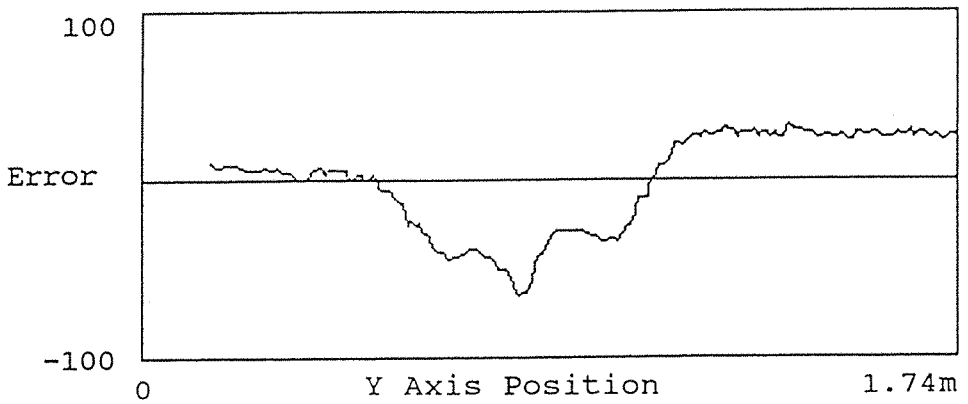

X axis velocity command plotted against Y axis position

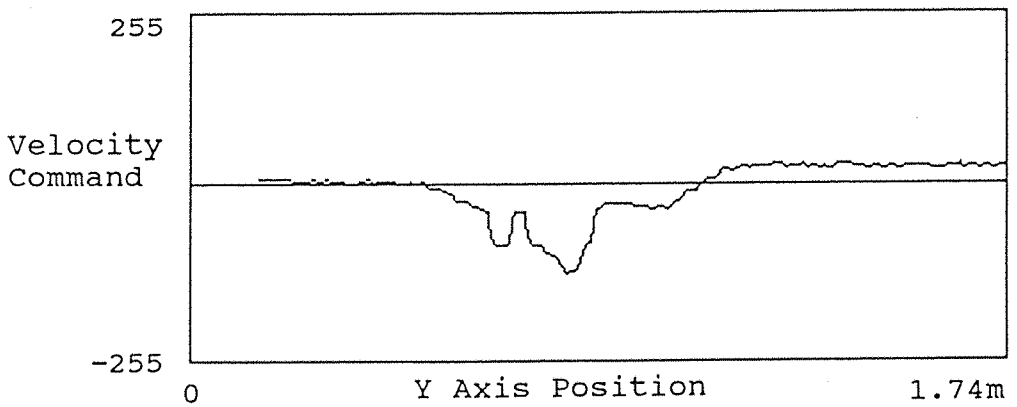

X axis position plotted against Y axis position

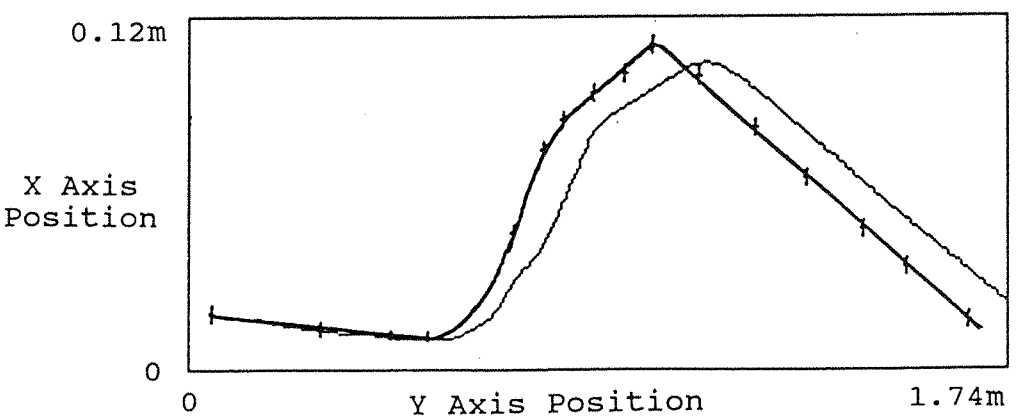

Fig.32(c) Seam tracking results

Tracking Speed = 25mm/s
Acceleration/Deceleration time = 0.5s

Measured error plotted against Y axis position

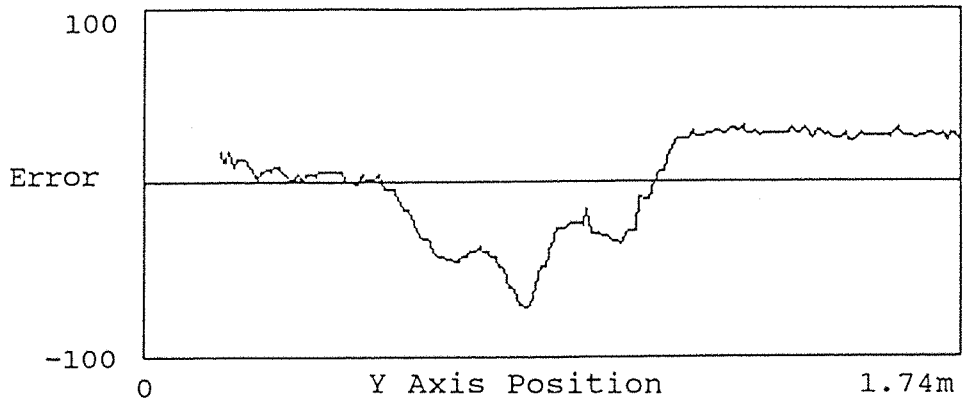

X axis velocity command plotted against Y axis position

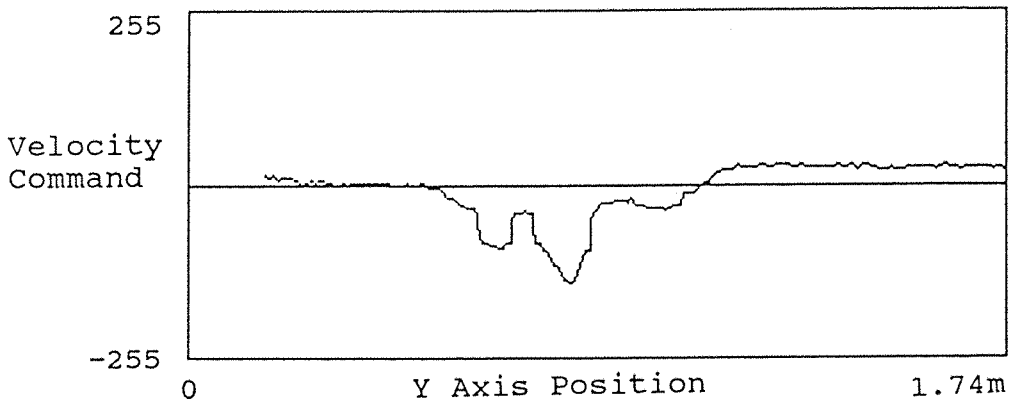

X axis position plotted against Y axis position

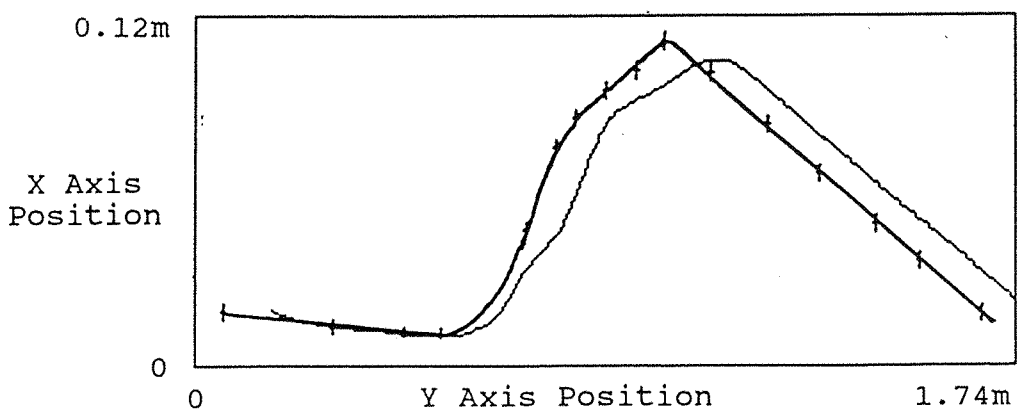

Fig.32(d) Seam tracking results

Tracking Speed = 25mm/s
Acceleration/Deceleration time = 0.117s

Measured error plotted against Y axis position

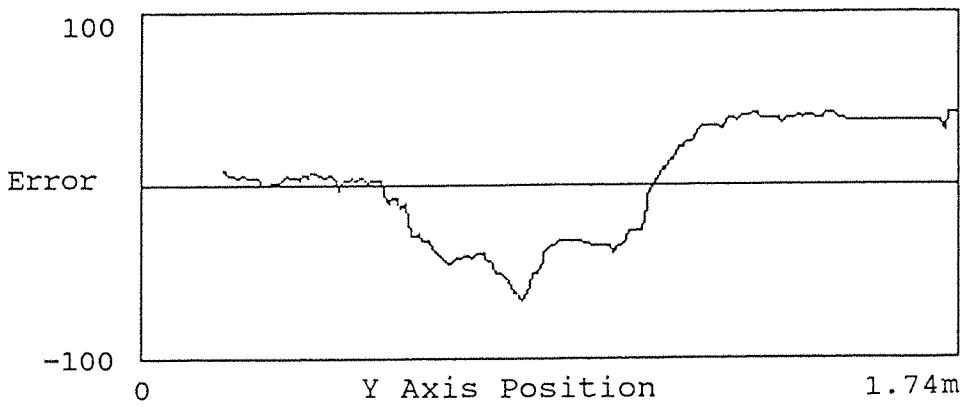

X axis velocity command plotted against Y axis position

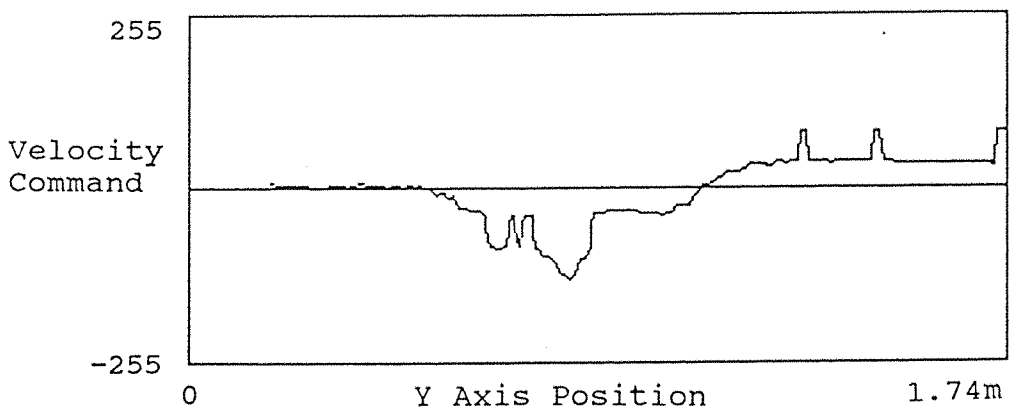

X axis position plotted against Y axis position

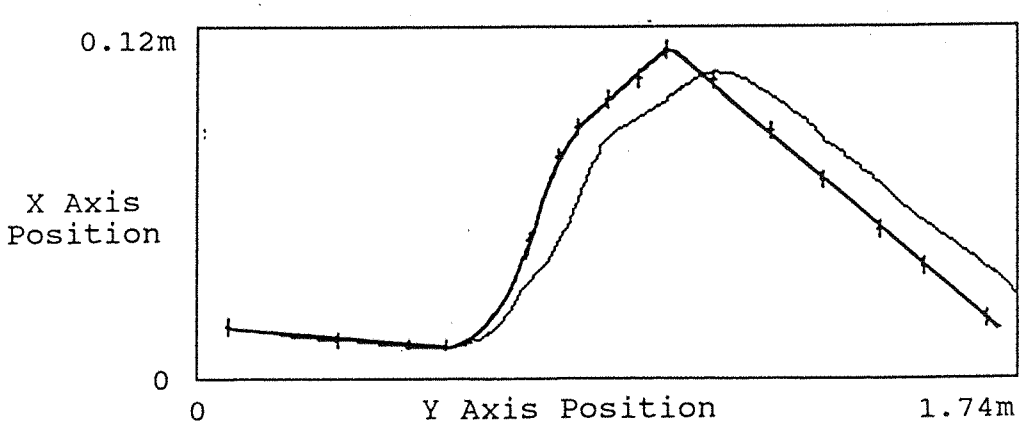

Fig.32(e) Seam tracking results

Tracking Speed = 50mm/s
Acceleration/Deceleration time = 0.25s

Measured error plotted against Y axis position

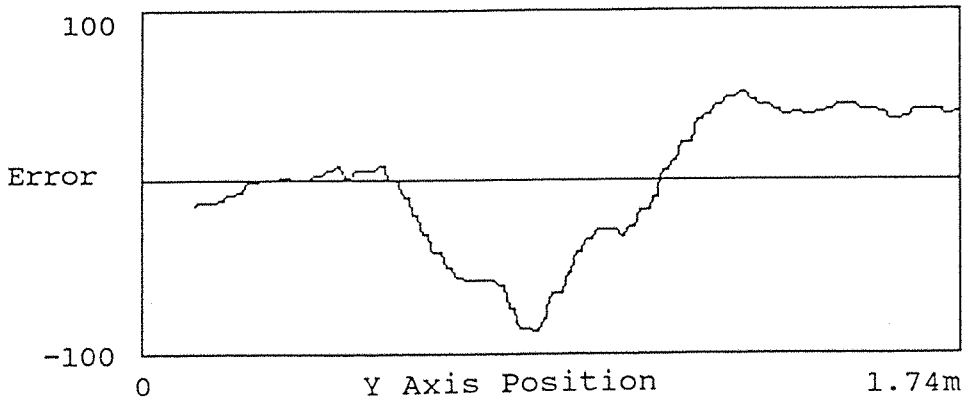

X axis velocity command plotted against Y axis position

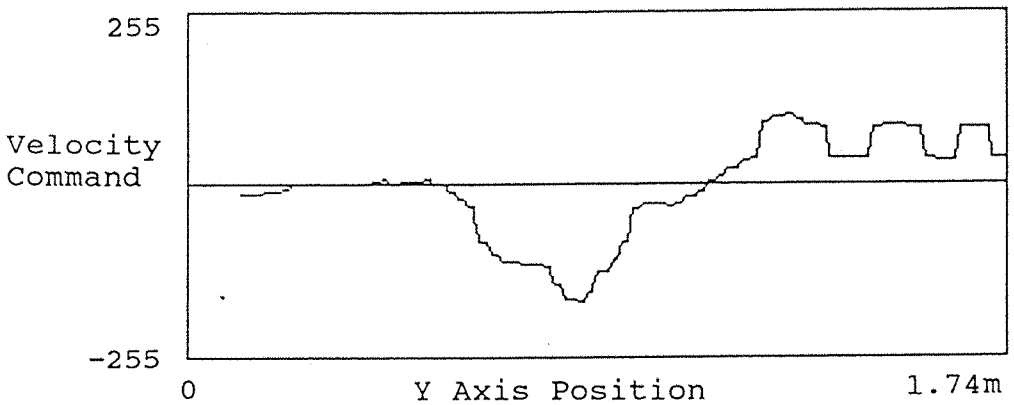

X axis position plotted against Y axis position

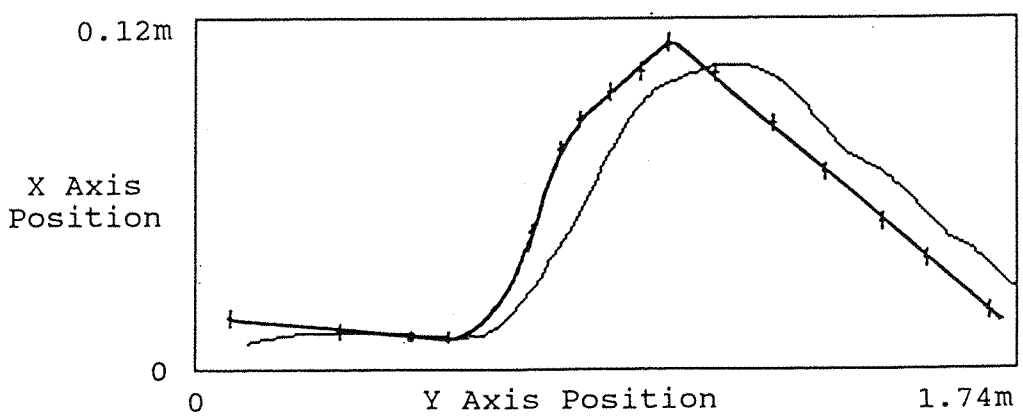

Fig.32(f) Seam tracking results

Tracking Speed = 10mm/s
Acceleration/Deceleration time = 0.25s

Measured error plotted against Y axis position

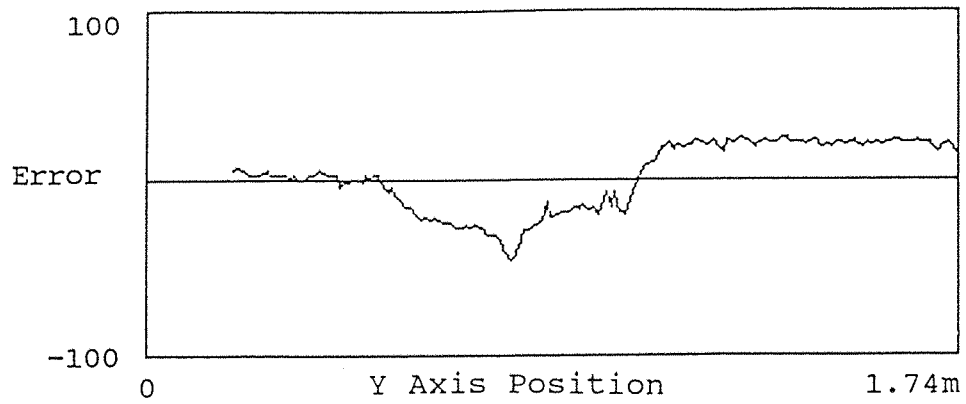

X axis velocity command plotted against Y axis position

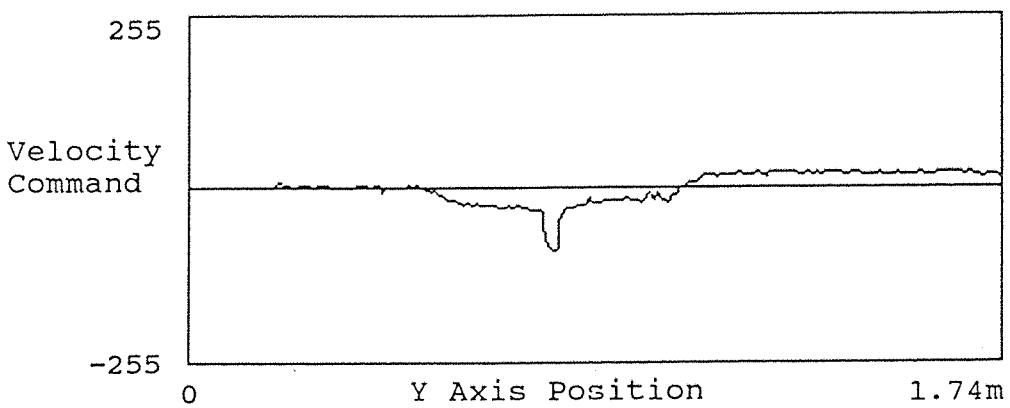

X axis position plotted against Y axis position

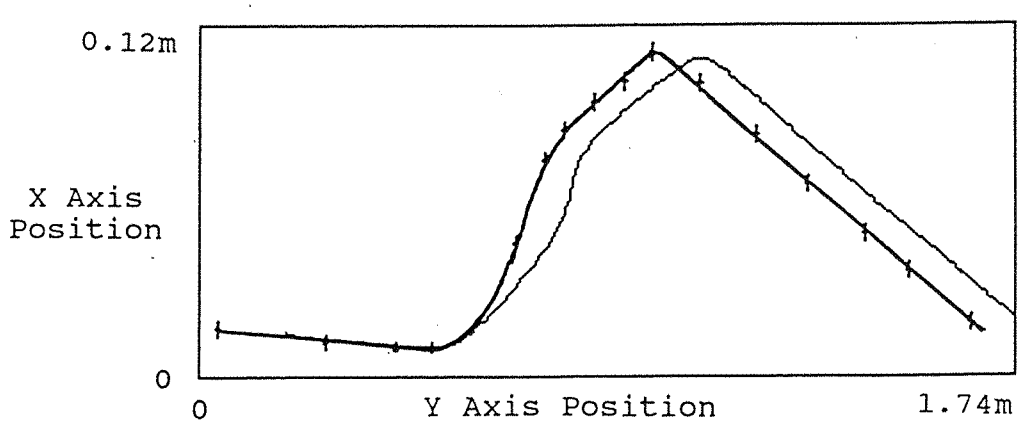

Fig.32(g) Seam tracking results

Tracking Speed = 25mm/s (Filter Selected)
Acceleration/Deceleration time = 0.25s

Measured error plotted against Y axis position

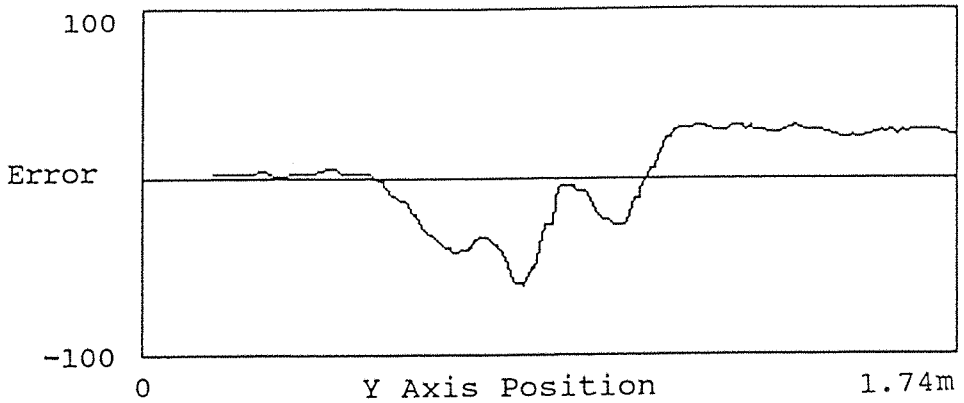

X axis velocity command plotted against Y axis position

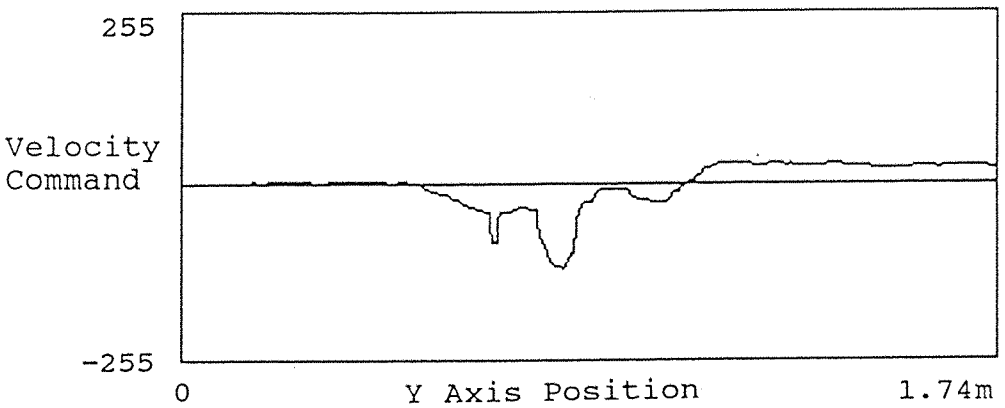

X axis position plotted against Y axis position

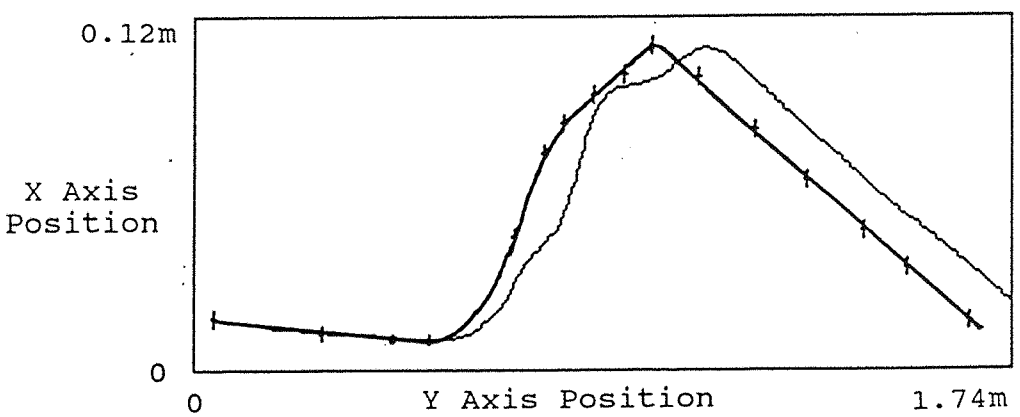

Fig.32(h) Seam tracking results

Chapter 7
Vision Sensors

7.1 Introduction

Potential application areas for vision sensors are numerous and the following examples are intended to illustrate the range of tasks which have successfully used some form of machine vision.

Example 1 - Visual Guidance

A robot with visual guidance has been used to assemble power diodes [72]. Diodes are constructed from five separate components which are assembled in a jig prior to soldering. The robot has a multi-function end-effector which incorporates a low resolution camera. A second low resolution camera is used to inspect individual components before assembly, while an overhead Vidicon camera is used to view the entire work-cell. Image processing is performed using two separate processors, one for low resolution vision and the second for system control and high resolution vision. A third microprocessor is used to communicate with the robot controller. The authors report that the use of sensory feedback increased the total assembly time from 166s to 294s however, the reliability also increased, from 81.5% to 99.55%.

Example 2 - Visual Inspection

Marchant [73] describes a grading system which can be used to inspect fruit and vegetables, rejecting those which do not conform to preset size, shape or colour requirements. The objects to be inspected are presented to the camera using a conveyor consisting of linked rollers which rotate the produce as they move forward. All sides of the object are presented to the camera which is mounted above the conveyor. Three rows of produce are contained within the field of view simultaneously and data reduction is performed by encoding the boundaries of each object. A hardware encoding system is used which can differentiate between objects which are touching.

Concurrent image processing is performed using three 16-bit microprocessors, one for each row of produce. A fourth microprocessor is used to coordinate the activity of the slave processors and operate the electro-mechanical sorting mechanism. Blemish detection is handled using a fifth microprocessor which makes use of the boundary data to identify the position of an object. In use, the system is capable of grading 40 objects per second and the weight of each object can be estimated from the measured volume.

Example 3 - Image Recognition

Paint spraying of small components has been partially automated using a vision system [74]. The operator mounts a component on a conveyor with the aid of a computer screen which shows how each component should be suspended. A vision system is used to identify the component type and check for correct orientation on the conveyor. Image processing is performed using a multi-processor system, with a serial communication link installed between the loading station and the spraying cabin. The object proceeds to the spraying cabin, where control codes sent to the controller indicate the position of the object and select the appropriate spray painting program for the robot.

7.2 Machine Vision

During the first half of the 1980s machine vision was widely heralded as the solution to all sensing and inspection problems [75]. With the benefit of hindsight it is clear that the predictions of massive growth in the machine vision market were wildly optimistic. Vision systems were large, expensive, slow and often plagued by poor reliability. Consequently, machine vision gained a reputation for being expensive and unreliable, a reputation which has been difficult to lose.

> "Many systems that were installed failed to live up to expectations and are now gathering dust, sitting unused on the factory floor."
>
> (Coulthard, 1991)

Increased competition in the marketplace due to recession and the creation of a single European market has placed renewed emphasis on quality control and process monitoring. Quality control is of particular importance in the food manufacturing industry where food safety standards reflect universal public concern. It has been estimated that human visual checks are only 30% effective [76] and a new generation of machine vision systems are required for applications such as on-line inspection, sorting, gauging and process control.

Automated inspection systems may be used to form a simple pass/fail decision based on the general appearance of an item or to obtain specific quantitative measures of characteristics such as surface finish or component dimensions. The majority of machine vision systems use two-dimensional solid-state cameras. A typical camera has a resolution of 512 by 512 pixels and a scan rate of 20ms. Such devices are expensive and require a high performance image processing system. One-dimensional sensors are often preferred in applications where the product is moving. The continuous movement of the workpiece on a conveyor may be used to synthesise a two-dimensional image and these devices are less expensive than array cameras.

Coulthard [75] asserts that while considerable research has been directed at advanced vision systems, this has led to relatively few successful shop-floor installations. Instead, simple inspection tasks can be performed effectively using low cost vision systems. A simple machine vision application will require a simple pass/fail decision based on unambiguous inspection criteria. One flat face of the workpiece will be inspected and the defect must be clearly visible without sophisticated lighting techniques. Image processing algorithms will be implemented using an inexpensive hardware platform and the workpiece should be presented to the camera using an existing conveyor.

7.3 Solid State Cameras

Conventional machine vision systems use solid state CCD or CID cameras [77]. Such devices are available in two-dimensional or line scan configurations. Line scan cameras use an array of photosensitive elements arranged in a single line and these devices are often used in place of area array cameras when the product is moving. Loughlin [78] describes the operation of the line scan camera and identifies the following advantages when compared with array cameras:

1) The line scan camera offers high resolution. Devices are available with up to 2048 pixels, compared with the 512 by 512 resolution generally available from area array cameras.
2) Line scan cameras can be used to monitor the entire width of a continuously moving production line and hence a series of scans can be used to construct an image of an infinitely long production line or product. The array camera must construct an image from a large number of rectangular sections.
3) The line scan camera has a short scan time (typically less than 1ms) compared with the 20ms of an area array camera. Long exposure times can result in blurring of the image and hence inaccuracies in dimensional measurements. Unfortunately, short exposure times require high levels of illumination because of the short time available to integrate the light falling onto a pixel and convert this level into an electrical signal.

Low cost machine vision systems may be constructed around a line scan camera and an IBM compatible PC [79]. A system using a 1024 pixel camera has been used successfully for applications which include measuring the diameter of steel pipe and detecting defects in a flow of material carried on a conveyor. Image processing is performed by the PC and this offers a number of advantages; the hardware is inexpensive, interfacing is generally easy and the PC is well suited to many operator interface requirements.

7.4 Flying Spot Laser Scanners

Flying spot laser scanners [57] are frequently used for inspecting strip products such as steel, aluminium, glass, plastic or paper. The flying spot technique permits a linear scan across the width of the strip, however a number of problems exist:

1) The angles of illumination and detection must be carefully chosen to ensure that subtle defects will be detected.
2) Complex arrangements of lenses and mirrors may be required to ensure that the sensor has a linear response.
3) Insensitive to fine defects running along the length of the strip. Specular surfaces will reflect large amounts of light using the simple rule "angle of reflection is equal to angle of incidence". A linear defect, such as a scratch, running along the length of the strip will scatter light towards the detector and this is indistinguishable from light reflected directly from the surface.
4) Dimensional measurements are best performed using solid state cameras, although laser scanners have the advantage of potentially higher resolution.

Laser scanning cameras offer a large depth of focus, have no ancillary lighting requirements, and are relatively insensitive to radiation. In addition, different laser scanner designs may be produced for use in areas which are difficult to access using conventional cameras [80].

Retro-reflective scanning systems are used for inspecting glass and clear plastics [81]. A retro-reflective sheet, placed under the material to be inspected, will reflect the laser beam back towards the projector where it is sensed using a suitable light detector. The retro-reflector has the property of sending the reflected light beam back along the same path as the received beam, but diverging the return beam slightly. A complex optical arrangement incorporating a beam splitter directs the returned beam onto two separate photo-

multipliers and the analogue signals are used to detect defects in the glass sheet which may absorb, distort or scatter the light beam. Defect classification may be performed by an "Expert System" approach. Features are extracted from the image data and these are compared with the "rule set" for each defect type.

A commercial system has been produced by Sira using the retro-reflective technique. Linear defects down to 50μm wide and spot defects down to 300μm diameter can be detected in 1.5m wide photo-sensitive film at speeds of up to 200 metres/min **[82]**. In a second commercial application, a retro-reflective scanner has been installed for paint inspection at the Austin Rover Cowley works **[83]**. The scan rate and spot size are adjusted electronically to ensure 100% coverage of the workpiece, while image processing is performed by a hybrid hardware and software system. The weight of the scanner has been constrained by the 10kg capacity of the robot used to move the scanner over the vehicle body.

Some limited success has been reported in the use of linear CCD cameras for inspecting strip products. The major limitations are the large number of cameras which are required to achieved the necessary resolution and the bright light source needed with CCD devices **[81]**.

7.5 Concluding Remarks

Vision sensors are used in a wide range of applications; for example, inspection, sorting, gauging and process control. Solid-state cameras are flexible and offer high resolution. Such devices are often used in low-cost vision machine systems. Flying spot laser scanners, although less reliable than solid-state cameras, have a large depth of focus and are particulary suitable for use in radioactive environments.

Chapter 8
Visual Inspection and Surface Classification

The prototype laser scanner can be used for visual inspection, although the resolution will be limited by the sampling rate of the digital signal processing system, the rate at which the sensor is moved across the surface to be imaged and the scanning rate of the laser across the workpiece. Equation 5.3 gives a basic sensor resolution of 0.385mm for a scan rate of 20 s^{-1}. Figure 5 indicates that the scanning velocity must be limited to 40mm/s to ensure 100% coverage of the workpiece. There is a trade-off between sensor resolution and scan rate. Resolution is limited by the maximum sampling rate of the DSP system and the scan rate, while the scan rate will limit the maximum velocity at which the scanner can be operated.

The prototype mirror is inaccurate and this produces considerable variation in the amplitude of the scanner output signal (Figure 16). Detection of a seam position is relatively easy and compensation has been achieved by scaling the scan data and disregarding any intermittent loss of the seam position. Vision applications require 100% reliability and software routines are needed to reject abnormal scan data and ensure reliable operation of the scanner (with reduced performance) if any of the mirror faces are contaminated by dirt or grease or the light detector is temporarily occluded by smoke or fumes.

8.1 Noise Cancellation

The use of signal averaging for noise reduction is well known **[84]** (pp222-223). The scanner output signal is periodic and if the noise component is completely uncorrelated adding together (or averaging) n scans will improve the signal to noise ratio by a factor of $\sqrt{n}$.

The result of adding a number of separate scans is shown in Figure 33. It can be seen that the signal to noise ratio is improved by adding three scans, however adding five scans has increased the overall noise level due to slight differences in

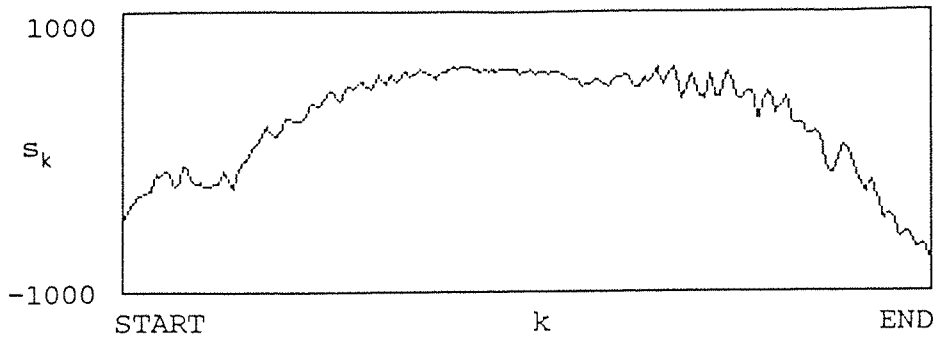

(a) A single scan

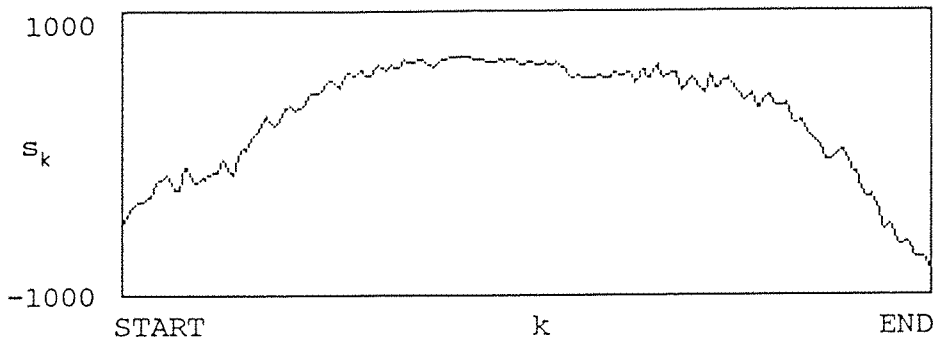

(b) Averaging three scans

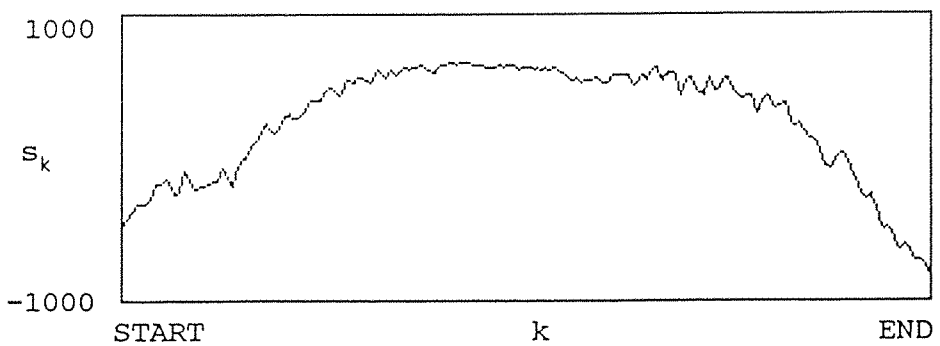

(c) Averaging five scans

s_k is the amplitude of the scan data

k is the sample number

START = 40*

END = 300*

* There is a 5ms delay (40 samples) before the laser is scanned across the leading edge of the light detector aperture. The scan time is 27.5ms (260 samples).

Fig.33 Averaging scan data for noise cancellation

the registration of the scan data. It was found that adequate noise reduction is provided by adding three scans, although this will reduce the effective scan rate and hence degrade the scanner performance.

Consider the addition of three successive scans produced using the prototype mirror which gives five good scans followed by three poor scans (Figure 16). The possible combinations are shown in Table 11.

Combination	Probability
3 good scans	3/8
2 good scans + 1 poor scan	2/8
1 good scan + 2 poor scans	2/8
3 poor scans	1/8

Table 11 Scan data from the prototype mirror

8.2 Rejection of Poor Scan Data

An effective grading technique is required to facilitate rejection of erroneous scan data. It will be insufficient to use the simple peak value of the scanner output as a comparative measure because if a surface discontinuity is located at either end of the detector aperture the peak value of the scan data will be considerably altered. A number of techniques are used to characterise a signal **[85]**:

8.2.1 Mean Value

The mean value is given by

$$\bar{X} = \frac{X_1 + X_2 + X_3 + \ldots X_n}{n} \qquad 8.1$$

If n = 2^k where k = 1,2,3 etc. the mean value can calculated quickly using integer arithmetic however this is unsuitable as a comparative measure because each scan is approximately symmetrical about zero giving a mean value approaching zero.

8.2.2 Standard Deviation

The standard deviation characterises the dispersion of a signal about the mean value and is given by

$$\sigma = \sqrt{\frac{(x_1-\bar{x})^2 + (x_2-\bar{x})^2 + (x_3-\bar{x})^2 + \ldots (x_n-\bar{x})^2}{n}} \qquad 8.2$$

The mean value of the scan signal is small and hence the standard deviation will approach the root mean square (RMS) value. In addition, evaluation of the standard deviation will be slower than the RMS value because of the additional calculations required.

8.2.3 RMS Value

The RMS value is given by

$$X = \sqrt{\frac{x_1^2 + x_2^2 + x_3^2 + \ldots x_n^2}{n}} \qquad 8.3$$

The RMS value is determined using floating point arithmetic from the magnitude of each sample in the data and will be relatively unchanged by slight fluctuations in the scanner signal due to varying surface texture.

Evaluation of the RMS value can be carried out using the variation in the output signal from the prototype scanner. It has been noted that adding three successive scans will result in one of four possible outcomes. If the RMS value is an effective comparative measure it should be possible to distinguish between these separate scan combinations. To verify this the RMS value was calculated for 400 scans taken from a uniform surface. The results obtained are shown in Table 12 and these may be divided into four separate groups as shown in Table 13.

Range		Freq
200.0	219.9	0
220.0	239.9	9
240.0	259.9	38
260.0	279.9	0
280.0	299.9	0
300.0	319.9	0
320.0	339.9	0
340.0	359.9	0
360.0	379.9	0
380.0	399.9	6
400.0	419.9	17
420.0	439.9	26
440.0	459.9	3
460.0	479.9	14
480.0	499.9	29
500.0	519.9	11
520.0	539.9	0
540.0	559.9	0
560.0	579.9	0
580.0	599.9	0
600.0	619.9	0
620.0	639.9	0
640.0	659.9	0
660.0	679.9	1
680.0	699.9	3
700.0	719.9	9
720.0	739.9	12
740.0	759.9	25

Range		Freq
760.0	779.9	17
780.0	799.9	7
800.0	819.9	10
820.0	839.9	12
840.0	859.9	10
860.0	879.9	5
880.0	899.9	0
900.0	919.9	0
920.0	939.9	2
940.0	959.9	3
960.0	979.9	2
980.0	999.9	4
1000.0	1019.9	4
1020.0	1039.9	9
1040.0	1059.9	9
1060.0	1079.9	9
1080.0	1099.9	4
1100.0	1119.9	1
1120.0	1139.9	4
1140.0	1159.9	7
1160.0	1179.9	6
1180.0	1199.9	14
1200.0	1219.9	15
1220.0	1239.9	13
1240.0	1259.9	19
1260.0	1279.9	8
1280.0	1299.9	3
1300.0	1319.9	0

Table 12 Distribution of RMS values for 400 separate scans

Class	Combination of scans	Range	Observed Values	Expected Values
1	3 good	920.0-1299.9	136	150
2	2 good 1 poor	660.0-879.9	111	100
3	1 good 2 poor	380.0-519.9	106	100
4	3 poor	220.0-259.9	47	50

Table 13 RMS values partitioned into four classes

Using the Chi-Square test **[86]** (pp148-151) to verify the statistical significance of the results obtained, if the probability of a recorded RMS value falling in class i is P_i we have a Null Hypothesis, Ho

Ho: $P_1 = 0.375$

$P_2 = 0.25$

$P_3 = 0.25$

$P_4 = 0.125$

There are 4 mutually exclusive classes and hence 3 degrees of freedom. The test value χ_o^2 is given by

$$\chi_o^2 = \sum \frac{(observed - expected)^2}{expected} \qquad 8.4$$

$$\chi_o^2 = \frac{(136-150)^2}{150} + \frac{(111-100)^2}{100} + \frac{(106-100)^2}{100} + \frac{(47-50)^2}{50} \qquad 8.5$$

$$\chi_o^2 = 3.06 \qquad 8.6$$

For the χ^2 distribution with v degrees of freedom there is probability α of observing a test value larger than $\chi^2_{\alpha,v}$

With 5% uncertainty and 3 degrees of freedom $\chi^2_{0.05,3} = 7.81$

In this case $\chi_o^2 < \chi^2_{0.05,3}$

Therefore we can accept the Null Hypothesis and conclude that the RMS value can be used to classify the scan data.

8.2.4 Autocorrelation Function (ACF)

The autocorrelation function is a measure of the correlation between the present value of a signal and its value in the near future **[87][88]**. It is simply a measure of the average product of a signal with a time shifted version of itself. Formally, for a sampled data sequence of length 2N+1 the ACF is defined as

$$r_{xx}(k) = \sum x_m x_{m+k} \qquad for\ -N \le m \le N \qquad 8.7$$

The ACF of a periodic signal will always be periodic while a random signal will exhibit a high degree of correlation for small time shifts but this will tend towards zero as the time shift is increased.

The ACF can be used to detect the presence of a signal in noise, however the theoretical basis is for signals of infinite extent ($N \rightarrow \infty$) and in practise it may be necessary to use a large numbers of samples to achieve good results. Lynn observes the effect on the estimated ACF of a signal using 100, 50 and 25 samples and notes that while increasing the sample size improves the accuracy, the results in all cases are poor **[84]** (pp90-93).

It is apparent that while the ACF provides a robust method of detecting a noisy signal the computation time is large with accuracy dependant on a large sample sequence. The RMS value provides a satisfactory qualitative measure although it is recognised that the ACF has potentially greater reliability and may be essential if the signal to noise ratio is degraded by a particular application of the scanner.

8.3 Surface Inspection

Surface discontinuities can be detected by differentiating the scan data and using a threshold to determine the position of a significant surface defect or blemish. A global threshold

has been employed for seam tracking but this will only detect the position of a well defined defect situated near the ends of the detector aperture and this will not provide the discrimination necessary for surface inspection. Instead, consider the use of a local threshold, that is a threshold based on attributes of the scan data in the region of the point of interest. It is not possible to derive a general model of the light detector on which to base the threshold because the response is dependent on the surface that is being scanned; a specular surface will reflect the laser beam directly onto a single point on the detector, while a diffuse surface will scatter light, some towards the detector. Specular and diffuse surfaces thus give different output signals (Figure 34) and the response for a particular surface can be modelled using a polynomial, r(k) given by

$$r(k) = \sum a_n k^n \qquad for\ 0 \le n \le M \tag{8.8}$$

The polynomial has order M and can be fitted to the scan data using the method of least squares **[89][90]**. To determine the order of polynomial for the "best fit" consider the scan data for specular and diffuse surfaces shown in Figure 34. Polynomials have been fitted to this data with the correlation shown in Table 14.

Order M	Correlation Coefficient	
	Diffuse Surface	Specular Surface
2	0.950157	0.950337
3	0.952699	0.954850
4	0.952708	0.957670
5	0.952712	0.958340
6	0.952725	0.960923

Table 14 Correlation of fitted polynomials

Coefficients of order higher than six are negligible and a third order polynomial was selected as increasing M gives only a small improvement in correlation. Third order polynomials

Diffuse Surface

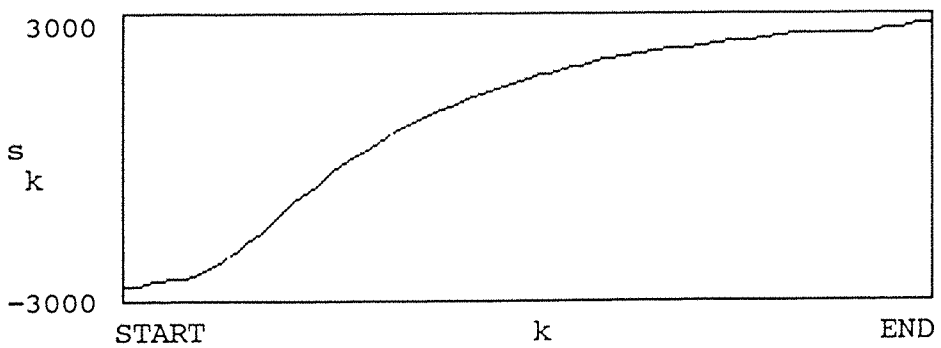

Specular Surface

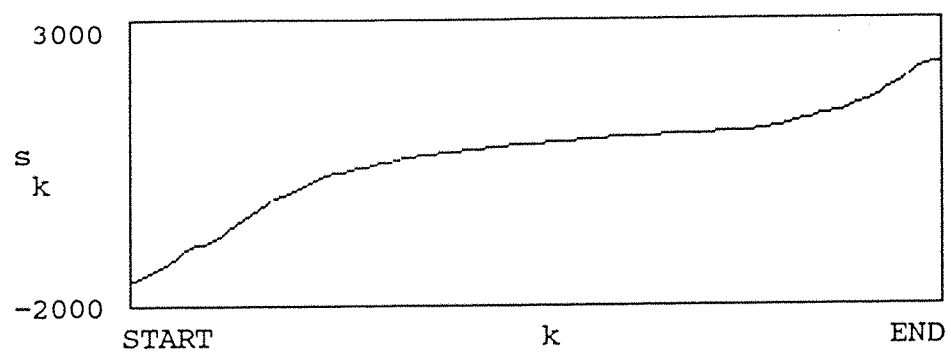

s_k is the amplitude of the scan data

k is the sample number

START = 40

END = 300

Fig.34 Scan data from specular and diffuse surfaces

have been fitted to the scan data from Figure 34 and the results are shown in Figure 35.

Surface inspection can be performed by differentiating the scan data and then applying a local threshold based on the polynomial model of the sensor output. The local threshold is given by

$$Local\ Threshold = \frac{d}{dt} r(k) \pm K_T \qquad 8.9$$

Where K_T is the threshold constant.

Figure 36 shows how this technique can be used to inspect a specular surface. Noise cancellation has been provided by averaging three separate scans. The RMS value for each scan is calculated and if this value is less than a reference level the data is rejected. The reference level is set during sensor initialisation so that approximately 38% of scans are discarded, effectively rejecting data from Class 3 and Class 4 (Section 8.2.3). The scan data in Figure 36 has three significant surface defects and these are clearly detected using the local threshold.

Comments

1) Differentiation has been performed using the central difference operator for seam detection in order to reduce noise caused by surface texture or small defects, however the first order backwards difference operator is preferred for surface inspection in order to maximise the sensitivity.
2) It is difficult to relate the pulse produced by the light detector to the severity of the defect (as judged by a visual inspection) and the threshold constant must be established empirically.
3) This technique can be used to detect the position of relatively well defined surface defects near the ends of the detector aperture. To ensure 100% coverage of the workpiece separate passes with the sensor must be interwoven so that the entire surface is covered by the

Diffuse Surface

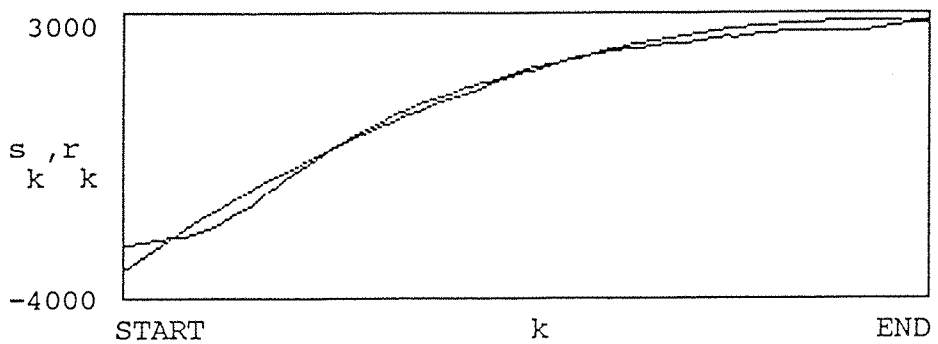

Specular Surface

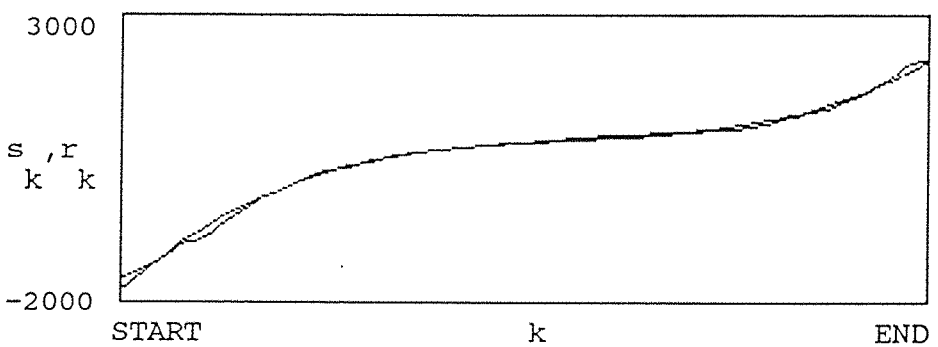

s_k is the amplitude of the scan data

r_k is the third-order polynomial model

k is the sample number

START = 40

END = 300

Fig.35 Fitting a third-order polynomial to the scan data

s_k is the amplitude of the scan data

r_k is the third-order polynomial model given by:

$$r_k = a_0 + a_1 k + a_2 k^2 + a_3 k^3$$

k is the sample number

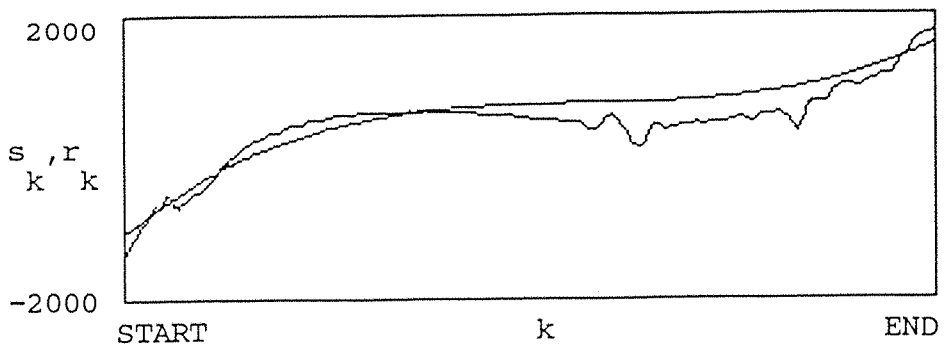

START = 40

END = 300

Differentiate scan data $\frac{d}{dt} s_k = s_k - s_{k-1}$

Differentiate polynomial $\frac{d}{dt} r_k = a_1 + 2a_2 k + 3a_3 k^2$

Local Threshold = $\frac{d}{dt} r_k \pm K_T$

Where K_T is the threshold constant

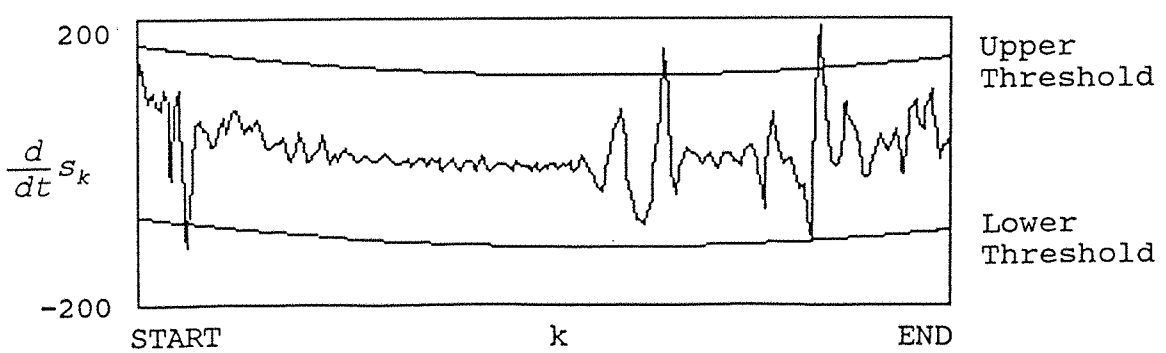

Fig.36 Surface inspection using a local threshold

sensitive regions of the detector. Alternatively, for diffuse surfaces which scatter light, two separate light detectors may be used in conjunction with a single projector. The detectors should be displaced such that the insensitive area of one is aligned with a sensitive region of the second.

4) Satisfactory results have been obtained for a range of surface types and defects, although the threshold constant must be evaluated separately for each operating condition.

5) The performance of the prototype laser scanner is poor when compared with traditional machine vision systems. Resolution is approximately 0.4mm with a basic scan rate of 20 s^{-1}. Software routines reject 38% of the scan data and average three successive scans giving an overall scan rate in the order of 4 s^{-1}. As a consequence, the operating speed of the scanner must be restricted to prevent blurring.

A simple qualitative measure of surface finish can be obtained by differentiating the scan data and using the dispersion of the data as an indication of surface texture **[91]**. The scan data must be scaled before differentiation to permit comparison of different surfaces. Typical results are shown in Figure 37. The scan data from a steel plate with good finish and a steel plate with some corrosion have been scaled such that the peak value in each case is 2048 and the data has been differentiated using the first order backwards difference operator. The mean value and the standard deviation of the differentiated data have been calculated, with the mean values close to zero because the differentiated data are approximately symmetrical about zero. Standard deviation characterises the dispersion of a set of samples about the mean value. In this case, the figure of 171.167 indicates poor surface finish compared with a value of 57.625.

8.4 Simple Geometric Inspection

The sensor can be used to form a simple pass/fail decision based on the general shape of an object. Consider the

X_k is the amplitude of the scan data from a steel plate with good finish

Y_k is the amplitude of the scan data from a steel plate with poor finish

k is the sample number

START = 40

END = 300

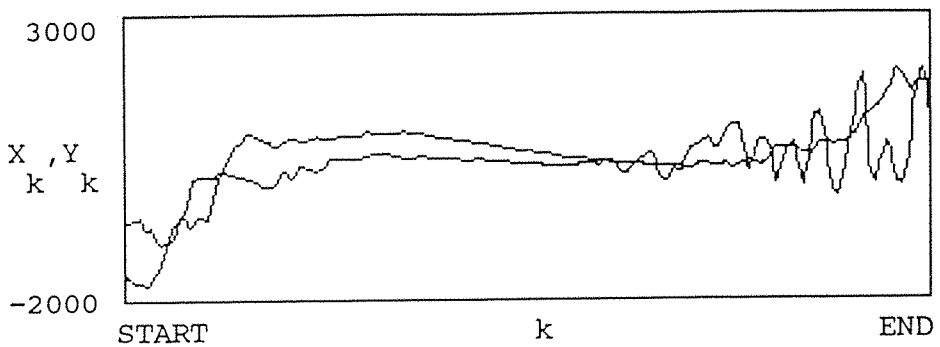

Differentiate scan data

$$\frac{d}{dt}X_k = X_k - X_{k-1} \qquad \frac{d}{dt}Y_k = Y_k - Y_{k-1}$$

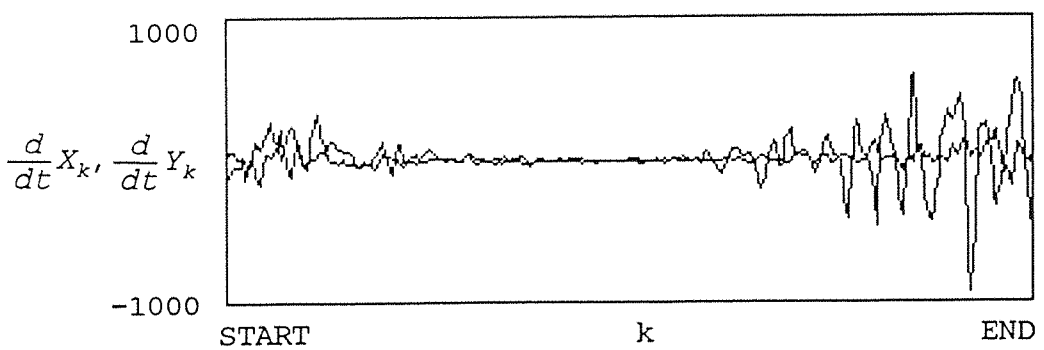

$$Mean\left(\frac{d}{dt}X_k\right) = 13.579 \qquad Stdev\left(\frac{d}{dt}X_k\right) = 57.625$$

$$Mean\left(\frac{d}{dt}Y_k\right) = 8.3 \qquad Stdev\left(\frac{d}{dt}Y_k\right) = 171.167$$

Fig.37 Qualitative surface inspection

inspection of biscuits travelling at constant speed on a conveyor. The edges of a biscuit can be sensed as it passes under the scanner and hence the width can be measured. If the biscuit is circular, the maximum width that is measured will be the diameter of the biscuit. Figure 38 shows a typical scan from a circular biscuit. The coarse surface texture of the biscuit can be distinguished from the uniform background, while the height of the biscuit and the geometry of the scanning mechanism cause a shadow adjacent to one side. A temporary loss of reflected laser light caused by the shadowing effect must be considered when devising an edge detection algorithm and the following solution has been employed; the scan data is differentiated and the leading edge of the biscuit is sensed using a positive threshold to detect the first peak in the differentiated signal. A negative threshold is then used to detect the trailing edge of the biscuit. Threshold levels are set using the polynomial modelling technique described in Section 8.3 and testing was carried out by measuring a series of dimensions using a circular biscuit with diameter 67mm. The results are summarised in Table 15.

Width (samples)	Measured Width (mm)	Actual Width (mm)
85	34.0	33.0
121	48.4	49.0
144	57.6	58.0
152	60.8	62.0
163	65.2	65.0
165	66.0	67.0

Table 15 Edge detection results

Comments

1) The measurement error is 3% which is adequate for many simple inspection applications, although the operating speed of the prototype sensor is limited because of the

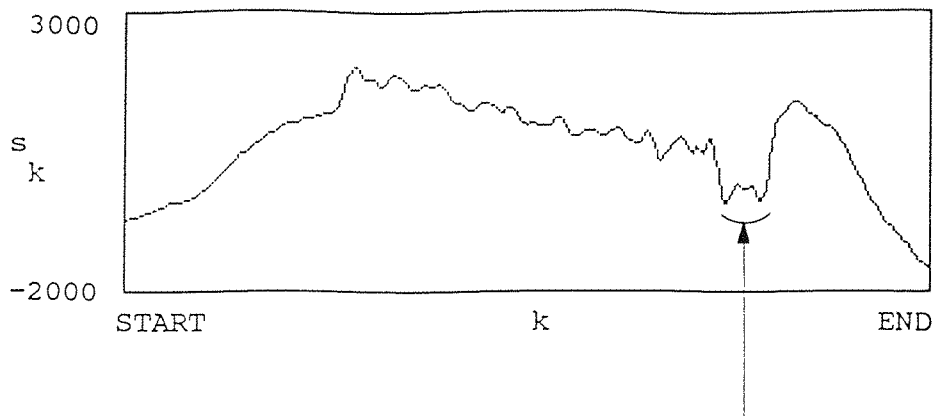

s_k is the amplitude of the scan data

k is the sample number

START = 40

END = 300

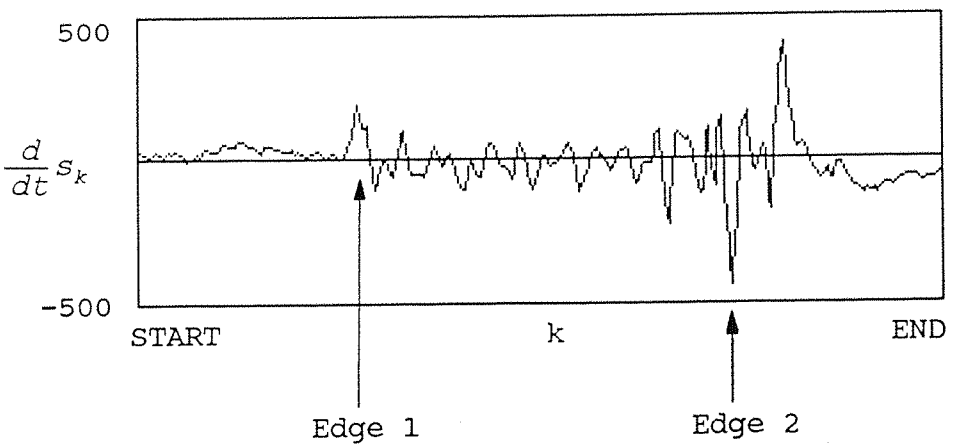

Edge 1 position = 111

Edge 2 position = 232

Separation = 232 - 111 = 121 samples

The sensor resolution is 0.4mm and hence the total separation is 48.4mm

Fig.38 Simple geometric inspection

low scan rate and the measured dimensions must be less than 100mm.

2) Edge detection is simplified by the height difference between the object under inspection and the background. In addition, surface texture may be used to discriminate between an object and the background.

3) Geometrical inspection of circular objects can be performed with relative ease as the measured width will change when the object is passed under the scanner, reaching a maximum when the diameter is measured. The maximum width can be compared with the nominal diameter of the object and the result used to signal a reject. Rectangular objects aligned with the scanner will have a measured width that remains relatively unchanged, while complex shapes can be inspected by constructing a two-dimensional profile from a number of individual scans. Precise control of the scan rate is essential, in addition to feedback of conveyor speed.

8.5 Surface Classification

It was observed in Section 8.3 that the output signal obtained from the scanner is dependent on the surface that is being scanned. This "signature" is dependent on the amount of light that is directly reflected from the workpiece. Specular and diffuse surfaces yield clearly different scan characteristics (Figure 34) and the scan signature can be used for surface classification.

A comparative measure is required to determine whether the difference between two scan signatures is significant or whether it arises from noise or other random effects. One such method is described by Chatfield **[86]** (pp143-146) and originates in statistical estimation techniques. A significance test is used to compare the mean values of two sets of samples. The standard error for each set is calculated and the test statistic is found by dividing the difference of the means by the standard error of the difference. The level of significance of a particular result will be interpreted in accordance with the normal distribution so that low figures

(less than 1.0) indicate a high level of confidence. Figure 39(a) shows the method applied to scan data from the same surface and Figure 39(b) is for scan data from two different surfaces. A test statistic of 0.235 indicates a very high level of confidence in the match, while 3.029 indicates low match probability.

8.6 Concluding Remarks

The prototype laser scanner has been used successfully for surface inspection, simple geometric inspection and surface classification. Reliability may be improved by using the RMS value of the sampled scan data as a measure of data integrity. Noise reduction can be achieved by averaging a number of separate scans, however this may cause blurring if the scanner is operated at high speed.

X_k is the amplitude of the scan data from a white diffuse surface

Y_k is the amplitude of the scan data from a white diffuse surface

k is the sample number

START = 40

END = 300

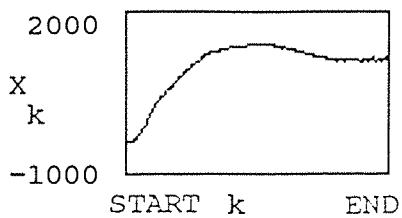

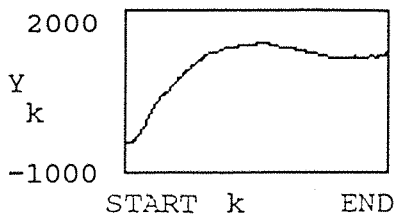

$Mean(X_k) = 992.6$

$Stdev(X_k) = 617.6$

$Mean(Y_k) = 979.7$

$Mean(Y_k) = 635.3$

Find the standard error in each case

$$\frac{617.6}{\sqrt{260}} = 38.3$$

$$\frac{635.3}{\sqrt{260}} = 39.4$$

Find the standard error of the difference

$$\sqrt{38.3^2 + 39.4^2} = 54.9$$

Calculate the ratio of the standard error of the difference to the difference of the means

$$r = \frac{992.6 - 979.7}{54.9}$$

$$|r| = 0.235$$

Fig. 39(a) Comparing scan data

X_k is the amplitude of the scan data from a black specular surface

Y_k is the amplitude of the scan data from a grey specular surface

k is the sample number

START = 40

END = 300

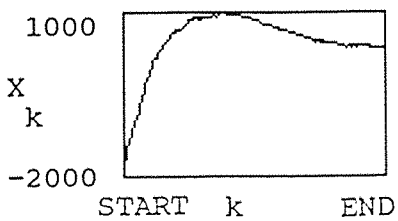

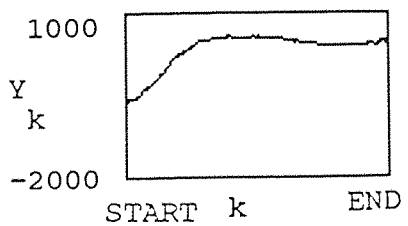

$Mean(X_k)$ = 472.2

$Stdev(X_k)$ = 691.7

$Mean(Y_k)$ = 321.3

$Mean(Y_k)$ = 409.6

Find the standard error in each case

$$\frac{691.7}{\sqrt{260}} = 42.9$$

$$\frac{409.6}{\sqrt{260}} = 25.4$$

Find the standard error of the difference

$$\sqrt{42.9^2 + 25.4^2} = 49.9$$

Calculate the ratio of the standard error of the difference to the difference of the means

$$r = \frac{472.2 - 321.3}{49.9}$$

$$|r| = 3.029$$

Fig. 39(b) Comparing scan data

Chapter 9
Discussion

9.1 The Scanner Optics

Two main problems are apparent with the simple projection technique used by the laser scanner:

1) The angle of reflection of the laser beam from the surface of the workpiece varies with scan position.
2) The scanning speed varies with scan position.

Commercial laser scanning systems employ specially designed lenses situated between the scanning element and the workpiece and adjust the laser spot size automatically to cope with the necessary depth of focus [58]. This solution is expensive and it has been shown that seam tracking and simple vision tasks can be performed effectively without recourse to complex projector optics.

Certain colour features cannot be detected using the laser scanner because the laser light is monochromatic. Three separate lasers having different wavelengths may be used to resolve colour, but such systems are very expensive [57].

Multiple reflections may occur when the laser beam is reflected from the workpiece and then, after reflection from the laser chassis, back onto the workpiece. Specular surfaces are more susceptible to this problem because more light is directly reflected and the front panel of the scanner chassis must be coated with a non-reflecting material.

The major shortcomings of the simple laser scanner are caused by the laser beam which originates from a single point and hence is scanned through an arc. Referring to Figure 40 it can be seen that if the polygon mirror is rotated by θ_p the laser will be scanned through a total angle of $2\theta_p$ (optical lever principle). The mirror has eight faces and for one complete scan θ_p will increase from 0° to 45° and the laser will be

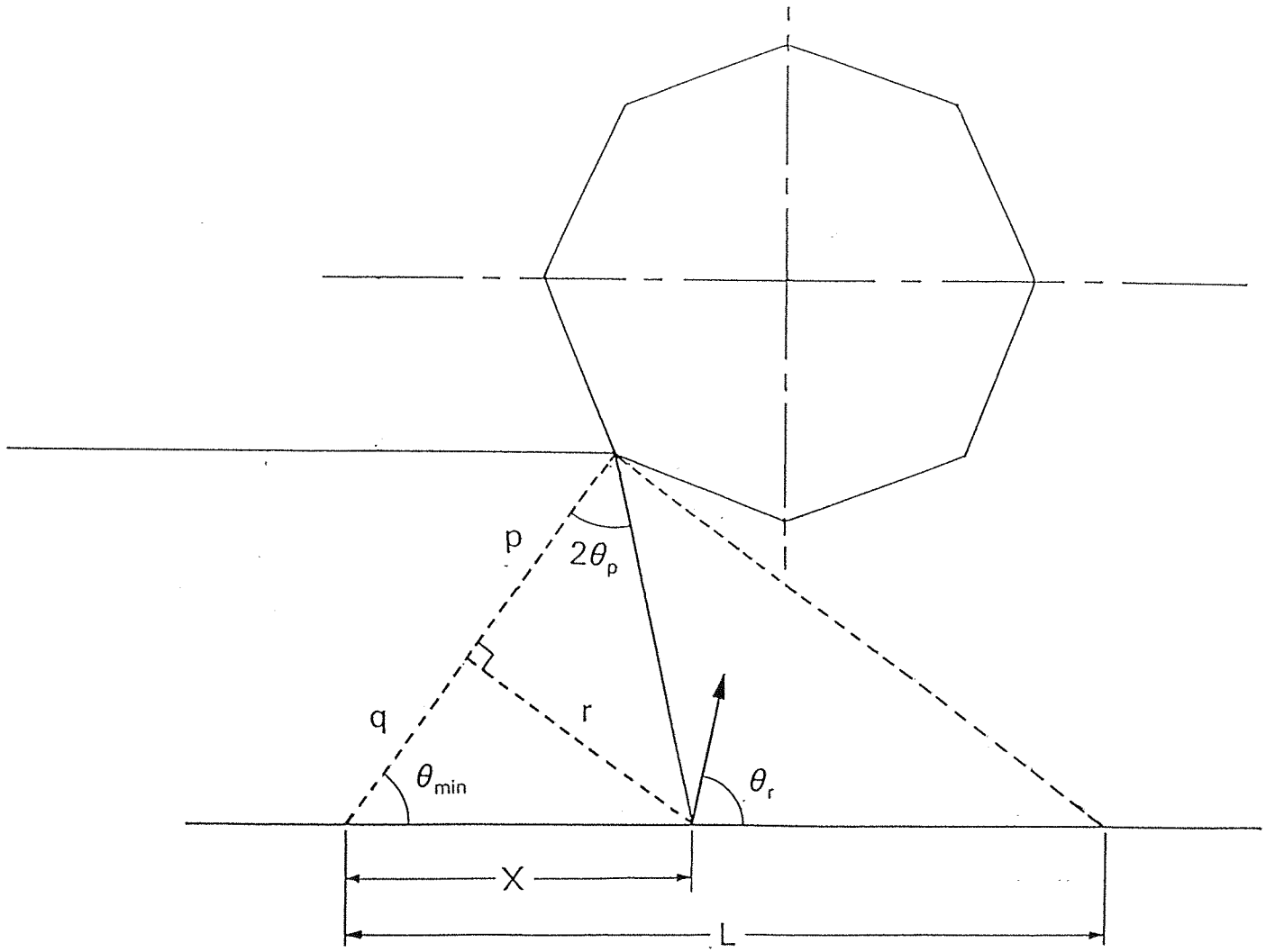

Fig.40 Determination of scan speed

scanned through a total angle of 90°. The angle of reflection of the laser from the workpiece is given by

$$\theta_r = 180 - (\theta_{min} + 2\theta_p) \qquad 9.1$$

The position of a discontinuity is determined using the optical signal received by the light detector. The relationship between the position of a discontinuity on the surface of the workpiece and the measured position will be dependent on a number of factors; the scan position, the vertical position of the discontinuity, the stand-off height and the surface finish. Sensor error due to the angle of reflection from the workpiece is minimised by placing the light detector close to the workpiece, although this places the light detector in a vulnerable position, especially when the sensor is used for weld seam tracking. Varying the stand-off height will cause an error in the measured position of the discontinuity. A maximum position error of 4mm was observed for a ±5mm variation in the vertical position of the scanner.

The scan speed of the laser may be determined using Figure 40 and a derivation is shown in Appendix 3. The scan speed is given by Equation A3.12 and this is clearly a non-linear function of the mirror position. The position of a discontinuity is determined when light is either reflected directly from the discontinuity and collected by the detector or scattered causing a reduction in the measured light level. Position is resolved from the point on the light detector which receives this change in light level and this will be independent of the scan velocity, although the duration of the transient disturbance in the optical signal will be contingent on the position of the discontinuity.

The sensor must be operated with a constant stand-off height. A cartesian robot has been used for testing the laser scanner, and a constant stand-off height is achieved simply by fixing the Z axis position. If the vertical position cannot be fixed accurately an additional sensor must be used to measure the distance between the laser scanner and the workpiece.

Transducers using optical triangulation are widely used for distance measurement and such a device has been successfully used to measure the stand-off height of a laser scanner in another application [36].

9.2 Light Collection System

The overall response of the sensor is non-linear, with poor sensitivity at the centre of the scan. Signals from two photo-diodes are subtracted to cancel variations in ambient light levels and reduce common mode noise. The disadvantage of this differential configuration is that when a discontinuity is located near the centre of the light detector, signals of approximately equal amplitude will be received by the photo-diodes, resulting in a low output voltage from the differential amplifier.

During seam tracking the robot will attempt to position the centre of the light detector above the seam. The light detector sensitivity is poor in this region, causing some difficulty in extracting the seam position when the end-effector is located close to the seam. Tracking algorithms have been devised using the pre-programmed seam width to locate the seam which is normally a fairly significant feature. Surface inspection may be performed by overlapping a number of sweeps with the laser scanner. Alternatively, for diffuse surfaces which scatter light, two separate light detectors, suitably displaced, may be used with a single projector.

9.3 Seam Tracking

Seam tracking is achieved by mounting the sensor ahead of the tool at the robot end effector. One major advantage of this look-ahead configuration is that compensation is possible for the delayed reaction of the robot controller. Smith and Lucas [50] have reported good results using a sensor sited 10mm ahead of the weld pool. This distance will prevent corruption of the sensor signal due to the molten weld pool, but is close enough to compensate for any heat distortion of the workpiece.

The performance of the prototype laser scanner is limited by the maximum scan rate of the laser across the workpiece and the maximum sampling rate of the DSP system. The prototype scanning mechanism gave a maximum scan rate of 40 scans/s using a polygon mirror with 8 sides and a stepping motor having 1.8° step size operated at 300 rpm. The DSP routines are implemented using an IBM PC/AT computer which can achieve a maximum useful sampling rate of 8KHz when the converted values are stored directly in memory. The design resolution of the scanner is 0.4mm and this has limited the scan rate to 20 s^{-1}. Software has been written using a High Level Language (HLL) and a typical software loop time of 200ms has been achieved for seam tracking. The scan period is 50ms, with a further 150ms required to process the data and extract the seam position.

A two-stage seam tracking algorithm has been employed. One complete scan is sampled and the converted values are stored in memory. The scan data must be scaled to compensate for variations in light detector output caused by the hardware tolerances of the scanning mechanism. Differentiation is used to highlight edges in the scan data, with satisfactory results obtained using the central difference operator. Initially a global threshold is applied to the differentiated data. The light detector has a non-linear response and this threshold may not establish the position of a seam close to the centre of the detector aperture. In this situation the absence of reflected light may be used to recognise the seam position. The height difference inherent with some seam configurations will cause a shadow, while a gap between two components will give no reflected light. Reliability is improved by disregarding scan data when the seam position cannot be determined, thus introducing a variable dead-time into the sensor transfer function. Tracking is discontinued when five successive scans indicate that no seam is present.

The sensor has been interfaced to a gantry robot and seam tracking has been performed successfully at a typical MIG welding speed of 25mm/s. A proportional control law has been

adopted, where the robot is moved along the Y axis at a constant speed, with the X axis speed proportional to the sensed error. The Z axis position (sensor stand-off height) is fixed.

The proportional gain settings, controller dead-band and robot feed rate control parameters have been adjusted during a series of tests. Poor results have been obtained using a constant proportional controller gain. Large gain values cause an oscillatory response, while reducing the gain gives a sluggish response and large tracking errors. The control law which has been employed has unity gain for small position errors and a gain of two for larger position errors. This two-stage characteristic gives a rapid response when the error is large and then reduces the controller gain when the error is small, thus preventing overshoot. The X axis velocity is set to zero when the error is less than 3 to prevent the robot oscillating about the seam when the tracking error is small.

The results obtained using this control algorithm are summarised in Table 16. As expected, tracking accuracy is increased by reducing the tracking speed. Reducing the robot acceleration/deceleration time has no discernable effect as the robot is unable to respond quickly to programmed speed changes. Increasing the acceleration/deceleration time restrains the response to changes in seam position and hence increases the tracking error.

Measurement noise can be reduced by smoothing the sensor output. In this case averaging the last three seam positions has increased the tracking accuracy, but the high frequency performance of the system has been degraded.

Test Parameter	Acc/Dec Time (s)	Tracking Speed (mm/s)	Max Error (mm)
Varying the tracking speed	0.25	10	18.4
	0.25	25	26.0
	0.25	50	34.0
Varying the Acc/Dec time	0.5	25	28.4
	0.117	25	26.0
Filtering the error data	0.25	25	24.4

Table 16 Seam tracking results

It was decided not to pursue an optimum set of robot control parameters because the tracking accuracy is governed by a number of factors in addition to the performance of the sensor system. External factors include the dynamics of the robot, the software loop time of the robot controller and the operating speed of the serial link used to connect the robot controller to the intelligent axis control cards. The sensor has a resolution of 0.4mm which is adequate for many seam tracking applications.

Steady state following errors result when tracking inclined sections of the seam. These errors cannot be eliminated using a proportional control law. One solution is to employ a two-term "proportional plus integral" controller **[71]**. The integral control action will reduce steady state errors.

TIG welding is performed at a typical speed of 10mm/s compared with 25mm/s for MIG welding. Despite the slower tracking speeds, considerable problems have been experienced with commercial TIG welding systems. The welding process generates considerable RF interference and extensive screening and protection is required for electronic equipment close to the torch **[18]**. The prototype laser scanner uses a range of noise reduction techniques; differential amplifiers provide common mode noise cancellation and screened cables are used for all sensor signals. The photo-diode signals are amplified close to

the light detector and all subsequent signal processing is performed using analogue electronics and DSP techniques at the sensor controller, situated approximately 2m from the robot end effector. Considerable interference will be present in any industrial environment and low noise design techniques have been employed at each stage in the laser scanning system.

Weld seam tracking requires a compact sensor package to reduce accessibility problems. The prototype laser scanner can be used to track lap joints with a minimum plate thickness of 4mm, single V-butt joints and square butt joints having a minimum root gap of 4mm. Fillet joints cannot be tracked because of the laser scanner configuration (Figure 41). Protection of the sensor can be achieved using baffles, disposable windows or a gas shroud. Cooling may be necessary to regulate the scanner temperature and this can be effected using a supply of cold water or a forced air flow **[43]**. The Helium-Neon laser has a wavelength of 633nm which corresponds to a window in the broad spectrum of radiation produced by the arc **[30]** and a narrow band spectral filter may be used to isolate the laser light from the background radiation **[55]**.

Seam sealing is used extensively during car production and this process is notoriously difficult to automate. Uniform application of the adhesive or sealant is essential and high precision volume dosage devices must be used because of variation in sealant viscosity with temperature. Test runs are used during commissioning because the actual path of the robot may differ from the programmed path, especially when the robot is operated at high speed. Many industrial robot controllers provide analogue outputs of total nozzle movement which are used to meter adhesive or sealant dosage **[92]**.

One successful seam tracking system is described by Sawano *et al* **[93]**. A solid state camera is used to track the seam at speeds of up to 440mm/s. The sensor has a software loop time of approximately 34ms and gives a tracking accuracy of ±2mm. It may be inferred from the results obtained using the prototype laser scanner that the system may be enhanced to

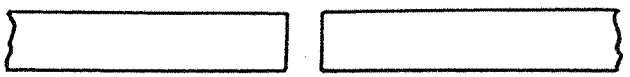

Square Butt

Single V

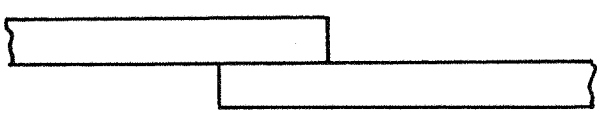

Lap

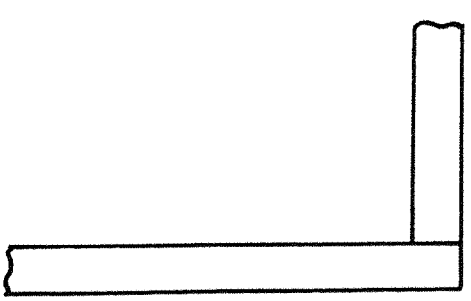

Fillet

Fig.41 Types of weld seam

allow successful seam tracking at this higher speed. Performance may be increased by using an autonomous I/O technique to acquire the scan signal and porting the signal processing algorithms to a dedicated DSP processor.

Automated Guided Vehicles are widely used for moving material between processing stations, shipping docks and storage areas. Vehicles are available for a variety of applications; these include towing, load carrying and pallet collection. Carts are propelled by electric motors powered from lead-acid batteries mounted in the AGV at speeds ranging from 200 to 1000mm/s **[94]**. The majority of AGVs follow cables embedded in the floor which carry low voltage AC signals. Such systems are inflexible, but the wires are almost immune to damage **[95]**. Optical guidance systems use lines or marks on the floor which are sensed by a detector mounted on the vehicle. These lines are prone to damage and consequently this technique is only used in "clean" environments, although it permits a high degree of flexibility.

The laser scanner has been used for seam tracking at a maximum speed of 50mm/s compared with a maximum AGV tracking speed of 1000mm/s. In general, AGV positioning accuracy will be application dependent; vehicles used to deliver components to an automated manufacturing system may require high precision, while a stop accuracy of ±10mm is sufficient for a simple load carrying cart. Again, sensor performance can be enhanced to permit AGV guidance by modifying the scan rate and using a faster DSP platform.

Some existing AGV systems make use of bar-coded instructions and it is speculated that the laser scanner may be used to read such track-side codes, although the sensor resolution must be improved by increasing the sampling rate of the DSP system.

9.4 Vision Applications

High reliability is an essential feature of any machine vision system and a number of techniques are used to enhance the

performance of the prototype laser scanner. It was found that the RMS value provides a reliable qualitative measure for the integrity of the sampled scan data. After quantisation the RMS value of the scan data is calculated and compared with a threshold level. The threshold level is set during the initialisation of the sensor so that 38% of scans with low RMS values are rejected. Noise reduction is achieved by averaging three successive scans, however this must be used with care when the scanner is operated at high speed. Successive scans may detect a single discontinuity at different positions, especially when the scanner is moved laterally across the discontinuity at high speed. Adding these separate scans will not give a well defined signal from the discontinuity. Instead, the image will be "smeared" so that the position cannot be resolved successfully. The effect of the software routines which reject poor scan data and average scans for noise cancellation is to reduce the overall scan rate to 4 s^{-1}.

Surface inspection can be carried out by differentiating the scan data and using a local threshold to determine the position of any significant surface defect or blemish. The local threshold is based on a polynomial model of the scanner output signal and hence the threshold level is effectively determined by applying a low-pass filter function to the scan data itself. In practice it is difficult to relate the magnitude of the scanner output pulse to the severity of a defect and a separate threshold constant must be established for every operating condition.

Poor surface finish will introduce a high frequency "noise" component into the scanner output signal. A qualitative measure of surface texture can be obtained by differentiating the scan data and considering the dispersion of the result. The standard deviation of the differentiated data is calculated, with low figures indicating good surface finish. The scan data must be scaled before differentiation to compensate for variations in the amplitude of the scan data.

Surface inspection is limited by the pass-band of the anti-aliasing filter. The prototype sensor system uses a second-order Butterworth filter with a 2kHz cut-off frequency. This must be extended to detect small surface defects and any increase must be matched by the corresponding increase in sampling rate.

Geometric inspection can be used to verify the basic shape of an object. Tests have yielded a basic measurement accuracy of ±3% which is suitable for many simple inspection applications. The height difference between the object under inspection and the background simplifies the edge detection process, although care must be taken. The laser originates from a fixed point and the height difference may cause a shadow. The temporary loss of reflected laser light will cause a transient in the light detector output which must be separated from the true edge of the object.

The light detector output is dependent on the surface that is being scanned; a specular surface will reflect the laser beam directly onto a single point on the detector, while a diffuse surface will scatter light, some towards the detector. The output signal is thus dependent on the amount of light that is directly reflected or scattered from the surface and this scan signature can be used for surface classification. Scan signatures may be compared using a significance test and satisfactory results have been obtained using the ratio of the standard error of the difference to the difference of the means. The comparison will indicate whether the difference between two scan signatures is significant or whether it arises from noise or other random effects. The test statistic is related to the normal distribution, with low figures indicating high match probability.

Neural networks may be used for pattern classification and it is speculated that a neural computer may be used to classify the scan signatures. A neural computer has been used in a comparable application, that of predicting the quality of spot welds [96]. Weld voltage and current is recorded and these

parameters are forged into a time dependent function, the "weld signature". The neural network is used to predict the integrity of a weld from its signature. Training is performed using signatures from good welds only, found by destructive testing.

Scanner performance is limited because the scan rate cannot be increased without degrading the resolution. Sampling the light detector output using an autonomous I/O technique such as Direct Memory Access (DMA) will increase the maximum sampling rate and reduce the software loop time as scan data may be sampled while the previous scan is processed by the CPU. Additional hardware will be required and high performance analogue input/output cards are available for use with the PC/AT bus (also known as Industry Standard Architecture). A typical single channel data acquisition board employing DMA may give a sampling rate in the order of 100kHz **[97]**.

The use of a high performance microprocessor or a specialised DSP processor will also improve system performance. Such devices are expensive and often lack comprehensive development tools. A large range of low cost software is available for the PC, the hardware is relatively inexpensive and considerable experience has been gained using the PC for a wide range of industrial applications.

9.5 Further Work

The work described in this thesis may be extended in the following areas:

1) The sensor may be packaged for practical one-pass weld seam tracking. A spectral filter, centred at 633nm, is required to isolate the laser from the background radiation. Satisfactory protection of a one-pass sensor is afforded using a disposable glass window in conjunction with a forced air flow, while cooling can be provided using a chilled water supply **[43]**.

2) The scanning mechanism may be refined in order to reduce the size of the sensor package and eliminate variation in the scan speed. Alternate scanning elements include oscillating mirrors and acousto-optic deflectors, while scanning the laser through an arc will give constant scan speed.

3) The laser scanner cannot resolve depth and a simple optical triangulation sensor could be integrated with the sensor package to measure stand-off height. Alternatively, a range finder could be used to synthesise the height profile of the workpiece. This information could be used to control the arc welding process. Parameters such as welding speed, heat input, filler metal deposition rate and orientation of the torch could be adjusted automatically.

4) Performance of the prototype sensor may be enhanced by using some form of autonomous I/O technique to quantise the light detector output. The software loop time will be improved considerably by porting the algorithms to a specialised DSP processor.

5) Surface inspection has been performed using differentiation to highlight transients in the scan signal. The sensor has a non-linear response and it is difficult to relate the signal produced by the light detector to the severity of a surface defect. This classification may be possible using a neural network. Perhaps the network could be trained to differentiate between "good" and "bad" scan data as judged by a visual inspection.

6) The laser scanner has been used for surface classification, with a statistical technique employed to characterise surface type. Neural networks are widely used for pattern classification and this technique may allow a more reliable comparison.

Chapter 10
Conclusions

1) Seam tracking has been performed successfully at speeds used for MIG arc welding. The tracking accuracy is clearly influenced by the performance of the robot, however, the prototype sensor has a resolution of 0.4mm which is suitable for many seam tracking applications.

2) Sensor performance is constrained by two interrelated factors; the scan rate of the laser and the sampling rate of the DSP system. Increasing the scan rate will reduce the resolution unless the sampling rate is also increased. The maximum sampling rate is limited by the performance of the DSP system.

3) The sensor has a non-linear response caused by variation in the scan speed and the characteristics of the light detector. Surface discontinuities can be detected by differentiating the scan data and employing a thresholding technique. Well defined discontinuities can be detected using a global threshold, while a local threshold, based on the scan data itself, will detect subtle defects near the ends of the detector aperture. Edge detection is facilitated by a height difference; for example, when tracking a lap joint. If a seam cannot be detected using a suitable threshold its position may be resolved using the optical signal resulting either from a root gap, or the shadow caused by a height difference. During the course of this work a seam has been simulated using a strip of tape and the position may be resolved using the uniform reflection which results.

4) Surface inspection is best performed by interlacing passes with the scanner. In this way the entire surface of the workpiece may be covered by the sensitive regions of the detector.

5) The sensor must be operated at a fixed height above the workpiece. The angle of reflection of the laser varies with scan position and to minimise measurement error this stand-off height must be small, possibly placing the sensor in a vulnerable position.

6) A high precision scanning mechanism is not required. Software routines have been developed to correct or discard inconsistent scan data. These routines improve the noise performance of the sensor system and allow reliable operation if one or more faces of the polygon mirror are damaged.

7) Small surface defects will not be sensed unless the pass-band of the anti-aliasing filter is extended. This in turn will require an appropriate increase in sampling rate.

8) Results obtained using the prototype laser scanner indicate that the system may be easily enhanced for use in applications such as sealant application and AGV guidance.

9) The geometry of the scanning mechanism gives rise to a relatively bulky sensor package and this causes accessibility problems. These may be eased by fixing the sensor on a rotary mount. The additional degree of freedom will assist with sensor placement in confined spaces.

10) The PC/AT computer is a useful development platform, however, even with a floating point maths co-processor, performance is limited. No problems have been experienced with the speed of the DOS operating system.

References

1. British Robot Association, "Robot Facts 1990", Annual Report of UK Investment in Robot Automation in Manufacturing Industry.

2. A. Pugh, The Robot Story, In "IEE Computing and Control Engineering Journal", vol. 2 no. 1, pp13-21, January 1991.

3. J. P. Trevelyan, Sheep Shearing by Robot - An Update, In "The Industrial Robot", vol. 19 no. 1, pp23-24, March 1992.

4. M. P Groover, M. Weiss, R. N. Nagel and N. G. Odrey, Industrial Robotics: Technology Programming and Applications, M°Graw Hill, 1986.

5. J. Hartley, Robots at Work, IFS Publications, 1983.

6. P. Coiffet and M. Chirouze, An Introduction to Robot Technology, Kogan Page, 1982.

7. R. Miller, Fundamentals of Industrial Robots and Robotics, pp47-83, PWS-Kent Publishing, 1988.

8. T. Kenjo and S. Nagamori, Permanent-Magnet and Brushless DC Motors, Oxford University Press, 1985.

9. D. J. Todd, Fundamentals of Robot Technology, Kogan Page, 1986.

10. A. Pugh (ed.), Robot Sensors Vol. 1: Vision, IFS Publications, 1986.

11. A. Pugh (ed.), Robot Sensors Vol. 2: Tactile and Non-Vision, IFS Publications, 1986.

12. G. M. Mair, Industrial Robots, pp195-217, Prentice Hall, 1988.

13. V. J. Pavone, User-Friendly Programming for Arc Welding Robots, In "Robotic Welding", ed. J. D. Lane, pp295-315, IFS Publications, 1987.

14. J.J. Craig, Introduction to Robotics: Mechanics and Control, pp281-300, Addison-Wesley Publishing, 1986.

15. V. Mangold, Robot arc welding system design, In "The Industrial Robot", vol. 16 no. 3, pp143-148, September 1989.

16. R. Smith, Welding Technology for Competitive Manufacture, In "Assembly Automation", vol. 11 no. 2, pp18-22, 1991.

17. E. Appleton and D. J. Williams, Industrial Robot Applications, pp150-169, Open University Press, 1987.

18. B. Rooks, Welding robots - the state of the art, In Welding and Metal Fabrication, pp238-242, June 1991.

19. A. Pugh, Second generation robotics and robot vision, In "Robotic Technology" ed. A. Pugh, pp1-9, Peter Peregrinus, 1983.

20. E. Appleton and D. J. Williams, Industrial Robot Applications, pp150-169, The Open University Press, 1987.

21. R. Birrel, Choosing the right weld sensor, In "The Industrial Robot", vol. 17 no. 4, pp210-212, December 1990.

22. KUKA commercial literature, Robotics: Introduction with Examples of Applications, Verlag Moderne Industrie, 1987.

23. B. Rooks, Large fabrications can be welded by robot, In "The Industrial Robot", vol. 12 no. 3, pp175-177, September 1985.

24. D. J. Todd, Fundamentals of Robot Technology, pp107-108, Kogan Page, 1986.

25. G. E. Cook, K. Andersen, K. R. Fernadez, M. E. Shepard and A. M. Wells, Jr, Electric Arc Sensing for Robot Positional Control, In "Robotic Welding", ed. J. D. Lane, pp181-216, IFS Publications, 1987.

26. Y. Munezane, T. Watanabe, A. Iochi and T. Sekino, A Sensing System for Arc Welding Robots, In "Robotic Welding", ed. J. D. Lane, pp265-274, IFS Publications, 1987.

27. Z. Smati, D. Yapp and C. J. Smith, Laser Guidance System for Robots, In "Robotic Welding", ed. J. D. Lane, pp91-103, IFS Publications, 1987.

28. G. Edling and T. Porsander, Adaptive control of torch position and welding parameters in robotic arc welding - Examples and practical use, Proc. International Symposium on Industrial Robotics, pp359-363, 1984.

29. G. Edling, Programming, process control and use of sensors in robot arc welding, Proc. International Symposium on Automation, vol. 2, pp1819-1827, 1984.

30. W. J. P. A. Verbeek, L. J. H. F. Beckmann and G. L. Oomen, Control Strategy for an arc-welding robot under sensory guidance, Proc. International Conference on Robot Vision and Sensory Controls, pp541-550, 1985.

31. G. L. Oomen and W. J. P. A. Verbeek, A Real-Time Optical Profile Sensor for Robot Arc Welding, In "Robotic Welding", ed. J. D. Lane, pp117-128, IFS Publications, 1987.

32. G. L. Oomen, W. J. P. A. Verbeek and K. Ohlsen, ARC welding process control with an optical profile sensor, Proc. International Conference on Robot Vision and Sensory Controls, pp101-114, 1988.

33. S. Bangs, Laser vision robot guides welding arc, In "Welding design and fabrication", vol. 57 no. 11, pp45-48, November 1984.

34. M. Björkelund, A True Seam-Tracker for Arc Welding, In "Robotic Welding", ed. J. D. Lane, pp167-177, IFS Publications, 1987.

35. G. Edling, New generation of seam tracking systems, Proc. British Robot Association Conference, pp5-10, 1986.

36. Anon., Testing technologies for large-scale welding jobs, In "The Industrial Robot", vol. 15 no. 3, pp151-154, September 1988.

37. L. Yen, W. Lin and C. Dinghua, A new vision system of weld seam tracking, Proc. International Conference on Robot Vision and Sensory Controls, pp569-574, 1985.

38. H. C. F. M. Wezenbeek, weld puddle observation in the presence of the arc for seam tracking purposes, Proc. International Conference on Robot Vision and Sensory Controls, pp551-556, 1985.

39. P. Drews, B. Frassek and K. Willms, Optical Sensor Systems for Automated Arc Welding, Robotics, vol. 2, pp31-43, 1986.

40. P. Drews and A. H. Kuhne, An automatic welding system, Proc. International Conference on Advanced Welding Systems, pp191-198, 1987.

41. D. Brzakovic and D. T. Khani, Weld pool edge detection for automatic control of welding, IEEE Trans. Robotics and Automation, vol. 7 no. 3, pp397-403, 1991.

42. S. R. Ruocco, Robot Sensors and Transducers, The Open University Press, 1987.

43. W. F. Clocksin, J. S. E. Bromley, P.G. Davey, A. R. Vidler and C. G. Morgan, An Implementation of Model-Based Visual Feedback for Robot Arc Welding of Thin Sheet Steel, In "The International Journal of Robotics Research", vol. 4 no. 1, pp13-26, 1985.

44. B. Rooks, Advancing sensor technology into industry, In "The Industrial Robot", vol. 12 no. 1, pp10-13, March 1985.

45. B. Rooks, Advanced technology gives entry into new markets, In "The Industrial Robot", vol. 13 no. 3, pp157-159, September 1986.

46. Huang Nan, R. J. Beattie and P. G. Davey, A Rule-Based System for Interpreting Weld Seam Images, In "The International Journal of Advanced Manufacturing Technology", vol. 3 no. 2, pp111-121, 1988.

47. B. Rooks, Vision seam tracking extends to TIG, In "The Industrial Robot", vol. 14 no. 4, pp207-208, December 1987.

48. W. R. Koelbl and C. G. Morgan, An optical seam tracker in practical applications, Proc. International Symposium on Industrial Robotics, pp233-240, April 1988.

49. R. W. Richardson, D. A. Gutow, R. A. Anderson and D. F. Farson, Coaxial Arc Weld Pool Viewing for Process Monitoring and Control, In "Welding Journal", pp43-50, March 1984.

50. J. S. Smith and J. Lucas, A vision-based seam tracker for butt plate TIG welding, J. Phys. E: Sci. Instrum., vol. 22, pp739-744, 1989.

51. S. Clark, J. Lucas and A. B. Parker, Seam tracker for TIG welding, IEE Proceedings, vol. 132, pt. D, no. 4, 1985.

52. K. Koskinen, P. Kohola, J. Hirvonen, J. Annanpalo, H. Lehtinen and K. Vartiainen, Experimental vision based robot system for ARC welding, Proc. IFAC Workshop on Digital Image Processing in Industrial Applications, 1986.

53. M. A. Browne, E. R. D. Duckworth, R. A. Wainwright and J. Ashby, Practical industrial low cost vision for welding robots and automated welding machines, In "Robots and Automated Manufacture", ed. J. Billingsley, pp199-210, Peter Peregrinus, 1985.

54. T. C. Wang, White Light Seam Tracking System for Arc-Welding Robot, Proc. SPIE - The International Society for Optical Engineering, pp101-107, 1987.

55. B. S. Thomas, Optical Seam Trackers: Tough Requirements for Design and Laser Safety, In "Robotics Engineering", vol. 8 no. 6, pp8-11, June 1986.

56. M. C. Fairhurst, Computer Vision for Robotic Systems: An Introduction, pp8-10, 1988.

57. D. J. Purll and R. N. West, Flying Spot Laser Scanners, In "Automated Visual Inspection", ed. B. G. Batchelor, D. A. Hill, D. C. Hodgson, pp296-321, IFS Publications, 1985.

58. R. N. West and L. R. Baker, Laser scanning in inspection, Proc. SPIE, vol. 1012, In-Process Optical Measurements, pp163-169, 1988.

59. F. Slabodsky, Automatic inspection of glass, In "Sensor Review", vol. 10 no. 2, pp79-83, April 1990.

60. BS7192:1989 British Standard Specification for Radiation Safety of Laser Products, British Standards Institution, 1989.

61. P. Horowitz and W. Hill, The Art of Electronics (Second Edition), pp421-428, Cambridge University Press, 1989.

62. G. E. Tobey, J. G. Graeme and L. P. Huelsman, Operational Amplifiers Design And Applications, pp282-326, M°Graw Hill, 1986.

63. R. J. Beattie, A Low-cost Robot Guidance Vision System, IEE Colloquium on "Binary Image Processing - Techniques and Application", Digest No. 1991/059, pp5/1-5/3, March 1991.

64. Turbo C Reference Guide, Borland International, 1988.

65. C. S. Williams, Designing Digital Filters, pp13-18, Prentice Hall International, 1986.

66. R. C. Gonzalez and P. Wintz, Digital Image Processing, Addison Wesley, 1987.

67. C. S. Williams, Designing Digital Filters, Prentice Hall International, 1986.

68. M. C. Fairhurst, Computer Vision for Robotic Systems, pp23-30, Prentice Hall, 1988.

69. R. A. Roberts and C. T. Mullis, Digital Signal Processing, pp198-201, Addison Wesley, 1987.

70. T. Porsander and T.Sthen, An Adaptive Torch Positioner System, In "Robotic Welding", ed. J. D. Lane, pp157-165, IFS Publications, 1987.

71. C. L. Phillips and R. D. Harbor, Feedback Control Systems, pp363-376, Prentice Hall International, 1988.

72. J. J. Hill, D. C. Burgess and A. Pugh, Vision Guided Assembly of High Power Semiconductor Diodes, In "Robot Assembly", ed. K. Rathmill, pp305-315, IFS Publications, 1985.

73. J. A. Marchant, A mechatronic approach to produce grading, Proc. Mechatronics: Designing Intelligent Machines, pp159-164, IMechE, 1990.

74. P. G. Havas, Picture recognition for automated paint spraying of complex components, Proc. International Conference on Robot Vision and Sensory Controls, pp289-295, 1985.

75. M. Coulthard, Tile Inspection - The Right Application, In "Sensor Review", Vol. 11 No 2, pp15-18, 1991.

76. R. K. Dyche, INEX - 100 Per Cent On-Line Visual Inspection of Consumer Products, In "Sensor Review", Vol. 11 No. 4, pp14-16, 1991.

77. D. J. Purll, Solid-State Image Sensors, In "Automated Visual Inspection", ed. B. G. Batchelor, D. A. Hill and D. C. Hodgson, pp255-293, IFS Publications, 1985.

78. C. Loughlin, Tutorial: Line scan cameras, In "Sensor Review", Vol. 9 No. 4, pp195-202, 1989.

79. B. Vogeley, Vision systems or vision sensors? In "Sensor Review", Vol. 7 No. 3, pp152-160, 1987.

80. R. S. Adrain, I. A. Armour and J. H. Bach, Laser scanning cameras for in-reactor inspection, In "Sensor Review", Vol. 7 No. 2, pp68-76, 1987.

81. J. F. Claridge, Automatic Glass Inspection - Use of Retro-Reflective Laser Scanning, In "Sensor Review", Vol. 11 No. 1, pp17-21, 1991.

82. Sira (Image Automation) Commercial Literature, FastScan Retro-reflective scanner system.

83. C. A. J. Braganca, J. F. Claridge and R. M. Atkinson, A robot-based automatic paint inspection system, In "The Industrial Robot", vol. 14 no. 2, pp81-83, June 1987.

84. P. A. Lynn, An Introduction to the Analysis and Processing of Signals, Macmillan Publishers Ltd, 1984.

85. Open University Unit T292 - Instrumentation, Block 5 Part 1, Noise and Signals, pp27-28, The Open University Press, 1986.

86. C. Chatfield, Statistics for Technology: A Course in Applied Statistics, Chapman and Hall, 1983.

87. Open University Unit T326 - Electronic Signal Processing, Block IV - Random Signals and Signal Detection, pp13-18, The Open University Press, 1984.

88. D. Brook and R. J. Wynne, Signal Processing Principles and Applications, pp61-70, Edward Arnold, 1988.

89. K. A. Stroud, Engineering Mathematics, pp378-387, Macmillan, 1985.

90. A. C. Bajpai, L. R. Mustoe and D. Walker, Engineering Mathematics, pp391-398, Wiley, 1989.

91. S. J. Wellington and R. M. Crowder, A Non-Tactile Sensor for Robot Control, Proc. International Congress on Condition Monitoring and Diagnostic Engineering Management, pp326-330, Adam Hilger, 1991.

92. L. Bergstrom, Robotic seam sealing into the next generation, In "The Industrial Robot", Vol. 16 No. 3, pp138-142, September 1989.

93. S. Sawano, J. Ikeda, N. Utsumi, H. Kiba, Y. Ohtani and A. Kikuchi, A Sealing Robot with Visual Seam Tracking, Proc. International Conference on Advanced Robotics, pp351-358, 1983.

94. W. W. Luggen, Flexible Manufacturing Cells and Systems, pp250-260, Prentice Hall International, 1991.

95. I. A. Noble, Design of an automatic guided vehicle system, Proc. International Conference on Advanced Handling Systems - Applications and Experiences, pp21-26, IMechE, 1988.

96. P. J. C. Skitt, M. A. Javed, S. A. Sanders and A. M. Higginson, An artificial neural networks based quality monitor for resistance spot welding of coated steel, Proc. International Congress on Condition Monitoring and Diagnostic Engineering Management, pp40-45, Adam Hilger 1991.

97. J. Hicks, Data Acquisition Boards, In "Control and Instrumentation", pp31-35, March 1992.

Appendices

Appendix 1

Software Descriptions

Pseudo-code descriptions of the seam tracking software are presented in this section. Figure 23 shows a flowchart of the program.

1.1 Set Programmable Amplifier Gain

This routine is used to set the programmable gain amplifier so that the analogue input does not exceed the ±10V range of the analogue to digital converter, but is maintained close to these maximum values to minimise the quantisation error.

```
Amp_Gain=Break=0
REPEAT
     SET_AMP_GAIN=2^Amp_Gain
     Max=0
     FOR i=1 TO 4000
     DO
          Read=GET_ANALOGUE_INPUT
          Read=Read-2048
          IF ABS(Read) > Max
          THEN
               Max=ABS(Read)
          ENDIF
     ENDFOR
     IF Max >= 2047
     THEN
          Amp_Gain=Amp_Gain-1
     ELSEIF Max < 1024
     THEN
          Amp_Gain=Amp_Gain+1
     ELSE
          Break=1
     ENDIF
     IF Amp_Gain < 0
     THEN
          ABORT
     ELSEIF Amp_Gain > 4
```

```
    THEN
        ABORT
    ENDIF
UNTIL Break=1
```

NOTE

1) The software programmable gain amplifier (Analog Devices AD526) may be programmed to give a gain of 1, 2, 4, 8, or 16.
2) The A-D converter produces a 12-bit digital value given by the expression

$$V = 20\left(\frac{n}{4096} - \frac{1}{2}\right)$$

Where n is the decimal equivalent of the converted value (in the range 0 to 4095) and V is the analogue voltage (volts). A bipolar result is obtained by subtracting 2048 from the converted value.
3) The sampling rate of the A-D converter is controlled by a programmable hardware counter/timer.
4) With a sampling rate of 8kHz and a scan rate of 20 s^{-1} the analogue output will be sampled for 0.5s which corresponds to 1.25 complete revolutions of the 8-sided polygon mirror and this ensures that a minimum of one scan will be taken using each face of the mirror.

1.2 Sample Scan Data

This routine is used to sample one complete scan and store the converted values in memory. The programmable amplifier gain will be adjusted if necessary.

```
Inc=Dec=Break=0
REPEAT
    WAITFOR START_OF_SCAN
    FOR i=0 TO (NUMBER_OF_SAMPLES-1)
    DO
        Data[i]=GET_ANALOGUE_INPUT
        Data[i]=Data[i]-2048
    ENDFOR
```

```
      Max=0
      FOR i=START TO END
      DO
            IF ABS(Data[i]) > Max
            THEN
                  Max=ABS(Data[i])
            ENDIF
      ENDFOR
      IF Max >= 2047
      THEN
            Dec=Dec+1
      ELSEIF Max < 1024
      THEN
            Inc=Inc+1
      ELSE
            Break=1
      ENDIF
      IF Inc=5
      THEN
            INCREMENT_AMP_GAIN
            Inc=Dec=0
      ELSEIF Dec=5
      THEN
            DECREMENT_AMP_GAIN
            Inc=Dec=0
      ENDIF
UNTIL Break=1
Scale_Factor=2048/Max
FOR i=(START-1) TO (END+1)
DO
      Data[i]=Data[i]*Scale_Factor
ENDFOR
```

NOTE

1) A total of NUMBER_OF_SAMPLES samples are taken and stored in the global array Data. The values START and END are the first and last samples of the sensor output signal due to laser light reflected directly from the workpiece.

For a scan rate of 20 s^{-1} the following constants are used:

START=40

END=300

NUMBER_OF_SAMPLES=320

2) To compensate for variation in the amplitude of the scanner output signal due to the manufacturing tolerances of the polygon mirror, variations in surface texture and colour of the workpiece and the discrete amplifier gain settings the scan data is scaled such that the peak value is 2048. This process simplifies the thresholding algorithms used to detect the seam position.

1.3 Differentiate Scan Data

This routine is used to differentiate the scan data using the central difference technique.

```
FOR i=START TO END
DO
    Diff[i]=Data[i+1]-Data[i-1]
ENDFOR
```

NOTE

1) The value assigned to Diff[i] is twice the required value (Equation 5.4). To reduce the number of calculations and hence minimise the computation time, the differential values are not divided by two, instead, the threshold levels used for seam detection are simply scaled accordingly.

1.4 Detect Seam Position

This routine is used to determine the position of a seam relative to the start of scan pulse. The seam position is used to calculate an error value, with zero error indicating that the seam is located at the centre of the detector aperture. The error value is communicated to the robot controller in Sign-Magnitude format.

```
Seam_Lost=0
REPEAT
     Seam_Position=0
     Sample_Scan_Data
     Differentiate_Scan_Data
     Total=Max_Total=Width=Position=0
     FOR i=START TO END
     DO
          IF Diff[i] >= 0
          THEN
               Total=Total+Diff[i]
               Width=Width+1
          ELSE
               IF Total > Max_Total
               THEN
                    Position=i-Width/2
                    Max_Total=Total
               ENDIF
               Width=Total=0
          ENDIF
     ENDFOR
     IF Max_Total > THRESHOLD_1
     THEN
          Seam_Position=Position
     ELSE
          Width=Max_Width=0
          FOR i=START TO END
          DO
               IF (Diff[i] >= 0) AND (Diff[i] < THRESHOLD_2)
               THEN
                    Width=Width+1
               ELSE
                    IF Width > Max_Width
                    THEN
                         Position=i-Width/2
                         Max_Width=Width
                    ENDIF
               ENDIF
          ENDFOR
```

```
            IF Max_Width >= THRESHOLD_3
            THEN
                  Seam_Position=Position
            ENDIF
      ENDIF
      IF Seam_Position=0
      THEN
            Seam_Lost=Seam_Lost+1
      ELSE
            Seam_Position=Seam_Position-START
            Seam_Position=254*Seam_Position/(END-START)
            Error=Seam_Position-127
            IF Seam_Position < 127
            THEN
                  Error_MSB=1
            ENDIF
            SEND Error TO ROBOT
            IF ROBOT_OK = False
            THEN
                  ABORT
            ENDIF
            Seam_Lost=0
      ENDIF
UNTIL Seam_Lost=5
```

Appendix 2

The Prototype Polygon Mirror

The dimensions of the polygon mirror used to scan the laser are presented in this section.

2.1 Surface flatness

Table 1 gives the mean flatness of each mirror face.

Face	Flatness (mm)
A	0.005
B	0.030
C	0.004
D	0.012
E	0.005
F	0.040
G	0.006
H	0.008

Table 1 Mean flatness of each mirror face

2.1 Angles between the polygon faces

Table 2 gives the angles between the faces of the polygon mirror.

Face	Angle (Degrees and minutes)
A-B	44° 5′
B-C	44° 6′
C-D	45° 0′
D-E	45° 5′
E-F	45° 0′
F-G	45° 1′
G-H	45° 9′
H-A	44° 5′

Table 2 Angles between the polygon mirror faces

Appendix 3

Calculation of scanning speed

Referring to Figure 40 the scanning speed may be calculated as follows:

$$Tan2\theta_p = \frac{r}{p} \qquad \text{A3.1}$$

$$Tan\theta_{min} = \frac{r}{q} \qquad \text{A3.2}$$

$$Sin\theta_{min} = \frac{r}{X} \qquad \text{A3.3}$$

Thus from Equation A3.3

$$r = XSin\theta_{min} \qquad \text{A3.4}$$

Substituting Equation A3.4 into A3.1 yields

$$p = \frac{XSin\theta_{min}}{Tan2\theta_p} \qquad \text{A3.5}$$

and substituting Equation A3.4 into A3.2 yields

$$q = \frac{XSin\theta_{min}}{Tan\theta_{min}} \qquad \text{A3.6}$$

Now, from Figure 40

$$p+q = LCos\theta_{min} \qquad \text{A3.7}$$

Substituting Equation A3.5 and A3.6 gives

$$LCos\theta_{min} = \frac{XSin\theta_{min}}{Tan2\theta_p} + \frac{XSin\theta_{min}}{Tan\theta_{min}} \qquad \text{A3.8}$$

and by algebraic manipulation

$$X = \frac{L\,Tan2\theta_p}{Tan\theta_{min} + Tan2\theta_p} \qquad \text{A3.9}$$

Where: X = Position of the laser beam

L = Scan Length

θ_{min} = Minimum angle of reflection of the laser from the polygon mirror

θ_p = Angular position of the polygon mirror

Differentiating Equation A3.9 yields

$$\frac{dX}{d\theta_p} = \frac{2L\,Tan\theta_{min}(1 + Tan^2 2\theta_p)}{(Tan\theta_{min} + Tan2\theta_p)^2} \qquad \text{A3.10}$$

Now, for a constant motor speed

$$\frac{d\theta_p}{dt} = K \qquad \text{A3.11}$$

Hence scan speed is given by

$$\frac{dX}{dt} = K\left(\frac{2L\,Tan\theta_{min}(1 + Tan^2 2\theta_p)}{(Tan\theta_{min} + Tan2\theta_p)^2}\right) \qquad \text{A3.12}$$

Where: K = Motor speed constant

Appendix 4
Published Papers

1) A tracking vision sensor system, IEE Colloquium "Binary Image Processing - Techniques and Applications", Digest No. 1991/059, pp3/1-3/5, March 1991.

2) A non-tactile sensor for robot control, Proc. International Congress on Condition Monitoring and Diagnostic Engineering Management, pp326-330, Adam Hilger, July 1991.

The following published papers were included in the bound thesis. These have not been digitised due to copyright restrictions, but the links are provided.

S.J. Williamson (1991) “A tracking vision sensor system.” IEE Colloquium Binary Image Processing – Techniques and Applications, No. 1991/059, pp.1-3/5, March 1991.

https://doi.org/10.1049/cp:19940239